PSERC

Estimation of Synchronous Generator Parameters from On-line Measurements

Final Project Report

Power Systems Engineering Research Center

A National Science Foundation
Industry/University Cooperative Research Center
since 1996

Power Systems Engineering Research Center

Estimation of Synchronous Generator Parameters from On-line Measurements

Final Project Report

Project Team

Gerald T. Heydt
Elias Kyriakides
George Karady
Keith Holbert
Sandeep Borkar
Winter Gu
Arizona State University

Vijay Vittal
Iowa State University

Garng Huang
K. Men
Texas A&M University

PSERC Publication 05-36

June 2005

Information about this project

For information about this project contact:

Gerald T. Heydt, Ph.D.
Arizona State University
Department of Electrical Engineering
Tempe, AZ 85287
Tel: 480-965-8307
Fax: 480-965-0745
Email: heydt@asu.edu

Power Systems Engineering Research Center

This is a project report from the Power Systems Engineering Research Center (PSERC). PSERC is a multi-university Center conducting research on challenges facing a restructuring electric power industry and educating the next generation of power engineers. More information about PSERC can be found at the Center's website: http://www.pserc.org.

For additional information, contact:

Power Systems Engineering Research Center
Cornell University
428 Phillips Hall
Ithaca, New York 14853
Phone: 607-255-5601
Fax: 607-255-8871

Notice Concerning Copyright Material

Acknowledgements

The Power Systems Engineering Research Center sponsored the research project titled "Extended State Estimation for Synchronous Generator Parameters." The project began in 2003. This is the final report for the project.

We express our appreciation for the support provided by PSERC's industrial members and by the National Science Foundation under grant NSF EEC-0001880 received from the Industry / University Cooperative Research Center program.

The authors thank all PSERC members for their technical advice on the project, especially Dale Krummen (AEP), Dale Bradshaw (TVA), Mike Ingram (TVA), Ralph McKoskey (TVA), Baj Agrawal (Arizona Public Service), Douglas Selin (Arizona Public Service), John Demcko (Arizona Public Service), and Bill Price (GE Energy). Dale Bradshaw and Baj Agrawal served as the industry advisors for the work.

An earlier Masters thesis was done at ASU, and the authors liberally used the work of Warren Rees. Mr. Rees is presently with the U. S. Bureau of Reclamation in Denver.

The authors also acknowledge Drs. Ali Abur and A. P. Sakis Meliopoulos of Texas A&M University and Georgia Tech respectively who contributed technical advice and data to this work. Dr. S. Suryanarayanan, of Florida State University, formerly of Arizona State, provided useful comments.

Executive Summary

This is the final report on a research project on identification of synchronous machine parameters using on-line measurements. The concept is to utilize the dynamic operational data in combination with manufacturers' estimates of synchronous machine parameters to 'force' the machine model to agree with measurements. Park's model is used with three damper windings. The method uses a mathematical tool from state estimation technology to formulate a minimum squared error solution. A particular difficulty relates to modeling magnetic saturation. A combination of classical model with a new approach is used so that saturated and unsaturated data are calculated. The mathematical details are given in equations and flow charts. Also, the method has been programmed in an object-oriented Graphic User Interface (GUI) in which the user attaches the machine measurement data file, and manufacturers' estimates. The calculation is displayed on a GUI menu. The method has been tested with data from approximately six large generating units (all machines with field circuit brushes). Estimates of model resistances and unsaturated inductances agree with manufacturers' estimates as well as operating data. The authors conjecture that the parameters calculated in this way actually may be more accurate for the given operating conditions than the manufacturer's parameters which may have been obtained from stand-still tests many years ago.

Applications of this work include:

- Utilization of accurate data and accurate models in transient stability studies, thus allowing more accurate and 'safe' operating practices (e.g., machine loading)
- The availability of a user friendly software tool to obtain synchronous generator parameters – even if these are missing from manufacturers' data
- The ability to track changes in machine parameters as the machine ages and undergoes normal 'wear' from operation.

The brushless exciter configuration has been examined, but results were disappointing. The results shown in Appendix F may indicate that our estimation method is not suitable for synchronous machine parameter estimation for brushless exciter installations.

The report also provides citations to several longer reports and published technical papers where additional project details are given.

Table of Contents

Table of Contents
(continued)

Table of Contents
(continued)

Table of Figures

Table of Figures
(continued)

Table of Figures
(continued)

Table of Tables

1 Modeling of Synchronous Generators

1.1 Background and Motivation

Synchronous generators are the mainstay of electric power generation in the World. These machines were invented in the late 1800s and further refined in the early 1900s. There is a huge literature of synchronous generators prior to 1930, but the main initial advance in synchronous machine analysis was the development of Park's model. The original paper by Park is [1]. Discussion of the model and classical references of the field appear in [2-9].

Park's model was not the only synchronous machine model: Jackson and Winchester [10] developed direct and quadrature axis equivalent circuits for round rotor synchronous generators. During the same period, Canay [11] focused on developing equivalent circuits for field and damper windings to estimate generator parameters. A significant contribution was made by Yu and Moussa in 1971 [12] who reported a systematic procedure that can be implemented to determine the parameters of the equivalent circuits of synchronous generators. A further alternative is to appeal to the finite element approach in which the magnetic circuits in a synchronous machine are modeled at the microscopic level, and a translation is made to the mesoscopic level.

It suffices to say that in all but the most unusual cases, the Park model is used. And this model has survived the 'test of time.' If modifications and refinements are made on the Park model, the usual approach is to add 'windings' to the model. This procedure entails the addition of RL circuits that are magnetically coupled to the classical model. By this procedure, second order effects can be captured by relatively minor additions to the classical model.

Models are needed for most engineering applications in any area. Applications of synchronous generators and their steady state and dynamic responses are no different. It is standard practice in power engineering to utilize Park's model of a synchronous generator for all engineering applications. As examples, the following are typical application areas:

- Standard steady state operations analysis, including calculation of voltage regulation, response to exciter signals
- Post-mortem analyses of failures and misoperation
- Identification of incipient failures of electrical windings in the machine
- Response analysis to disturbances, both large and small
- Design of exciters, power system stabilizers, and other controls.

However, modeling of synchronous machines always entails calculation or measurement of model parameters. In Park's model, there are at least three resistances and three inductances that need to be known. If machine damper windings are to be included in the model (essential for most transient analyses), at least two more resistances and two more

inductances must be known. Oftentimes, the model has in the order of ten R-L parameters that must be known. Some of these parameters are readily correlated to actual resistances or inductances – but some are not. Standardized tests have been developed to establish these parameters, and references [13-14] document these tests. One issue in these tests is that most standard tests require that the machine under test be taken off-line. The operation of modern power systems, and the judicious use of large synchronous machines often suggest that taking a machine down for testing is clearly undesirable. Therefore, there is strong motivation for on-line methods to establish machine parameters.

This report contains the details of an on-line procedure to accurately determine synchronous generator parameters using Park's model, and using a technology similar to state estimation. The state estimation utilized is actually parameter estimation, and the method is based on a mathematical tool known as the method of least squares. References [15-19] contain a full description of that technology.

1.2 Off Line Alternatives for Obtaining Synchronous Machine Model

Off-line methods, however, are neither practical nor accurate in most cases. Decommiting a generator for parameter measuring is not economical for a utility – especially if the specific generator is a base unit. Furthermore, under different loading conditions certain generator parameters may vary slightly and therefore off-line methods may not be accurate enough for certain applications. Finally, the effect of saturation of generator inductances cannot be accounted for in off-line studies. Saturation is a critical concept in generator operation; in order to consider it in the estimation process, one has to account for the operating level of the generator at the particular estimation interval [20]-[22].

Contrary to off-line methods, on-line methods to identify machine parameters are very attractive to utilities because of their minimal interference in the normal operation of the generator. Ideally, generator parameters may be calculated under different operating conditions, both in steady state and transient operation. In 1977 Lee and Tan [22] proposed an algorithm to determine the parameters of a salient pole generator from data obtained during a sudden short circuit. In 1981, Dandeno [23] used on-line frequency response measurements from two large turbo generators to identify machine parameters; during the same period, Nishiwaki [24] used the extended Kalman filter to identify dynamic stability constants for small disturbances under steady state operating conditions. In 1982 Bollinger [25] proposed a technique to estimate system parameters by utilizing wide bandwidth noise signals in an excitation signal which acts as a disturbance to the system.

1.3 Project Objectives

The main objective of this research work is to develop a method to identify synchronous generator parameters from on-line measurements. It is also desired to develop a graphic user interface (GUI) application which will be user friendly and self guiding so as to facilitate prompt estimation of the desired parameters. In this way, possible fault conditions can be detected and remedy action can be undertaken. Moreover, it is necessary to develop an algorithm that will enable bad measurement detection and rejection so as to

increase the reliability of the results. Another objective of this research work is to develop the saturation model of the inductances of a synchronous machine. A number of inductances in the synchronous machine model experience significant change in their values depending on the operating condition of the machine. The effect of saturation is modeled and incorporated it in the GUI so as to obtain accurate estimates that reflect the true status of the machine at every operating point.

Secondary objectives of the research include:

- Development of an observer for damper currents
- Calculation of the error characteristics of the estimation
- Development of an index of confidence
- Calculation of a range of values for each estimated parameter
- Study of which machine parameters can be estimated, and which can not
- Evaluation of alternative GUI features.

Fig. 1.1 shows the activities related to a synchronous generator, their relation to the graphic user interface, and the estimation method utilized in this research work.

1.4 Technical Documentation of the Project

This project was executed over three years at three universities and with the cooperative efforts of over eleven researchers – including industry liaisons and contributors. The main university contributions were made at Arizona State University (the 'lead' university); Iowa State University; and Texas A & M University. One of the authors of the report was affiliated with Iowa State University during the execution of this work – but has since left that position for a position at Arizona State University.

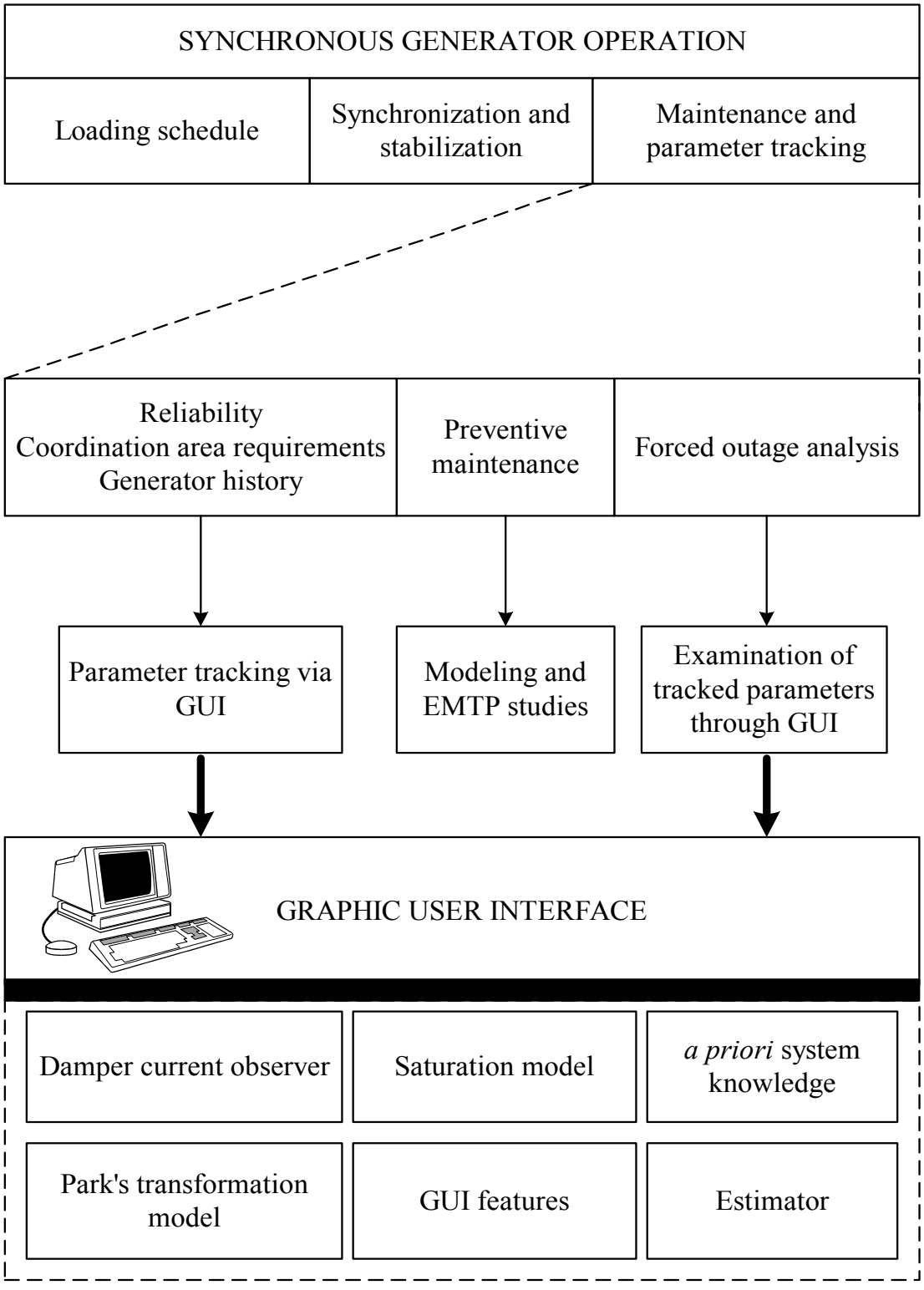

Fig. 1.1 Synchronous generator operation and graphic user interface implementation

Approximately 15 technical reports, theses and papers were prepared for the project, and these fully document the project. These are:

- S. U. Borkar, K. E. Holbert, "Digital Filtering of Synchronous Generator Measurements for Parameter Estimation," *Proceedings of the Seventh IASTED International Conference on Power and Energy Systems*, Clearwater, FL, Nov. 28-Dec. 1, 2004, pp. 454-459. This is reprinted in part in Appendix E.
- S. U. Borkar, K. E. Holbert, "Digital Filtering and Bad Data Rejection for Synchronous Generator Parameter Estimation," *Proceedings of the Thirty-fifth Annual North American Power Symposium* (NAPS 2003), Rolla, MO, October 20-21, 2003, pp. 591-598. This is reprinted in part in Appendix D.
- E. Kyriakides, "Innovative Concepts For On-Line Synchronous Generator Parameter Estimation," PhD. Thesis, Arizona State University, Tempe AZ, December, 2003. The main results appear in Chapters 1 – 5 of this report.
- S. U. Borkar, "Design of a Digital Filter for Synchronous Generator Parameter Estimation," M. S. E. E. Thesis, Arizona State University, Tempe, AZ, August 2004
- E. Kyriakides, G. T. Heydt, and V. Vittal, "On-line estimation of synchronous generator parameters using an observer for damper currents and a graphical user interface," *IEEE Transactions on Energy Conversion*, Aug. 2003, to be published.
- E. Kyriakides, G. T. Heydt, "An observer for the estimation of synchronous generator damper currents use in parameter identification," *IEEE Transactions on Energy Conversion*, Vol. 18, March 2002, pp. 175-177.
- N. Logic, E. Kyriakides, G. T. Heydt, "*Lp* state estimators for power systems," Journal of Electric Power Components and Systems, v. 33, No. 7, July 2005.
- E. Kyriakides, G. Heydt, "Estimation of Synchronous Generator Parameters Using an Observer for Damper Currents and a Graphical User Interface," J. Electric Power Systems Research, No. 69, v. 2004, pp. 7-16, February 2004 .
- Elias Kyriakides, Gerald T. Heydt, Vijay Vittal, "On-Line parameter estimation of round rotor synchronous generators including magnetic saturation," Accepted for publication, 2004, IEEE Transactions on Power Systems.
- E. Kyriakides, G. Heydt, "An observer for the estimation of synchronous generator damper currents for use in parameter identification," IEEE Power Engineering Letters, IEEE Transactions on Energy Conversion, v. 18, No. 1, ITCNE4, pp. 175 – 7, 2003.
- E. Kyriakides, G. T. Heydt, "A graphical user interface for synchronous machine parameter identification," 2001 North American Power Symposium, October, 2001, College Station, TX, pp. 112 – 119.
- E. Kyriakides, G. T. Heydt, "Synchronous machine parameter estimation using a visual platform," Proceedings of the IEEE Power Engineering Society Summer Meeting, 2001, v. 3, pp. 1381 – 1386.
- N. Logić, E. Kyriakides, G. T. Heydt, *"L_p* state estimators for power systems," Proceedings of the North American Power Symposium, October 14 – 15 2002, Tempe AZ, pp. 48 – 51.

- M. Bakroun, A. İnan, G. T. Heydt, "A comparison of L_p state estimators for power engineering applications," Proceedings of the North American Power Symposium, October 14 – 15 2002, Tempe AZ, pp. 520 – 526.
- E. Kyriakides, G. Heydt, "Damper winding representation and magnetic saturation in synchronous generator modeling," Proceedings of the 2003 North American Power Symposium, pp. 522 – 529, Rolla MO, October, 2003.

1.5 Research Staff

Table 1.1 shows the research staff on the project and their main roles.

1.6 A Guide to the Appendices

This report contains six appendices. The appendices mainly contain technical details to the main body of the report. Their content is indicated in Table 1.2. The special topic of brushless exciters (i.e., field current supplied to the machine electromagnetically) is discussed in Appendix F.

1.7 Analysis and Modeling of Synchronous Generators

The classic Westinghouse Transmission and Distribution Handbook provides information for the construction and operation of synchronous machines [26]. Another useful handbook in the field of electrical machinery is the *Electric Motor Repair* by Rosenberg [27]. It is a handbook for the "practically minded" concentrating on the winding, repair, and troubleshooting of a large number of AC and DC motors and controllers. *Power System Stability and Control* by Kundur [20] and *Power System Control and Stability* by Anderson and Fouad [21] provide an extensive and detailed analysis of synchronous machines, in both theory and modeling. They dedicate three chapters on this topic and, among others, they cover the *dq0* transformation, the per unit representation, equivalent circuits, and analysis in both steady state and transient operation. Saadat in *Power System Analysis* [28] concentrates on the transient analysis of the synchronous generator and on balanced and unbalanced faults. Saadat offers coverage on the Park's transformation and on deriving the generator equation in the rotor frame of reference.

Anderson, Agrawal, and Van Ness [29] provide an extensive analysis of synchronous machines. They dedicate a chapter on synchronous machine modeling and provide an extensive analysis of the direct and quadrature axis equations. They also examine thoroughly Park's transformation, while in one of their chapters they concentrate on parameter computation, measured data from field tests, and sample test results. Very useful sources of information are the books *Electric Machinery* [30] and *Analysis of Electric Machinery* [31]. Both books contain the theory of synchronous machines and analysis of steady state operation. In addition, [31] offers interesting details on operational impedances and time constants, linearized equations, and a chapter on the asynchronous and unbalanced operation of synchronous machines.

Table 1.1 University research staff

Staff member	Institution where work was done	Main project role
Sandeep Borkar	Arizona State University	Researched instrumentation signal filtering
Winter Gu	Arizona State University	Investigated brushless exciter applications
Gerald T. Heydt	Arizona State University	Principal investigator
Keith E. Holbert	Arizona State University	Researched instrumentation signal filtering
Garng Huang	Texas A&M University	Investigated brushless exciter applications
George Karady	Arizona State University	Investigated brushless exciter applications
Elias Kyriakides*	Arizona State University	Main researcher and developer of the computer implementation
K. Men	Texas A&M University	Investigated brushless exciter applications
Vijay Vittal **	Iowa State University	Investigated saturation, report preparation

*Dr. Kyriakides is presently with the University of Cyprus, Nicosia, Cyprus.
** Dr. Vittal is presently with Arizona State University.

Table 1.2 Report appendices

Appendix	Subject area	Content	Main subject matter reprinted from this reference
A	Modeling	Modeling of the damper currents using a device known as an observer	[69]
B	Bad data	Elimination of bad measurement data via preprocessing	[69]
C	Modeling	Modeling magnetic saturation	[67], [69]
D	Data acquisition, measurement filtering	Design of specific numerical filters (e.g., Butterworth, Chebyshev) for synchronous machine instrumentation	[68]
E	Measurement filtering	Maintaining phase relationships among AC voltages and currents in measurements during noise filtering; harmonics in measurements	[71]
F	Brushless excitation	An attempt was made to modify the parameter estimation algorithm for brushless machines. No data were available for this type of machine for cases of known model of the brushless exciter. Some progress was made, but the concepts were not integrated into the algorithm developed.	

1.8 Estimation of Parameters of Synchronous Generators

Keyhani, who has conducted research on parameter estimation using a number of different techniques, has offered extensive literature on this topic. One of the methods used by Keyhani was the estimation of parameters from Standstill Frequency Response (SSFR) test data [31], [32]. In this approach, curve fitting techniques are used to derive the transfer functions of the direct axis and quadrature axis using the available test data. The parameters of the model are then calculated from nonlinear equations, which relate the machine parameters and the time constants corresponding to the transfer functions [32]. However, noise-corrupted data cause multiple parameter sets to be estimated. To obtain a unique set of parameters, Keyhani used a maximum likelihood estimation (ML) technique [31]. The results indicate that a unique and relatively accurate parameter set is estimated even though the data are corrupted with noise.

Keyhani in [33] offers an evaluation of the performance of the ML method using case studies and SSFR data from tests on a 722 MVA generator. It is shown that the ML method gives estimates with very small error, while the noise has no noticeable effect on the estimator. The ML algorithm and SSFR data were also used in [32] to estimate parameters of a three phase salient pole 5 kVA synchronous machine. The equivalent circuit models were developed and online dynamic responses were performed to validate the identified models.

Tsai, Keyhani, Demcko, and Farmer used small-disturbance responses and the ML estimation technique to identify an online synchronous generator model [35]. The first step was to identify the machine linear model parameters. Consequently, the saturation models of the machine were identified using the estimated mutual inductances under a wide range of operating conditions. It was shown that when the MMF saturation model was used, the simulated responses of the developed model matched closely with the measured responses.

Another method used by Keyhani was the identification of synchronous machine linear parameters from standstill step voltage input data [36]. The procedure involves applying a step voltage as an input and estimation of the parameters of the time constant and equivalent circuit models. The initial values of the parameters to be estimated are extracted from the operational inductances which are derived from the measured time domain data.

Tsai, Keyhani, Demcko, and Selin presented a new approach to develop a model of the saturated synchronous generator using artificial neural networks (ANN) [37]. ANN are possible to be trained after being arranged in a certain pattern. The pattern used in this network is a feed-forward network and the learning scheme is of the error back-propagation form. Moreover, the training pattern was based on online small disturbance responses and the ML algorithm. The important conclusion of this paper is the fact that the developed ANN saturation model is capable of predicting the machine nonlinear changes which were not used in the training process.

Eitelberg in [38] uses a linearly formulated least squares problem to obtain approximate parameter values. Consequently, a numerical search method is used to solve the nonlinear problem of magnitude and phase fitting. Boje [39] proposes time domain measurements for determining selected parameters of synchronous machines. These are proposed as an alternative to standstill frequency domain tests, since as the authors argue, the proposed method uses simpler equipment and model parameters are obtained directly in parametric form. However, as with traditional SSFR testing, this method does not model the machine at normal operating conditions.

Karayaka, Keyhani, Agrawal, Selin, and Heydt in [40]-[42] concentrated on large synchronous utility generators to develop a procedure of parameter estimation from online measurements. In [40] a one-machine infinite bus system is simulated in the *abc* frame of reference using parameters provided by the manufacturer. The armature circuit pa-

rameters are hence calculated using the recursive maximum likelihood (RML) estimation technique. Based on these estimates, the field winding and some damper parameters are estimated using an Output Error Estimation (OEM) technique. It is found that even with highly corrupted data the estimated and actual parameters are in good agreement. In [41] the authors present a method to estimate machine parameters using synthetic data as previously, but also real time operating data from a utility generator. This study showed that noise-corrupted data could be handled up to a certain point. Below a certain signal-to-noise ratio (SNR), estimation of machine parameters was not possible. The estimation of machine parameters using data obtained online showed that there was a reasonable agreement between estimated and actual curves.

The above methods were repeated by the authors using Artificial Neural Networks [42]. The data used to train the ANN were taken from real time operating data and the developed models were validated with measurements not used in the training of ANN and with large disturbance responses. It was shown that ANN models could correctly interpolate between patterns not used in training.

Rico, Heydt, Keyhani, Agrawal, and Selin attempted to estimate machine parameters using orthogonal series expansions such as Fourier, Walsh, and Hartley series [43], [44]. In [43] the authors propose the use of the Hartley series for fitting operating data such as voltage and current measurements and the use of linear state estimation to identify the coefficients of the series. In this way, the machine parameters can be identified. At the same time, this method is tested for noise corruption in the measurements. The authors show that the error in the estimation is below 1% even for SNR of 50:1. In [44] the authors expand their previous study to include Walsh and Fourier series in machine parameter estimation. A matrix of coefficients common to all orthogonal series expansions is used. The results show that the estimated parameters are in good agreement with the actual parameters. Also, this method takes into account the dependence of the parameters with respect to the operating point. More information on orthogonal series expansions for various power system components such as synchronous generators and transmission lines can be found in [45].

Finally, Kyriakides and Heydt in [46] and [47] offer an algorithm for the estimation of synchronous generator parameters from measurements that are taken at the machine terminals while the generator serves its load. This report is an extension of the idea presented in the papers.

1.9 Estimation Techniques

Estimation techniques such as state estimation, least squares, and maximum likelihood are used in engineering applications interchangeably. For the purposes of this research the mathematical model is desired to be transformed in a form realizable by a state estimation algorithm. State estimation is a process during which a number of unknown system state variables or parameters are assigned a value based on measurements from that system [48].

Schweppe [49]-[50] was one of the first to propose and develop the idea of state estimation for the monitoring of power systems. Wood and Wollenberg dedicate a chapter of their book on state estimation [50]. They offer insight to maximum likelihood concepts and derive the least squares equations used in state estimation. An introduction on advanced topics on state estimation and a lot of examples on AC network state estimation are offered. Advanced topics include bad data detection, estimation of quantities not being measured, network observability, and pseudo-measurements.

1.10 Noise Filtering

Generating stations are notorious for their poor electromagnetic interference (EMI) environment. This is a consequence of the high currents which produce high magnetic fields, and the high voltages which may produce electrostatic coupling as well as partial discharges. These usual test conditions, as well as general environmental issues that result in measurement error, are the basis for a specialized interest in noise filtering. There are some fortunate issues in that many power system noise issues relate to the 60 Hz supply, or to integral harmonics (e.g., fifth harmonic = 300 Hz). In between the data acquisition and the estimator implementation there are a number of other processes that need to be performed to prepare the data in a form that can be used by the estimator. One of the most fundamental processes is the filtering of the measured data for the removal of inconsistent measurements and noise. Various filters have been developed and implemented for the purposes of noise filtering. The filters considered for this work are digital discrete filters. Representative types of digital filters are the Butterworth, Chebyshev, Bessel, and moving average filters [51]-[53].

A filter almost always introduces a phase shift to the filtered signal. This phase shift is not desired, since the various frequency components of the signal are phase shifted by a different amount. Therefore, a zero phase shift filter is desired to be implemented so that there is no phase difference between the original and filtered signals. Information on zero phase shift filters can be found in [59], [54]-[56]. Zero phase digital filters effectively filter the signal in both the forward and the reverse directions. The resulting sequence has zero phase distortion and twice the filter order.

In all measurement technologies, there are the possibilities of bad measurements or missing measurements. Bad data detection and rejection algorithms have been considered and implemented to remove outliers from the measurements. Such outliers appear in the form of spikes in the data sets and are inconsistent measurements. References [57]-[59] propose new methods for the implementation of bad data detection and rejection algorithms in power system state estimation problems.

The issues of missing data (e.g., a datum inadvertently ‘dropped’ from a clocked measurement) are discussed by Heydt in [60].

1.11 Magnetic Saturation

Saturation is a phenomenon in which a functional or physical relationship $y = f(x)$ experiences a condition in which for sufficiently large x, the values of y no longer change significantly. This occurs in magnetic circuits when a large number of the magnetic domains align, and the application of a magnetic field no longer produces significant increase in magnetic intensity. Saturation of the generator magnetic circuits is an important concept in this research work. The effect of saturation has been the subject of many scientific papers and is still a subject of active research due to the importance of the change of the generator parameters with operating conditions and the difficulty for modeling saturation accurately. Reference [61] identifies saturation representation as the most important factor in the improvement of synchronous machine models. Saturation and different methods to model it are considered in IEEE standards such as [5], as well as a number of research articles and books [11], [20]-[22], [62], [63]. Fig. 1.2 shows a sample saturation curve for a synchronous generator.

It has been stated that the modeling of magnetic saturation is one of the most difficult engineering problems in existence. In [22], [62] the authors propose two quadratic saturation functions to represent saturation and they fit the proposed functions with measured data from two generators. This is performed using the method of finite element analysis. Reference [64] compares two methods of saturation representation by examining results of calculations and available test data for a specific synchronous generator. Saturation in both the direct and quadrature axes is considered. Authors in [65] describe a maximum likelihood estimation algorithm to identify saturated inductances of a synchronous machine. The saturation was modeled from operating data that were generated from small voltage excitation disturbances. An alternative method to model saturation by using a linearized generator model and stochastic approximation to solve for the parameters of the model is presented in [63]. The authors in [66] present a saturation representation by using a finite element numerical analysis technique. However, the method does not apply to all operating conditions.

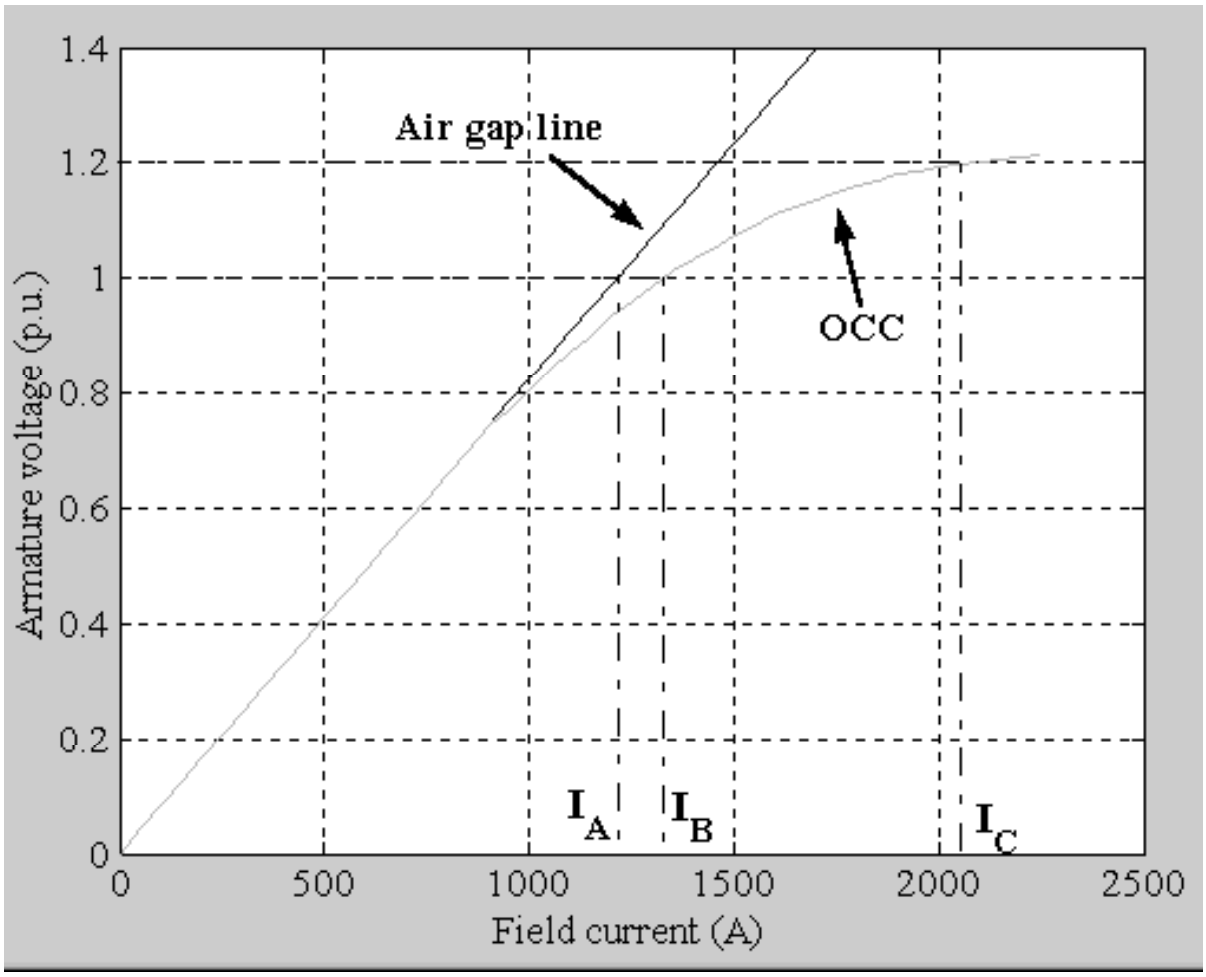

Fig. 1.2 Sample saturation curve for a synchronous generator

1.12 Organization of the Report

The report is organized into 5 chapters and 5 appendices. Chapter one is introductory and leads the reader to additional references as well as further reports of this work.
The main theory is shown in Chapter 2. Chapter 3 relates to the implementation and testing of the computer code. Examples are shown. Chapter 4 gives the details of a graphic user interface in an object oriented (menu driven) implementation. Chapter 5 contains conclusions, recommendations, and input received from industry for the project.
The appendices cover:

- A. Modeling of the damper currents using a device known as an *observer*
- B Elimination of bad measurement data via preprocessing
- C. Modeling magnetic saturation

- D. Design of specific numerical filters (e.g., Butterworth, Chebyshev) for synchronous machine instrumentation
- E. Maintaining phase relationships among AC voltages and currents in measurements during noise filtering; harmonics in measurements
- F. Brushless exciters.

2 Modeling of Synchronous Machines

2.1 Introduction

In this chapter, Park's model is explained. References to reports giving added detail are also given. The main enhancements to Park's model are described in the context of obtaining a method to identify synchronous machine parameters

2.2 Park's Model of a Synchronous Generator

In order to formulate the state estimation equations for a synchronous generator, it is necessary to employ a mathematical model which represents the synchronous generator in the conditions under study. The model used in this research work consists of three stator windings, one field winding and three damper windings as shown in Fig. 2.1. Magnetic coupling is a function of the rotor position and therefore, the flux linking each winding is also a function of the rotor position. The instantaneous terminal voltage of any winding takes the form,

$$v = -ri - \dot{\lambda} \tag{2.1}$$

where r is the winding resistance, i is the current and λ is the flux linkage. It should be noted that in this notation it is assumed that the direction of positive stator currents is out of the terminals, since the synchronous machine under consideration is a generator.
In (2.1) the voltage is expressed in terms of both currents and flux linkages. This is not desirable and therefore one of the two variables has to be replaced. The flux linkage variables can be substituted by appropriate expressions that relate them to generator currents via machine inductances.

This substitution will result in differential equations with time-varying coefficients. It is convenient to refer all quantities to a rotor frame of reference through Park's transformation,

$$\mathrm{P} = \sqrt{2/3}\begin{bmatrix} \frac{1}{\sqrt{2}} & \frac{1}{\sqrt{2}} & \frac{1}{\sqrt{2}} \\ \cos\theta & \cos(\theta - 2\pi/3) & \cos(\theta + 2\pi/3) \\ \sin\theta & \sin(\theta - 2\pi/3) & \sin(\theta + 2\pi/3) \end{bmatrix}.$$

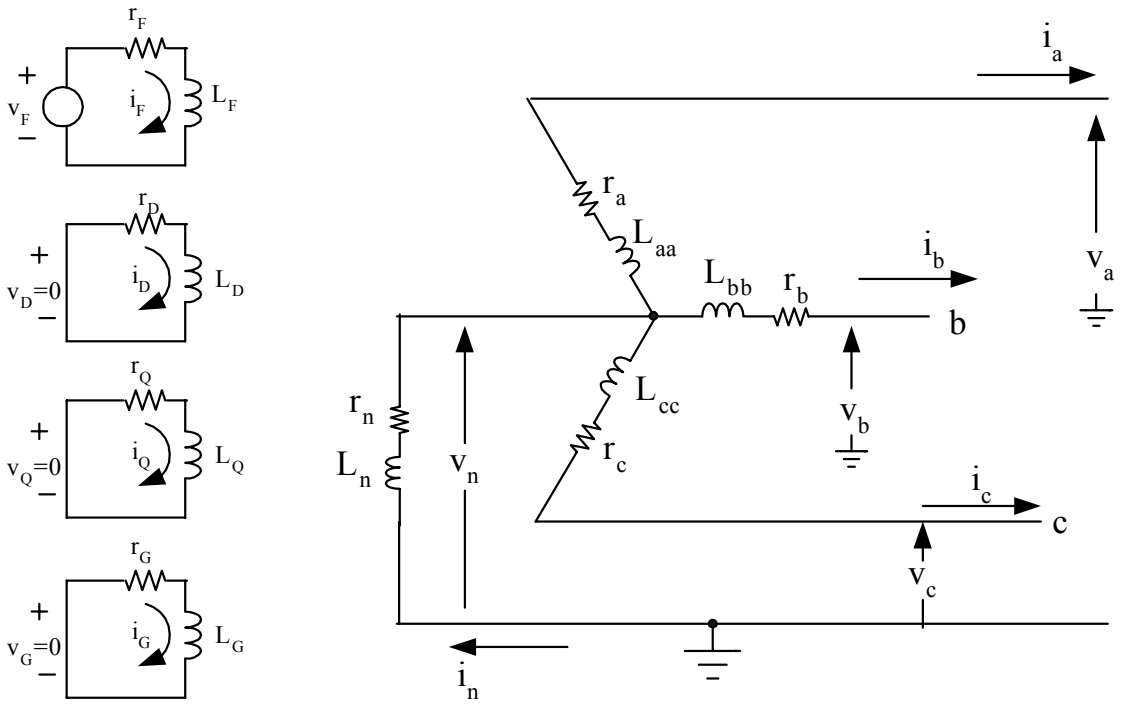

Fig. 2.1 Schematic diagram of a synchronous machine

The angle θ is given by [12],

$$\theta = \omega_R t + \delta + \pi/2$$

where ω_R is the rated (synchronous) angular frequency in rad/s and δ is the synchronous torque angle in electrical radians. The transformed currents are,

$$i_{0dq} = P i_{abc}$$

where the current vectors are defined as,

$$i_{0dq} = \begin{bmatrix} i_0 \\ i_d \\ i_q \end{bmatrix} \qquad \text{and} \qquad i_{abc} = \begin{bmatrix} i_a \\ i_b \\ i_c \end{bmatrix}.$$

Similarly, the transformed voltages and flux linkages are,

$$v_{0dq} = P v_{abc} \qquad \text{and} \qquad \lambda_{0dq} = P \lambda_{abc}.$$

Equation (2.1) in its expanded form becomes,

$$\begin{bmatrix} v_a \\ v_b \\ v_c \\ -v_F \\ -v_D \\ -v_G \\ -v_Q \end{bmatrix} = -\begin{bmatrix} r_a & 0 & 0 & 0 & 0 & 0 & 0 \\ 0 & r_b & 0 & 0 & 0 & 0 & 0 \\ 0 & 0 & r_c & 0 & 0 & 0 & 0 \\ 0 & 0 & 0 & r_F & 0 & 0 & 0 \\ 0 & 0 & 0 & 0 & r_D & 0 & 0 \\ 0 & 0 & 0 & 0 & 0 & r_G & 0 \\ 0 & 0 & 0 & 0 & 0 & 0 & r_Q \end{bmatrix} \begin{bmatrix} i_a \\ i_b \\ i_c \\ i_F \\ i_D \\ i_G \\ i_Q \end{bmatrix} - \begin{bmatrix} \dot{\lambda}_a \\ \dot{\lambda}_b \\ \dot{\lambda}_c \\ \dot{\lambda}_F \\ \dot{\lambda}_D \\ \dot{\lambda}_G \\ \dot{\lambda}_Q \end{bmatrix} + \begin{bmatrix} v_n \\ v_n \\ v_n \\ 0 \\ 0 \\ 0 \\ 0 \end{bmatrix} \tag{2.2}$$

Equation (2.2) is transformed into a 0*dq* frame of reference through a Park's transformation. The system of equations is converted into its per unit form and the following relations are used to simplify the model,

$$\begin{aligned} L_d &= L_{AD} + \ell_d \\ L_F &= L_{AD} + \ell_F \\ L_D &= L_{AD} + \ell_D \\ L_q &= L_{AD} + \ell_q \\ L_G &= L_{AD} + \ell_G \\ L_Q &= L_{AD} + \ell_Q \\ kM_F &= kM_D = M_X = L_{AD} \\ kM_G &= kM_Q = M_Y = L_{AQ} \end{aligned}$$

The resulting synchronous generator model that is used for the parameter estimation is thus given by,

$$\begin{bmatrix} v_0 \\ v_d \\ v_q \\ -v_F \\ -v_D \\ -v_G \\ -v_Q \end{bmatrix} = -\begin{bmatrix} r+3r_n & 0 & 0 & 0 & 0 & 0 & 0 \\ 0 & r & \omega(L_{AQ}+\ell_q) & 0 & 0 & \omega L_{AQ} & \omega L_{AQ} \\ 0 & -\omega(L_{AD}+\ell_d) & r & -\omega L_{AD} & -\omega L_{AD} & 0 & 0 \\ 0 & 0 & 0 & r_F & 0 & 0 & 0 \\ 0 & 0 & 0 & 0 & r_D & 0 & 0 \\ 0 & 0 & 0 & 0 & 0 & r_G & 0 \\ 0 & 0 & 0 & 0 & 0 & 0 & r_Q \end{bmatrix} \begin{bmatrix} i_0 \\ i_d \\ i_q \\ i_F \\ i_D \\ i_G \\ i_Q \end{bmatrix}$$
$$-\frac{1}{\omega_B}\cdot \begin{bmatrix} L_0+3L_n & 0 & 0 & 0 & 0 & 0 & 0 \\ 0 & L_{AD}+\ell_d & 0 & L_{AD} & L_{AD} & 0 & 0 \\ 0 & 0 & L_{AQ}+\ell_q & 0 & 0 & L_{AQ} & L_{AQ} \\ 0 & L_{AD} & 0 & L_{AD}+\ell_F & L_{AD} & 0 & 0 \\ 0 & L_{AD} & 0 & L_{AD} & L_{AD}+\ell_D & 0 & 0 \\ 0 & 0 & L_{AQ} & 0 & 0 & L_{AQ}+\ell_G & L_{AQ} \\ 0 & 0 & L_{AQ} & 0 & 0 & L_{AQ} & L_{AQ}+\ell_Q \end{bmatrix} \begin{bmatrix} \dot{i}_0 \\ \dot{i}_d \\ \dot{i}_q \\ \dot{i}_F \\ \dot{i}_D \\ \dot{i}_G \\ \dot{i}_Q \end{bmatrix} \qquad (2.3)$$

where all quantities are in per unit except ω_B which is in rad/s and time which appears in the derivative terms in seconds.

All parameters in the coefficient matrices in (2.3) are constant. Furthermore, since the rotor speed is nearly constant if small time periods are studied, (2.3) can be considered as a linear time invariant differential equation.

2.3 Development of an Observer for the Damper Winding Currents

Usually, available data for synchronous generators are the stator phase currents and voltages at the terminals of the machine, and the field voltage and current. In order to formulate the parameter estimation problem, it is necessary to have measurements for the damper currents i_D, i_G, and i_Q. Since it is not possible to measure the damper currents directly using physical instruments, even in the case that the damper windings are not fictitious, it is necessary to estimate the damper currents by means of an *observer* prior to the implementation of the state estimator for the generator parameters.

The general concept of an observer is as follows: certain states of a physical system may be difficult to measure or calculate. These unobserved states may nonetheless be needed to calculate an estimate of the machine parameters. An 'observer' is a dynamic system that is constructed so that the unobserved states may be estimated. The observer is adaptive: parameters of the observer are adjusted methodically so that the output of the machine simulation agrees with the actual measured machine output. Fig. 2.2 shows the concept of an observer.

For the construction of the observer, the last three equations of the synchronous generator model in (2.3) can be rearranged so as to obtain expressions for the damper winding currents. The three equations are given by,

$$-v_D = 0 = -r_D i_D - \frac{1}{\omega_B} L_{AD} i'_d - \frac{1}{\omega_B} L_{AD} i'_F - \frac{1}{\omega_B} (L_{AD} + \ell_D) i'_D \tag{2.4}$$

$$-v_G = 0 = -r_G i_G - \frac{1}{\omega_B} L_{AQ} i'_q - \frac{1}{\omega_B} (L_{AQ} + \ell_G) i'_G - \frac{1}{\omega_B} L_{AQ} i'_Q \tag{2.5}$$

$$-v_Q = 0 = -r_Q i_Q - \frac{1}{\omega_B} L_{AQ} i'_q - \frac{1}{\omega_B} L_{AQ} i'_G - \frac{1}{\omega_B} (L_{AQ} + \ell_Q) i'_Q \tag{2.6}$$

where for the purposes of the development of the observer the current derivatives are replaced by the forward difference formula,

$$i'(t) \approx \frac{i(t + \Delta t) - i(t)}{\Delta t} \,. \tag{2.7}$$

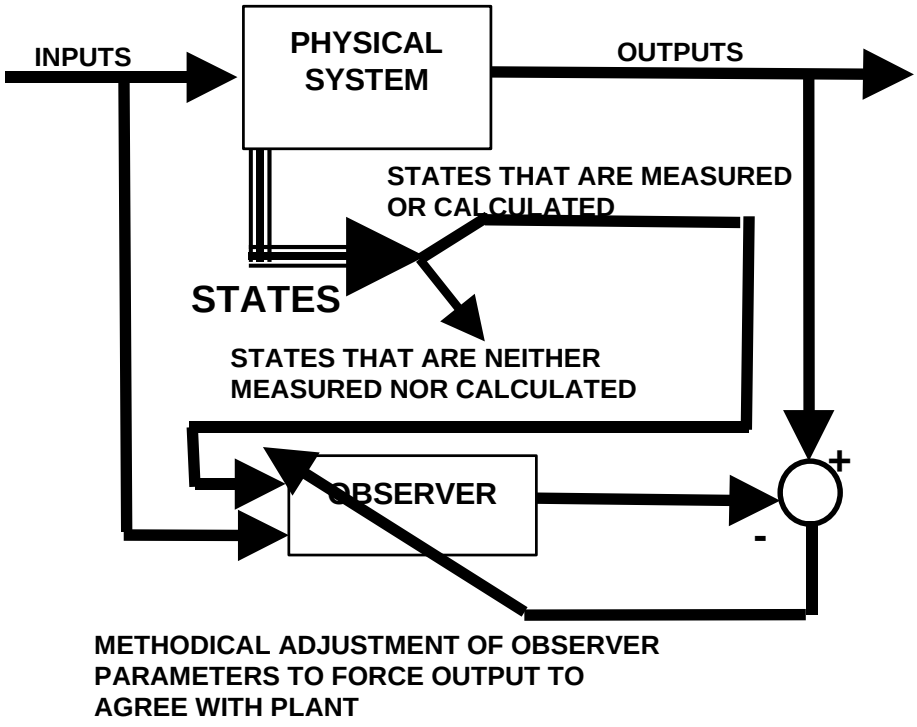

Fig. 2.2 Concept of an observer for a dynamic system

Solving (2.4) for i_D, an expression can be obtained in terms of known measurements and the value of i_D at the previous step.

$$i_D(n+1) = (1 - \frac{r_D \omega_B \Delta t}{L_{AD} + \ell_D}) i_D(n) - \frac{L_{AD} \Delta t}{L_{AD} + \ell_D} (i'_d(n) + i'_F(n)) \tag{2.8}$$

The quadrature axis damper winding currents i_G and i_Q can be obtained by the simultaneous solution of (2.5) and (2.6) and are given by,

$$i_G(n+1) = \left[1 - \frac{(L_{AQ} + \ell_Q) r_G \omega_B \Delta t}{k_{AQ}}\right] i_G(n) + \left[\frac{L_{AQ} r_Q \omega_B \Delta t}{k_{AQ}}\right] i_Q(n) + \frac{L_{AQ} \Delta t}{(L_{AQ} + \ell_G)} \left[\frac{L_{AQ} \ell_G}{k_{AQ}} - 1\right] i'_q(n) \tag{2.9}$$

$$i_Q(n+1) = \left[1 - \frac{(L_{AQ} + \ell_G) r_Q \omega_B \Delta t}{k_{AQ}}\right] i_Q(n) + \left[\frac{L_{AQ} r_G \omega_B \Delta t}{k_{AQ}}\right] i_G(n) - \left[\frac{L_{AQ} \ell_G \Delta t}{k_{AQ}}\right] i'_q(n), \tag{2.10}$$

where

$$k_{AQ} = (L_{AQ} + \ell_Q)(L_{AQ} + \ell_G) - L_{AQ}^2 .$$

Equations (2.8-2.10) enable the calculation of the damper currents. All parameters can be accurately calculated using manufacturer's data, while the time varying quantities are available measurements. The only ambiguity in the observer equations is the value of $i_D(0)$, $i_G(0)$, and $i_Q(0)$. These are needed to initiate the observation process. Nevertheless, the initial conditions can be assumed to be zero without loss of accuracy as will be shown in the two case studies in the next section.

2.4 Case Studies Using a Damper Winding Currents Observer

The foregoing concept of parameter estimation was tested in two ways: in simulated models; and utilizing actual generator measurements and manufacturer's data. The simulation approach is considered first.

A synchronous generator was simulated using the Electromagnetic Transients Program (EMTP) both in the steady state and in transient mode. EMTP is suitable for testing the estimation algorithm because data from the simulation are free of noise, and one has access to all machine parameters and signals. Furthermore, EMTP provides the simulated damper currents in the direct and quadrature axes. Therefore, a means of testing the observer is provided.

The machine under consideration is a cross-compound generator located in the southwest U.S.A. The generator contains a high pressure unit rated at 483 MVA and a low pressure unit rated at 426 MVA. Table 2.1 shows the parameters for the high pressure generator as calculated by manufacturer's data. These parameters are used in the EMTP program to obtain the required measurements. This example is chosen because subsequently, a real-life example of the same machine, with measurements taken by a digital fault recorder (DFR) will be used. At this point it suffices to state that the measurements re-

quired are the three phase stator voltages and currents, and the DC field voltage and current. The measurements are assumed to be error free for the simulation tests.

In the first case study, the machine is operating nearly in steady state. The damper winding currents are observed according to the observer equations (2.8)-(2.10) with the initial conditions assumed to be zero. All estimated damper currents match the simulated damper currents and are equal to zero to five decimal places, as expected from a synchronous generator that operates in steady state.

The error between the estimated and simulated currents can be calculated using the formula,

$$\%error = \frac{\left\| i_{simulated} - i_{observed} \right\|_2}{\left\| i_{simulated} \right\|_2} \times 100 ,$$

Table 2.1 Synchronous generator parameters:
483 MVA machine used in both synthetic and actual on-site tests

Parameter	Value (p.u.)	Parameter name
R	0.0046	Stator phase resistance
L_d	1.80	Equivalent direct axis reactance
L_q	1.72	Equivalent quadrature axis reactance
M_F	1.339054	Stator to field mutual inductance
M_D	1.339054	Stator to damper *D* mutual inductance
M_X	1.64	Rotor mutual inductance in the *d* axis circuit
r_F	9.722×10^{-4}	Equivalent field resistance
r_D	0.0125	Equivalent resistance of damper winding *D*
L_F	1.75791	Field winding self inductance
L_D	1.68125	Self inductance of damper winding *D*
M_G	1.2737	Stator to damper *G* mutual inductance
M_Q	1.2737	Stator to damper *Q* mutual inductance
M_Y	1.56	Rotor mutual inductance in the *q* axis circuit
r_G	0.01071	Equivalent resistance of damper winding *G*
r_Q	0.01632	Equivalent resistance of damper winding *Q*
L_G	1.978537	Self inductance of damper winding *G*
L_Q	1.593	Self inductance of damper winding *Q*
L_0	0.15	Equivalent zero sequence inductance
r_n	100	Equivalent neutral resistance
L_n	100	Equivalent neutral inductance

where $\|\cdot\|_2$ denotes the 2-norm (square root of the sum of the squares of all the elements). The errors in the three damper winding currents i_D, i_G, and i_Q for the steady state data case are 0.16%, 0.28% and 0.14% respectively.

In the second simulated case study, transient data were considered. A permanent line to line fault was applied at 0.25 seconds between phases *b* and *c*. The observed damper currents as compared to the EMTP simulated damper currents for each axis can be seen in Figs. 2.3, 2.4, and 2.5. As can be seen from the graphs, the estimated damper currents match the simulated damper currents. The percent errors between the simulated and estimated damper currents can be calculated in the same way as in the steady state case. The errors in the three damper winding currents i_D, i_G and i_Q for the transient data case are 0.03%, 0.63% and 0.16% respectively. Since the difference between the simulated and estimated signals is not discernible in Figs. 2.3, 2.4, and 2.5, a portion of i_Q as shown in Fig. 2.5 was magnified to visualize the difference between the two signals. This difference is shown in Fig. 2.6.

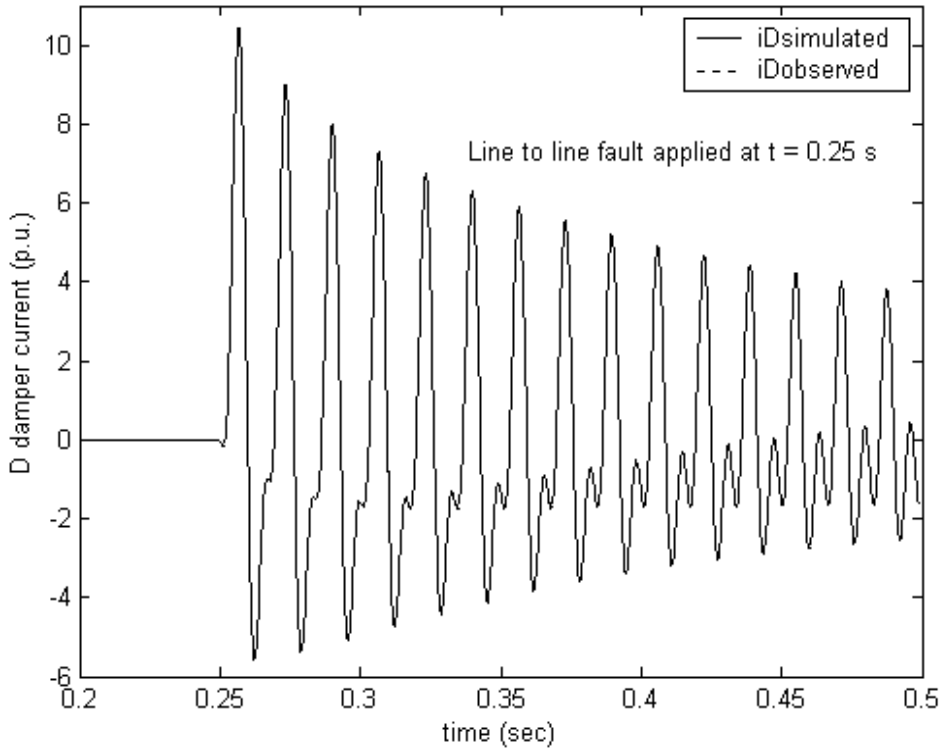

Fig. 2.3 Simulated and estimated damper current i_D using transient data

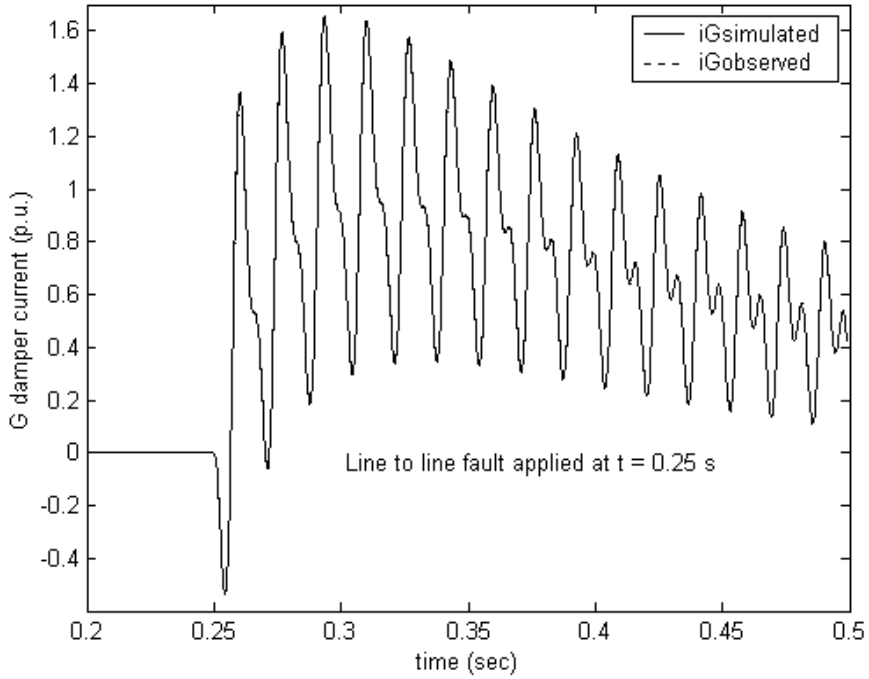

Fig. 2.4 Simulated and estimated damper current iG using transient data

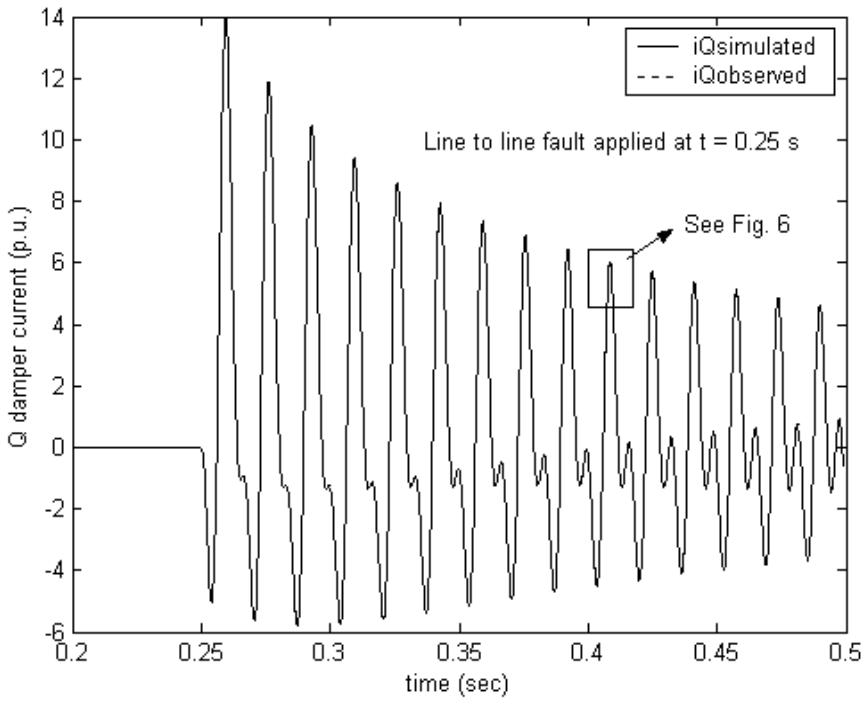

Fig. 2.5 Simulated and estimated damper current i_Q using transient data

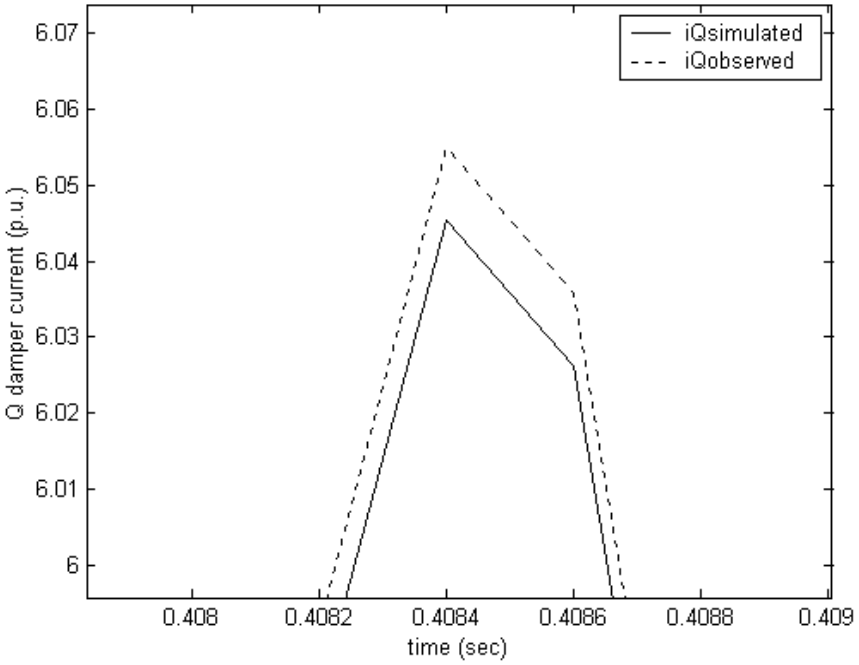

Fig. 2.6 Magnification of portion of i_Q to demonstrate the difference between the simulated and observed signals

2.5 Configuration of the State Estimator

State estimation is a process during which a number of unknown system state variables or parameters are assigned a value based on measurements from that system. Typically, the number of measurements (or number of equations) is much greater than the parameters to be estimated. In this case the system is overdetermined and the solution is found in a least squares sense. That is, the sum of the squares of the differences between the estimated and the measured parameters is minimized.

Since the last three equations of (2.9) have been used for the development of the observer, the remaining four equations of (2.9) are rearranged into the form $Hx = z$ to obtain the estimated parameters by $\hat{x} = H^{+} z$, where H^{+} is the pseudoinverse of H. Matrix H (the *process matrix*) is of dimension $m \times n$ and contains the coefficients of the unknowns, which are either obtained by direct measurements of current and voltages, or via the observer in the case of the damper currents, or via calculation in the case of the derivatives. The formula for the derivatives is the forward difference formula (2.11). The vector z has dimension m and it contains known parameters, or measurements or a combination of the two. Fig. 2.7 illustrates in block diagram form the idea of the observer, the data manipulation and the parameter estimation algorithm.

For example, if parameters L_{AD}, L_{AQ} and r_F are to be estimated, (2.9) can be rearranged in the form $Hx = z$ to obtain,

$$\begin{bmatrix} 0 & 0 & 0 \\ \dfrac{(i'_d + i'_F + i'_D)}{\omega_B} & \omega(i_q + i_G + i_Q) & 0 \\ -\omega(i_d + i_F + i_D) & \dfrac{(i'_q + i'_G + i'_Q)}{\omega_B} & 0 \\ \dfrac{(i'_d + i'_F + i'_D)}{\omega_B} & 0 & i_F \end{bmatrix} \begin{bmatrix} L_{AD} \\ L_{AQ} \\ r_F \end{bmatrix} = -\begin{bmatrix} r+3r_n & 0 & 0 & 0\,0\,0\,0 \\ 0 & r & \omega\ell_q & 0\,0\,0\,0 \\ 0 & -\omega\ell_d & r & 0\,0\,0\,0 \\ 0 & 0 & 0 & 0\,0\,0\,0 \end{bmatrix} \begin{bmatrix} i_0 \\ i_d \\ i_q \\ i_F \\ i_D \\ i_G \\ i_Q \end{bmatrix}$$

$$-\frac{1}{\omega_B} \cdot \begin{bmatrix} L_0+3L_n & 0 & 0 & 0 & 0\,0\,0 \\ 0 & \ell_d & 0 & 0 & 0\,0\,0 \\ 0 & 0 & \ell_q & 0 & 0\,0\,0 \\ 0 & 0 & 0 & \ell_F & 0\,0\,0 \end{bmatrix} \begin{bmatrix} \dot{i}_0 \\ \dot{i}_d \\ \dot{i}_q \\ \dot{i}_F \\ \dot{i}_D \\ \dot{i}_G \\ \dot{i}_Q \end{bmatrix} - \begin{bmatrix} v_0 \\ v_d \\ v_q \\ -v_F \\ -v_D \\ -v_G \\ -v_Q \end{bmatrix}$$

In this way, the three unknown parameters and their coefficients are isolated on the left hand side, and all elements of the right hand side are known. Moreover, the right hand side reduces to a vector and therefore the system takes the final form $Hx = z$.
The linear system $Hx = z$ represents multiple time steps. Each measurement results in an equation of the form $Hx = z$. At each subsequent time step, the new data are augmented to the existing H matrix and z vector to create an overdetermined system.

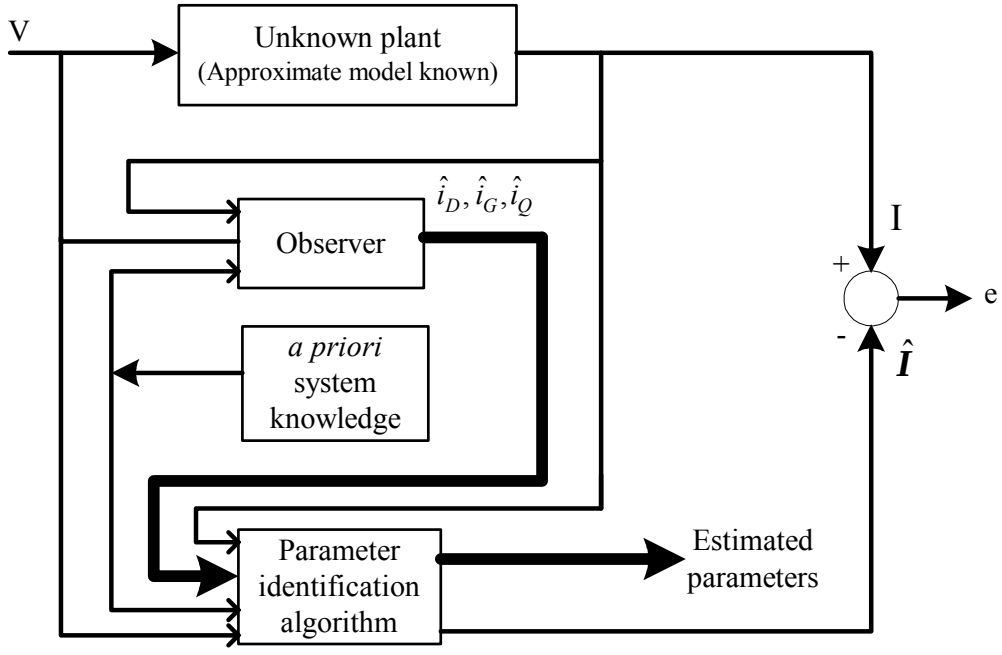

Fig. 2.7 Block diagram for observer implementation and parameter identification algorithm

2.6 Bad Data Detection, Rejection and Filtering

Real data have errors resulting mainly from meter and communication errors, incomplete metering, or inaccuracy of metering equipment. Therefore, prior to any estimation it is necessary to perform bad data detection and rejection, and filtering of the noise.

In the field circuit, the main frequency components of interest are at or near DC. On the other hand, in the stator measurements it is possible to perform filtering in the AC measurements (50-60 Hz range), or in the 0*dq* transformed signals (at or near DC). In the synchronous machine parameter estimation application, it was found that the stator measurements are most effectively filtered after the 0*dq* transformation. Fig. 2.8 shows the filtering and bad data detection/rejection configuration.

After the transformation of the *abc* voltages and currents into 0*dq* signals through Park's transformation, a filter is applied to remove outliers from the measurements. Such outliers appear in the form of spikes, in the time domain plot of each signal. They are caused by metering errors and can be safely removed without risking inaccuracies in the estimation process. If a spike in any one signal is detected, then the whole measurement at that time is removed from the data set.

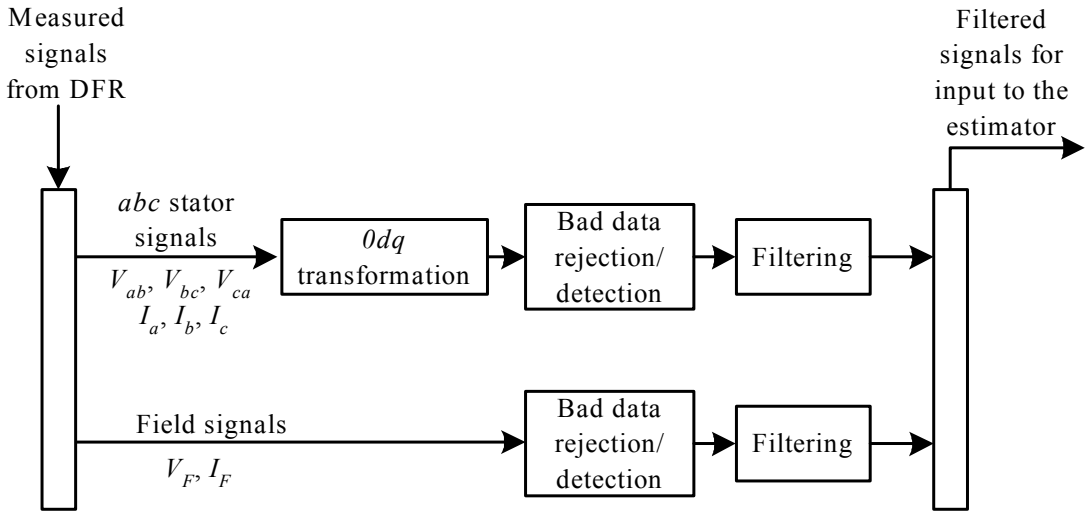

Fig. 2.8 Filtering and bad data detection/rejection configuration

A second filter was implemented for the removal of random noise. Frequency domain plots of the measured signals indicate the existence of noise in a wide range of frequencies from the main frequency component up to the Nyquist frequency. This noise is detrimental to the estimation process, especially in the calculation of derivatives. A small random noise content in consecutive measurements is amplified when divided by the time step between the measurements (Δt is in the order of 0.1 ms). A Butterworth filter is used to implement the filtering. Butterworth filters are characterized by a magnitude response

that is maximally flat in the passband and is characterized by monotonicity in the passband and stopband regions.

To compensate for the shallower rolloff characteristic of a Butterworth filter, the data are filtered successively by passing them through the same filter until the frequency components that are due to noise are minimized. Filter characteristics are chosen depending on the location and on the size of the noisy frequency components, but in general, the filters for all the signals have a cutoff frequency of approximately 10 Hz and a stopband frequency of 100 Hz with a stopband attenuation of about 60-80 dB. Fig. 2.9 depicts the direct axis voltage component in the time domain as calculated from measurements obtained at the generator terminals, while Fig. 2.10 shows the filtered signal after applying a spike filter and multiple Butterworth filters.

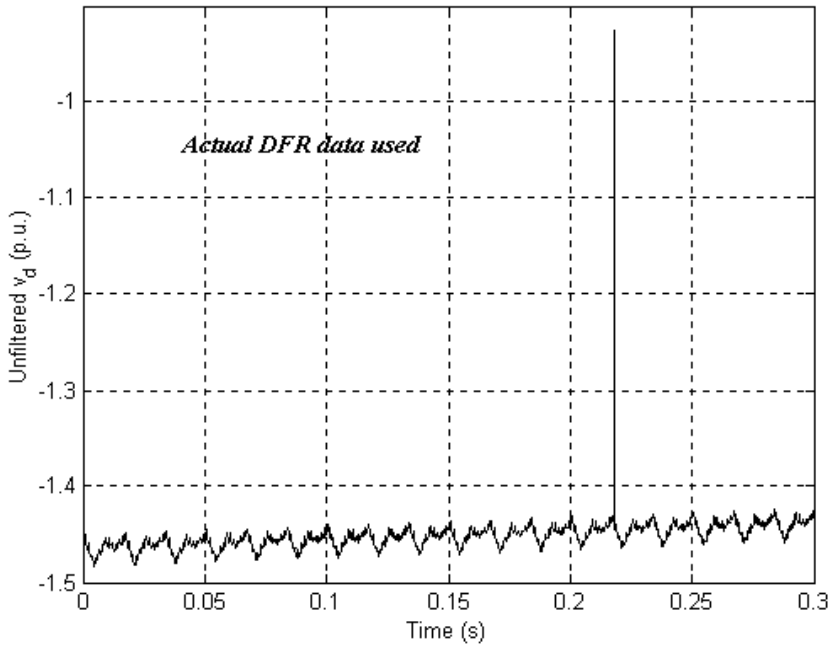

Fig. 2.9 Unfiltered direct axis voltage in the time domain

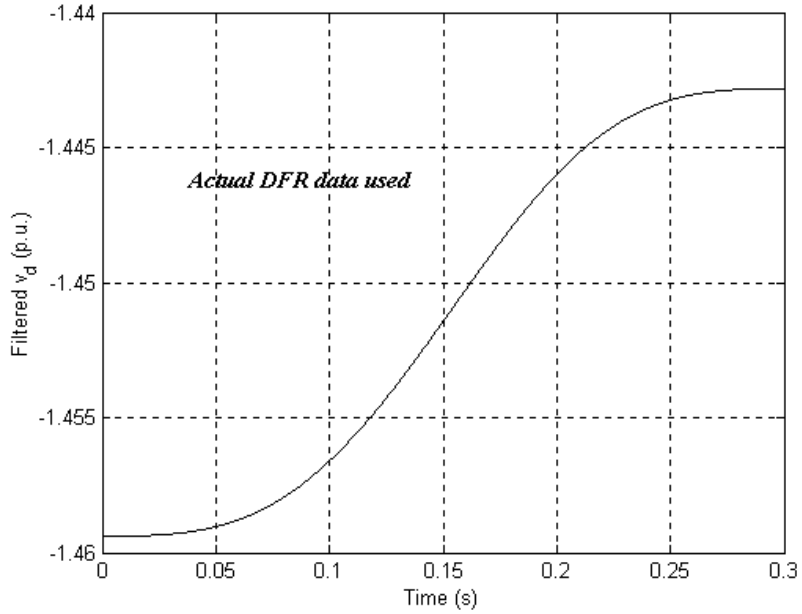

Fig. 2.10 Filtered direct axis voltage in the time domain

2.7 Magnetic Saturation

In order to represent saturation in stability studies several assumptions are made. The reason for this is that a rigorous treatment of synchronous machine performance including saturation is a futile exercise. Hence, one typically looks for a practical method for dealing with saturation effects based on semi-heuristic reasoning, carefully chosen approximations, simplicity of model structure, data availability, and accuracy of results.
The elementary approaches to including saturation are documented in [30. In this approach several simplifying assumptions are made in determining saturation. The effects of saturation are represented as,

$$L_{AD} = K_{sd} L_{ADu}$$

$$L_{AQ} = K_{sq} L_{AQu}$$

where L_{ADu} and L_{AQu} are unsaturated values of L_{AD} and L_{AQ}. The saturation factors K_{sd} and K_{sq} identify the degrees of saturation in the direct and quadrature axis, respectively. The saturation factors are less than 1.000 The *d*-axis saturation is determined from the open circuit characteristic. Typically the saturation curve is divided into three segments, which are defined by threshold values of the flux linkage λ. Suitable approximations for the behavior of λ are made based on the operating segment and thus, appropriated expressions for K_{sd} are derived. It is commonly assumed that for salient pole machines, since the path for the *q*-axis flux is largely in air, L_{AQ} does not vary significantly with saturation of the iron portion of the path. Hence, typically the saturation factor K_{sq} is assumed to be equal to 1.0 for all loading conditions.

In the case of round rotor machines, magnetic saturation should be accounted for in both axes. In general the saturation factor K_{sq} can be determined from the no-load saturation characteristic of the q-axis. However, q-axis saturation data are typically not available. As a result one normally makes the assumption that K_{sq} is equal to K_{sd}. This essentially assumes that the reluctance of the magnetic path is homogeneous around the periphery of the rotor.

An approach to improved saturation modeling using q-axis saturation characteristics derived from finite-element analysis is shown in [70] and discussed in [69]. Kundur [20] shows a method to calculate the saturation function. In the parameter estimation method shown in the present paper, L_{AD} and L_{AQ} (as well as other parameters) are estimated for a given set of operating data. Estimation of parameters using data from an actual synchronous generator operating at different load levels, indicates that inductances L_{AD} and L_{AQ} are the inductances that are most affected by saturation and these quantities vary considerably.

2.8 Brushless exciters

Many modern synchronous generators utilize brushless excitation. In this configuration, the field current is delivered to the rotor by induction. The AC in the field winding is then rectified on the rotor. There are no slip rings or brushes in this configuration.

Unfortunately, in the brushless configuration, there is no possibility of the direct measurement of the DC field current. And the nature of the waveshape and controls depends heavily on the type of exciter circuit used. In many cases, the exact exciter model is unknown and / or proprietary.

Power system small signal, transient, and dynamic stability studies are only as accurate as the underlying models used in the computer analysis. The validity of the results of these studies depends heavily on the accuracy of the model parameters of the system components. In practice, the parameters commonly used in stability studies are manufacturer specified values, or “typical” values. These typical values may be grossly inaccurate, as various parameters may drift over time or with operating condition. Thus, it is desirable to develop methods for estimating component parameters.

Accurate models of excitation systems are essential to transient simulation, which is a key part in power system planning and operation. Transient simulation is also used to analyze, explain and prevent the outage of the power system. One of the popular software packages is ETMSP (Extended Transient/Mid Term Stability Program) by EPRI. In order to obtain a reliable transient simulation, it is necessary to have accurate models and parameters of excitation systems, synchronous machines and other control systems such as a speed-governor system.

While parameter estimation of synchronous machines has been well documented, parameter estimation of excitation systems has only begun to receive thorough attention. The objective of this study is to establish a procedure to perform parameter estimation of

an AC1A type excitation system using least squares method. The details are shown in Appendix F. Unfortunately, very limited success was obtained in the brushless exciter case, and it is not known whether machine parameters may be calculated by the methods given in this report for the brushless case.

3 Estimation of Machine Parameters and Testing of the Algorithm

3.1 Description of a Testing Regimen

The parameter estimation algorithm was tested using real data collected from the terminals of a committed synchronous generator. The machine under consideration is the cross-compound generator described in Section 3.2. Measurements were collected using a digital fault recorder (DFR). The data were collected at steady state operation, while the machine served its load. The sampling frequency was 10 kHz and eight signals were measured: stator line currents and voltages (I_a, I_b, I_c, V_{ab}, V_{bc}, V_{ca}), and field current and voltage (I_F, V_F). Sample results are shown in Section 3.3.

3.2 Description of Tests

Implementation of any proposed algorithm using actual measurements is the ultimate test for its viability and applicability to the system under study. After the successful testing of the parameter estimation algorithm using both synthetic and EMTP data as demonstrated in [69], it is necessary to test the estimator using data obtained from synchronous generators and observe whether the proposed method agrees to the practical results.

Synchronous generator measurements for the purpose of this research work are obtained through a digital fault recorder (DFR). A DFR is effectively a data acquisition system that is used to monitor the performance of generation and transmission equipment, and therefore is connected permanently to utility generators. DFRs are typically used by the majority of the utilities to monitor the operation of generators. For this particular estimation methodology, the measurements are obtained at the terminals of committed synchronous generators (the units serve their typical loads). Different operating levels are considered to examine the accuracy of the proposed method with varying degrees of excitation and different saturation levels. The measurements are stored in a data file that can be read by the estimator. The data files are typically of the COMTRADE data file format, which is an approved IEEE data format for storage of measurements. The data can either be in ASCII format or binary format.

In between the data acquisition and the estimator implementation there are a number of other processes that need to be performed to prepare the data in a form that can be used by the estimator. Fig. 3.1 shows a flowchart of the procedure followed to perform the parameter estimation. The measurements obtained for the stator voltages are sometimes line to line measurements, and therefore it may be necessary to transform these signals into phase quantities. Further, the power angle δ needs to be calculated in order to perform the Park's transformation as explained in Chapter 2 and Appendices D - E. The above transformations and the procedure is illustrated in Fig. 3.1.

3.3 Results of Parameter Estimation from Actual Measurements

In contrast to the simulated data set, an examination of the actual data sets obtained from the synchronous generator terminals and used for the parameter estimation described in this section, indicates that the generators operate within the saturation region. Therefore, the estimator algorithm needs to adjust the parameters for saturation as explained in Chapter 2. The parameters obtained from the estimator reflect the true state of the system including saturation.

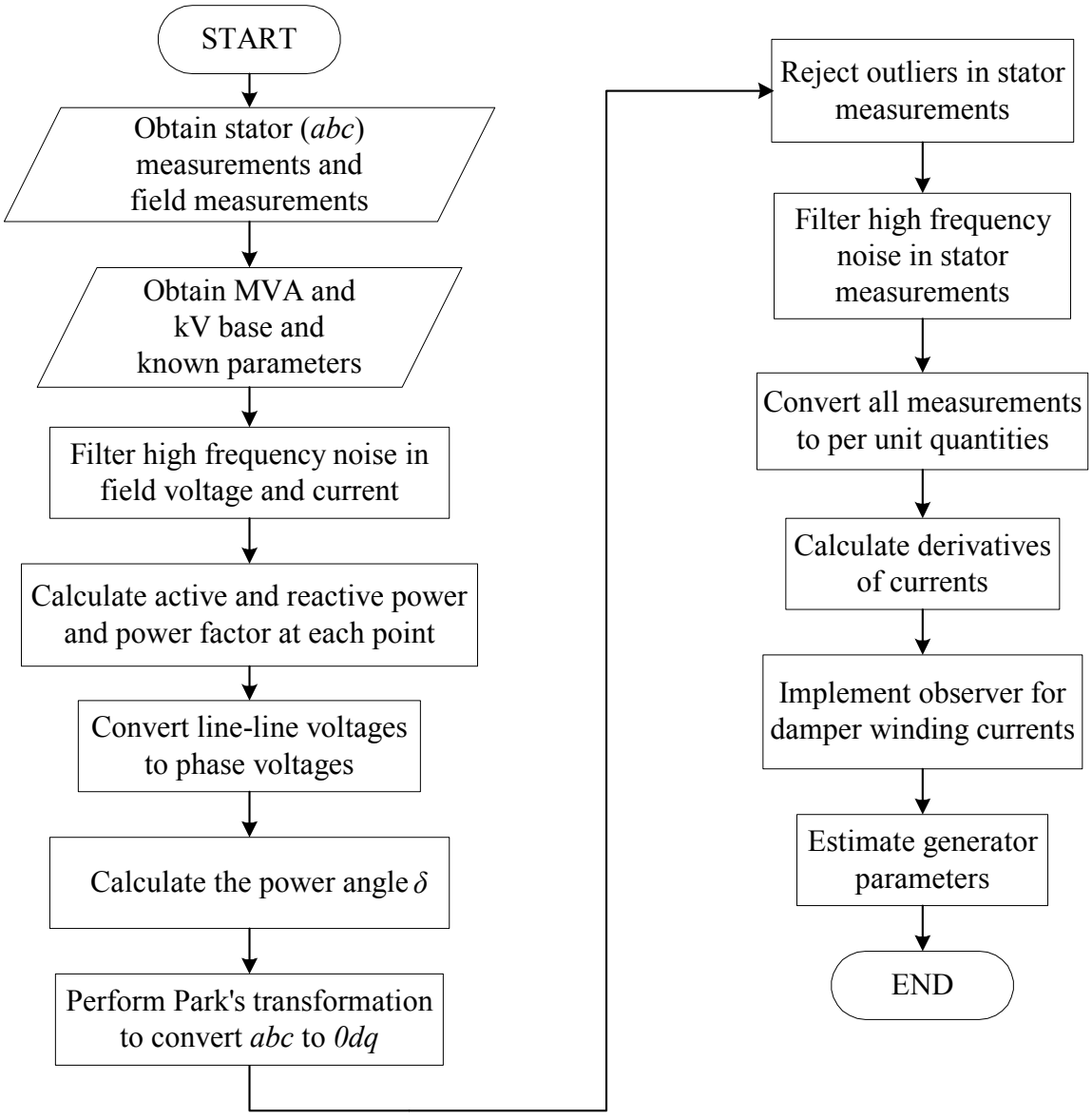

Fig. 3.1 Algorithm for estimator implementation for actual measurements

Table 3.1 depicts the estimated parameters in each of the three proposed models using actual measurements from generator FC5HP (case study R-NC-01-10). All parameters are individually estimated assuming that all other parameters are known. In the case of model 2.2x, L_{AD} and L_{AQ} are the only parameters affected by saturation since all other inductances have been expressed in terms of these mutual inductances. In the case of models 2.1 and 2.2 a number of parameters is affected by saturation and these parameters are adjusted prior to the estimation procedure if they are not desired to be estimated. Therefore, Table 3.1 depicts the saturated values of the parameters (where applicable).

Table 3.1 Estimated parameters for the three proposed models for generator FC5HP (case study R-NC-01-10)

Parameter (p.u.)	Model 2.1	Model 2.2	Model 2.2x
L_d	1.6146	1.6147	N/A
L_q	1.5648	1.5794	N/A
L_F	1.49493	1.49493	N/A
kM_F	1.5355	1.5355	N/A
L_{AD}	N/A	N/A	1.5963
L_{AQ}	N/A	N/A	1.4057
R	-0.0061185	-0.01273	-0.01273
r_F	$8.386x10^{-4}$	$8.386x10^{-4}$	$8.386x10^{-4}$

As mentioned above, the estimated inductances of Table 3.1 potentially reflect the true state of the system including the effect of saturation. Since the exact values of the parameters at every operating point are not known, it is not possible to derive any definite conclusions about the accuracy of the estimated parameters. Therefore, it is desired to nullify the effect of saturation by applying the inverse of the appropriate saturation factor to each of the saturated inductances. This will offer estimates of the unsaturated inductances and a comparison to the manufacturer values may be obtained. However, the manufacturer values of the parameters have been calculated by off-line tests and testing methods that may not necessarily reflect the operating point under consideration. Moreover, manufacturer values are typically design values for a series of manufactured generators, and consequently differences between designed and actual parameter values do exist. Therefore, the percent difference between the estimated parameters and the manufacturer parameters cannot be classified as a percent error as in the case of the simulated measurements. The difference between the estimates and their "nominal" values is re-

ferred to as a percent deviation. The percent deviation cannot be used as a verification or rejection of the proposed method, but it can offer an insight as to whether the estimates obtained are reasonable or not. In general, it is more important to have consistency in the estimated parameters between various data sets from the same generator, than to have results with varying degrees of accuracy.

Table 3.2 depicts the percent deviation of the estimated parameters from the manufacturer suggested values for the parameters, after the effect of saturation has been nullified to obtain an estimate of the unsaturated values of the inductances. All three models are considered to enable comparison of the estimation method between all the candidate models.

Table 3.2 Calculation of unsaturated parameters from the estimated parameters of generator FC5HP
(case study R-NC-01-10)

		Model 2.1		Model 2.2		Model 2.2x	
Parameter	Manufacturer value (p.u.)	Estimated parameter (p.u.)	% Deviation	Estimated parameter (p.u.)	% Deviation	Estimated parameter (p.u.)	% Deviation
L_d	1.80	1.757	2.4	1.757	2.4	N/A	N/A
L_q	1.72	1.702	1.0	1.724	0.2	N/A	N/A
L_F	1.75791	1.627	7.4	1.627	7.4	N/A	N/A
kM_F	1.64	1.671	1.9	1.671	1.9	N/A	N/A
L_{AD}	1.64	N/A	N/A	N/A	N/A	1.737	5.9
L_{AQ}	1.56	N/A	N/A	N/A	N/A	1.529	2.0
R	0.0046	-0.00612	233	-0.01273	377	-0.01273	377
r_F	$8.454x10^{-4}$	$8.386x10^{-4}$	0.8	$8.386x10^{-4}$	0.8	$8.386x10^{-4}$	0.8

Table 3.2 shows that the results obtained from all three models are similar. Results from models 2.2 and 2.2x are slightly improved due to the more accurate modeling of the quadrature axis. A discussion for some of the results from the three models is appropriate at this point. The field resistance is estimated with a deviation of 0.8% in all three models. Estimation of the field resistance is a critical aspect of the overall estimation procedure since one of the motivations for this research work is the tracking of the change in

the field resistance to detect and prevent short circuits in the field winding. The nominal field winding resistance noted as the manufacturer value in Table 8.2 is an approximate quantity since the generator under consideration has been rewound a number of times because of short circuits in the field winding. Therefore, no definite comparison can be performed between the estimated and the nominal value. Nevertheless, the estimation procedure gains considerable confidence from these results since the deviation between the two values is very small.

Values for L_d, L_q, and kM_F are estimated within a reasonable accuracy in both models 2.1 and 2.2, with L_q being estimated more accurately in model 2.2. The percent deviations for these parameters vary from 0.2 to 2.4%. In the case of the field inductance L_F, the percent deviation attained is in the order of 7.4%. This result is not considered satisfactory, but similarly to the case of the field resistance, the nominal value of L_F may not be accurate because of the rewinding of the field winding of this particular generator.
In the case of model 2.2x, L_{AQ} is estimated with a deviation of 2.0% from its nominal value, while L_{AD} is estimated with a deviation of 5.9%. A portion of the deviation of L_{AD} can be attributed to the field inductance L_F, since in model 2.2x the field inductance was expressed as $L_F = L_{AD} + l_F$, where l_F is the leakage inductance of the field winding. Therefore, the estimated L_{AD} will reflect any possible inaccuracy of l_F because of the rewinding of the field winding.

Finally, the results for the stator resistance in all three models show that currently the stator resistance cannot be estimated accurately. The amount of noise in the measurements and the representation of saturation are two of the reasons for the inaccuracy in the stator resistance. A number of case studies were performed to observe how using different saturation factors and various filtering mechanisms affect the stator resistance. For example, if no saturation is modeled, then the estimated stator resistance was positive and much higher than the manufacturer value of r. As saturation factors of increasing values were introduced to adjust L_{AD} and L_{AQ}, the value of the stator resistance reduced and in some cases the estimated value was negative as in the case of Table 3.2. The inability to estimate r within a satisfactory degree of accuracy is not an obstacle to this method of estimation. Typically, there is no interest in estimating r. The main parameters of interest are L_d, L_q (or L_{AD} and L_{AQ}), and r_F.

3.4 Multiple Parameter Estimation

Multiple parameter estimation from actual measurements is an important aspect of the estimator. In many cases (like the one under consideration in this research work) it is possible that there is uncertainty in more than one parameter. Therefore it is imperative that the feasibility of multiple parameter estimation is investigated. Ideally, it is desired that the percent deviation obtained for each parameter is the same in both individual parameter estimation and multiple parameter estimation.

Two case studies are performed. In the first case study (R-NC-03-11), L_d, L_q, and r_F are estimated simultaneously for models 2.1 and 2.2, while L_{AD}, L_{AQ}, and r_F are estimated simultaneously for model 2.2x. The estimated parameters are depicted in Table 3.3,

while the unsaturated parameters calculated from the estimated parameters are depicted in Table 3.4. It can be observed that for all three models the estimated parameters and their percent deviations are identical to the corresponding parameters in the individual parameter estimation of Table 3.1 and Table 3.2.

Table 3.3 Multiple simultaneous parameter estimation for generator FC5HP
(case study R-NC-03-11)

Parameter (p.u.)	Model 2.1	Model 2.2	Model 2.2x
L_d	1.6146	1.6147	N/A
L_q	1.5648	1.5794	N/A
L_{AD}	N/A	N/A	1.5963
L_{AQ}	N/A	N/A	1.4057
r_F	$8.386x10^{-4}$	$8.386x10^{-4}$	$8.386x10^{-4}$

Table 3.4 Calculation of unsaturated parameters for generator FC5HP
(case study R-NC-03-11)

		Model 2.1		Model 2.2		Model 2.2x	
Parameter	Manufacturer value (p.u.)	Estimated parameter (p.u.)	% Deviation	Estimated parameter (p.u.)	% Deviation	Estimated parameter (p.u.)	% Deviation
L_d	1.80	1.757	2.4	1.757	2.4	N/A	N/A
L_q	1.72	1.702	1.0	1.724	0.3	N/A	N/A
L_{AD}	1.64	N/A	N/A	N/A	N/A	1.737	5.9
L_{AQ}	1.56	N/A	N/A	N/A	N/A	1.529	2.0
r_F	$8.454x10^{-4}$	$8.386x10^{-4}$	0.8	$8.386x10^{-4}$	0.8	$8.386x10^{-4}$	0.8

In the second case study (R-NC-03-12), L_d, L_q, and L_F are estimated simultaneously for models 2.1 and 2.2, while L_{AD}, L_{AQ}, and L_F are estimated simultaneously for model 2.2x. The estimated parameters are depicted in Table 3.5, while the unsaturated parameters cal-

culated from the estimated parameters are depicted in Table 3.6. As in the previous case study, the estimated parameters and their percent deviations are identical to the corresponding parameters in the individual parameter estimation of Table 3.1 and Table 3.2.

Table 3.5 Multiple simultaneous parameter estimation for generator FC5HP
(case study R-NC-03-12)

Parameter	Model 2.1	Model 2.2	Model 2.2x
L_d	1.6146	1.6147	N/A
L_q	1.5648	1.5794	N/A
L_{AD}	N/A	N/A	1.5963
L_{AQ}	N/A	N/A	1.4057
L_F	1.49493	1.49493	N/A

The results of the multiple simultaneous parameter estimation case studies indicate that more than one parameter can be estimated at the same time. It was shown that there is no degradation of the percent deviation of the estimated parameters from their nominal values. Therefore, the confidence for the use of the estimator to estimate multiple parameters simultaneously is reinforced. In case that the confidence in some of the synchronous generator parameters is limited (for example, because of alterations to the generator circuitry), multiple parameter estimation holds the key to a reliable estimation procedure.

3.5 Application of the Algorithm to Different Machines and Operating Points

Sections 3.2 and 3.3 discussed the parameter estimation procedure and some of the results obtained using measurements from generator FC5HP. It is necessary to perform parameter estimation for different generators and at different operating points to ensure that the method is applicable to other generators as well. Using measurements from different generators enables the examination of the accuracy of the proposed method, while the estimation at various operating points for each generator ensures that the results are consistent.

Table 3.6 Calculation of unsaturated parameters for generator FC5HP
(case study R-NC-03-12)

		Model 2.1		Model 2.2		Model 2.2x	
Parameter	Manufacturer value (p.u.)	Estimated parameter (p.u.)	% Deviation	Estimated parameter (p.u.)	% Deviation	Estimated parameter (p.u.)	% Deviation
L_d	1.80	1.757	2.4	1.757	2.1	N/A	N/A
L_q	1.72	1.702	1.0	1.724	0.3	N/A	N/A
L_{AD}	1.64	N/A	N/A	N/A	N/A	1.737	5.9
L_{AQ}	1.56	N/A	N/A	N/A	N/A	1.529	2.0
L_F	1.75791	1.627	7.4	1.627	7.4	N/A	N/A

The case studies described in Sections 3.2 and 3.3 and a number of other case studies that were performed, permit the extraction of some conclusions pertaining to the model used in the estimation procedure. Clearly the estimates obtained from models 2.2 and 2.2x are superior to the ones obtained from model 2.1. This is due to the modeling of one extra damper winding in the quadrature axis of the generator; this winding causes the model to be symmetric with regards to the direct and quadrature axes. Results from models 2.2 and 2.2x are similar considering that the estimates of L_{AD} and L_{AQ} contain the error from the field winding inductance L_F and other quantities such as the mutual inductances between axes in the stator and the rotor (see [69] for a comparison of the two models. A clear advantage of model 2.2x is that it offers an easier way of representing the magnetic saturation in a synchronous generator. Therefore, model 2.2x is the preferred model. The parameter estimation results presented in this section and in Appendix F are obtained through the utilization of model 2.2x.

Table 3.7 shows the parameter estimation results for ten data sets obtained from two identically designed units at the Redhawk generating station of APS. Eight of the data sets are obtained from GT1, while two of the data sets are obtained from GT2. Although the two units may have some differences in their parameters since no two units are exactly identical, the use of more data sets will allow the extraction of useful results pertaining to the accuracy of the method when applied to different generators and the representation of saturation. The two units are gas turbine units rated at 213.7 MVA and 18 kV. Their characteristics are described in Table 3.1.

Table 3.7 Parameter estimation results for Redhawk gas turbines 1 and 2*

Case study	Unit #	$\hat{L}_{AD}$ (p.u.)	$\hat{L}_{AQ}$ (p.u.)	$\hat{r}_F$ (p.u.)	K_{sd}	i_F (A)	P (MW)	Q (MVAr)	$\hat{L}_{ADu}$ (p.u.)	$\hat{L}_{AQu}$ (p.u.)	% deviation L_{AD}	% deviation L_{AQ}
R-NC-03-13	GT1	1.5394	1.6787	$7.008x10^{-4}$	0.9479	1021.7	148.40	13.26	1.624	1.771	8.8	4.7
R-NC-03-14	GT1	1.6073	1.6735	$7.020x10^{-4}$	0.9487	982.72	145.2	10.87	1.694	1.764	4.9	4.3
R-NC-03-15	GT1	1.5998	1.6865	$7.205x10^{-4}$	0.9474	826.96	109.5	1.42	1.688	1.780	5.2	5.2
R-NC-03-16	GT1	1.5882	1.6724	$6.854x10^{-4}$	0.9485	853.08	111.13	5.69	1.674	1.763	6.0	4.2
R-NC-03-17	GT1	1.5748	1.6941	$6.730x10^{-4}$	0.9472	844.43	108.83	4.34	1.663	1.788	6.6	5.7
R-NC-03-18	GT1	1.6009	1.6387	$6.352x10^{-4}$	0.9473	874.65	119.14	4.43	1.690	1.730	4.7	3.6
R-NC-03-19	GT1	1.5682	1.7516	$7.716x10^{-4}$	0.9477	845.12	110.11	4.43	1.651	1.848	7.0	9.2
R-NC-03-20	GT1	1.5607	1.7557	$7.619x10^{-4}$	0.9511	921.00	119.87	15.63	1.641	1.846	7.8	8.3
R-NC-03-21	GT2	1.5795	1.6741	$6.980x10^{-4}$	0.9491	861.96	109.1	9.03	1.664	1.764	6.6	4.3
R-NC-03-22	GT2	1.5891	1.6760	$6.922x10^{-4}$	0.9495	863.21	108.40	10.61	1.674	1.765	6.0	4.3
Mean (μ)				$7.041\ x10^{-4}$					1.6667	1.782		
Standard deviation (σ)				$1.442\ x10^{-9}$					0.0225	0.0375		

* From the manufacturer data sheet: L_{AD} = 1.781 p.u., L_{AQ} = 1.692 p.u., while r_F is unavailable.

Three parameters were estimated from each data set: L_{AD}, L_{AQ}, and r_F. The operating point of the generator for each data set is shown, as well as the field current. The saturation factor for the direct axis is calculated and shown in the table for each case study. It is assumed that the saturation factor is the same in both the direct and quadrature axes.

It is necessary to apply the saturation factor (< 1.000) to the estimated saturated inductances in order to obtain the unsaturated inductances. This will allow comparison to the manufacturer data and enable the assessment of the estimation method. Table 3.7 depicts the estimated unsaturated mutual inductances and their deviation from the manufacturer supplied mutual inductances. It should be noted that the manufacturer inductances L_{AD} and L_{AQ} are 1.781 p.u. and 1.692 p.u. respectively.

It is of practical interest to examine the change of the two mutual inductances with excitation, using both the estimated saturated values as well as the values corrected for saturation to obtain the unsaturated values. Fig. 3.2 shows the change in the estimated direct axis mutual inductance L_{AD} with the field current. A linear regression model is fitted to observe the trend in the estimated inductance over increasing saturation levels. As expected there is a decrease in the apparent value of the inductance as the generator is driven to higher operating points.

Fig. 3.3 compares both the saturated and the unsaturated values of L_{AD} for all case studies. The stacked column graph shows the estimated parameters and the correction for saturation. An overall agreement between the unsaturated values is observed. The unsaturated values of L_{AD} have a mean of 1.6667 p.u. and a standard deviation of 0.0225 p.u. All of the values of the unsaturated L_{AD} agree to one decimal place.

The results of each case study for the quadrature axis mutual inductance L_{AQ} are summarized in Figs. 3.4 and 3.5. The estimated values of the quadrature axis mutual inductance at different operating points are shown in Fig. 3.4. The trend in the saturated value of the inductance is decreasing, although the decrease is not as evident as in the case of L_{AD}. It should be noted that the variation of L_{AQ} is slightly higher than that of L_{AD} since the standard deviation among the unsaturated parameters is 0.0375 p.u. The mean of the unsaturated parameters is 1.782. A comparison between the unsaturated values of L_{AQ} at each operating point is offered in Fig. 3.5, where the saturated inductances are corrected for saturation using the appropriate saturation factors at each operating point. With the exception of two data sets, the unsaturated values of the inductance agree to one decimal place.

Reference [69] presents parameter estimation results for two steam turbine generators located at the Redhawk generating station of APS. A number of case studies are performed and an analysis similar to the analysis of this section is offered.

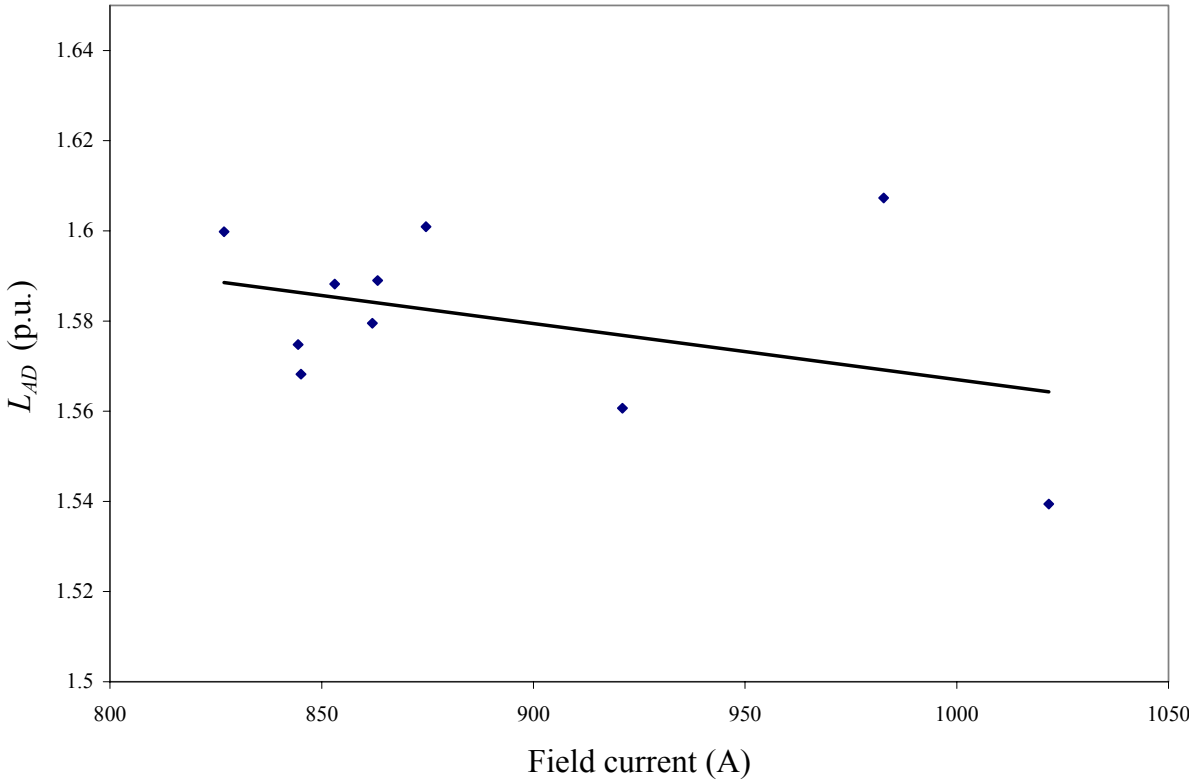

Fig. 3.2 Change of L_{AD} with operating point for Redhawk gas turbine generators

Note that the saturated inductances are smaller than the unsaturated values

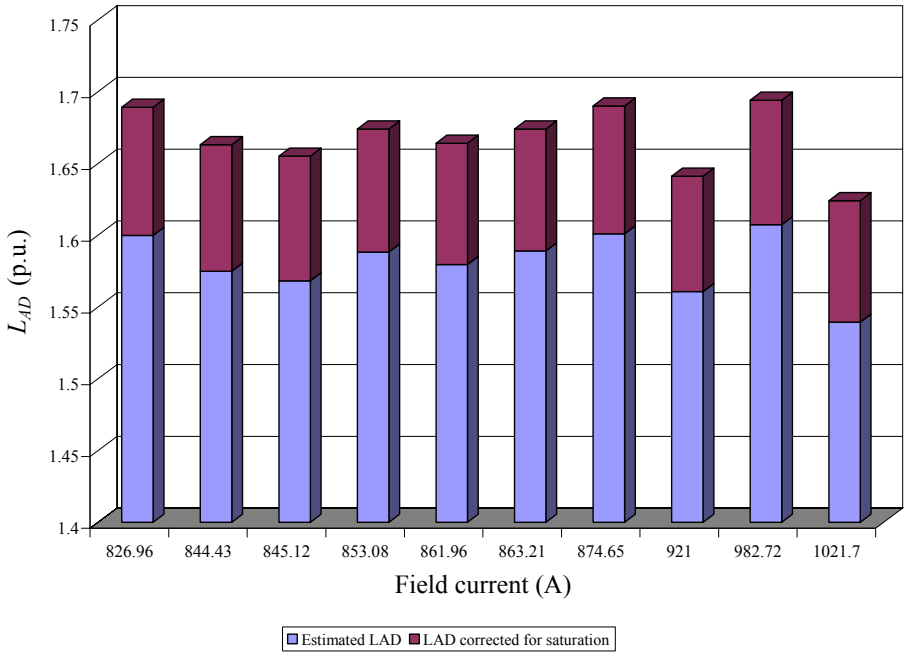

Fig. 3.3 Saturated and unsaturated values of L_{AD} for Redhawk gas turbine generators

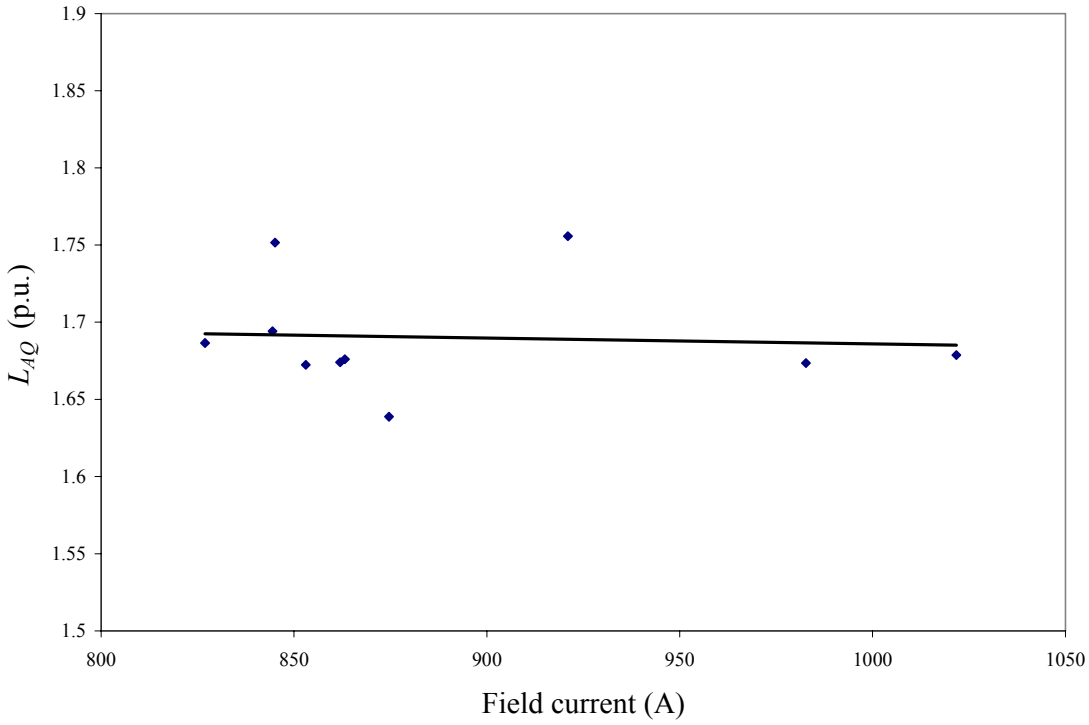

Fig. 3.4 Change of L_{AQ} with operating point for Redhawk gas turbine generators

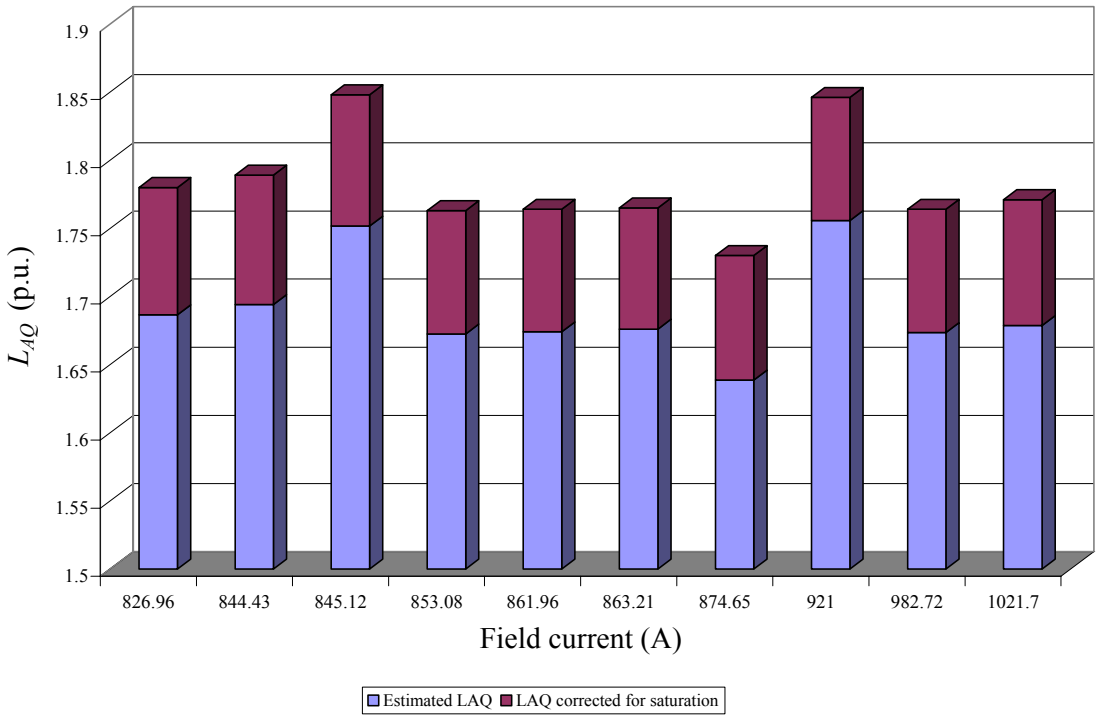

Fig. 3.5 Saturated and unsaturated values of L_{AQ} for Redhawk gas turbine generators.

3.6 Utilization of the Parameter Formulas to Obtain Machine Parameters

Typically machine parameters obtained from manufacturer data are as shown in [69]. These machine parameters are referred to as standard machine parameters and include the direct and quadrature axis reactances and their transient and subtransient counterparts, as well as the transient and subtransient time constants. However, the estimated parameters obtained through the model developed are derived parameters from these standard machine parameters.

Therefore, it is necessary to calculate the standard parameters from the estimated parameters obtained through the developed algorithm. Table 3.8 summarizes the formulae that are needed to perform the conversion from derived parameters to standard parameters. Table 3.9 compares estimated standard parameters to manufacturer standard parameters for case study R-NC-01-10 (generator FC5HP).

The results of Table 3.9 show a good correlation between the estimated standard parameters and the manufacturer standard parameters. The correction for saturation typically improves the estimates. Some of the parameters such as the transient and subtransient inductances are estimated with errors less than 0.3%. The highest error is observed for the direct axis transient open circuit time constant and it is equal to 5.5%.

Table 3.8 Calculation of standard parameters from the estimated derived parameters*

Parameter name	*Parameter symbol*	*Formula*
Equivalent direct axis reactance	x_d	$L_{AD} + \ell_d$
Transient direct axis reactance	x'_d	$\frac{\ell_F L_d + L_{AD}\ell_d}{L_{AD} + \ell_F}$
Subtransient direct axis reactance	x''_d	$\ell_d + \frac{1}{\frac{1}{L_{AD}} + \frac{1}{\ell_D} + \frac{1}{\ell_F}}$
Equivalent quadrature axis reactance	x_q	$L_{AQ} + \ell_q$
Transient quadrature axis reactance	x'_q	$\frac{\ell_G L_q + L_{AQ}\ell_q}{L_{AQ} + \ell_G}$
Subtransient quadrature axis reactance	x''_q	$\ell_q + \frac{1}{\frac{1}{L_{AQ}} + \frac{1}{\ell_G} + \frac{1}{\ell_Q}}$
Direct axis transient open circuit time constant	τ'_{d0}	$\frac{L_{AD} + \ell_F}{\omega_B r_F}$
Direct axis subtransient open circuit time constant	τ''_{d0}	$\frac{1}{\omega_B r_D}[\ell_D + \frac{1}{\frac{1}{L_{AD}} + \frac{1}{\ell_F}}]$
Quadrature axis transient open circuit time constant	τ'_{q0}	$\frac{L_{AQ} + \ell_G}{\omega_B r_G}$
Quadrature axis subtransient open circuit time constant	τ''_{q0}	$\frac{1}{\omega_B r_Q}[\ell_Q + \frac{1}{\frac{1}{L_{AQ}} + \frac{1}{\ell_G}}]$

*Note: Time constants are in seconds. All other quantities are in per unit.

Table 3.9 Comparison of estimated standard parameters to manufacturer standard parameters (case study R-NC-01-10)*

Parameter	Manufacturer value	Value at operating point	Unsaturated value	% Deviation
x_d	1.80	1.7563	1.897	5.4
x'_d	0.27	0.2698	0.2704	0.15
x''_d	0.19	0.18998	0.19003	0.02
x_q	1.72	1.5657	1.6894	1.78
x'_q	0.49	0.48251	0.48861	0.28
x''_q	0.19	0.18994	0.18999	0.005
τ'_{d0}	3.70	3.60802	3.90376	5.5
τ''_{d0}	0.032	0.03196	0.03209	0.28
τ'_{q0}	0.49	0.45179	0.48243	1.54
τ''_{q0}	0.059	0.05778	0.05877	0.39

*Note: Time constants are in seconds. All other quantities are in per unit. Note that the saturated L and X are less than the unsaturated values.

4 Graphic User Interface Implementation Using Visual C++

4.1 A Graphic User Interface

A particularly convenient way to estimate generator parameters in a practical engineering setting is through the use of a GUI. To be consistent with other engineering tools, the GUI might be in the form of a Windows application. A GUI utilizing on-line DFR data enables the practicing engineer and interested utilities to estimate parameters of a synchronous machine without having to decommit the unit.

In order to facilitate use of the estimation procedure described, an on-line implementation was developed and tested in a limited environment. The GUI enables on-line parameter estimation for a given synchronous machine based on measurements of the field and stator voltages and currents. Such measurements are usually available. An application of this nature should be portable and able to be installed on any personal computer operating under Windows. User friendly interaction is achieved by means of the dialogs and context-sensitive help provided on request. In the subsequent section, the GUI developed is described in greater detail. The implementation is offered as an example of what might be done to implement the estimation algorithm described in this report.

4.2 A Sample Input / Output Dialog And Estimator Configuration

It is useful to configure the main window of a GUI to implement the estimator described above to offer a variety of options on its toolbar, like any other Windows program. To begin the process of estimating machine parameters, the user must open the input screen as shown in Fig. 4.1. This is achieved by selecting the option *Estimator* on the toolbar of the main window, and then selecting the *Set up Estimator* option.

The user can set up the *Estimator* and calculate the parameters of the synchronous machine that is to be studied by following the directions on the input screen. The name of the data file is entered in the edit box as shown in Fig. 4.1. The file can be of any data format type (for example .dat or .txt). If applicable, the user can select the IEEE COMTRADE option by clicking on the respective radio button and the *Estimator* will read the measurements as obtained directly from the measuring device that is connected to the machine.

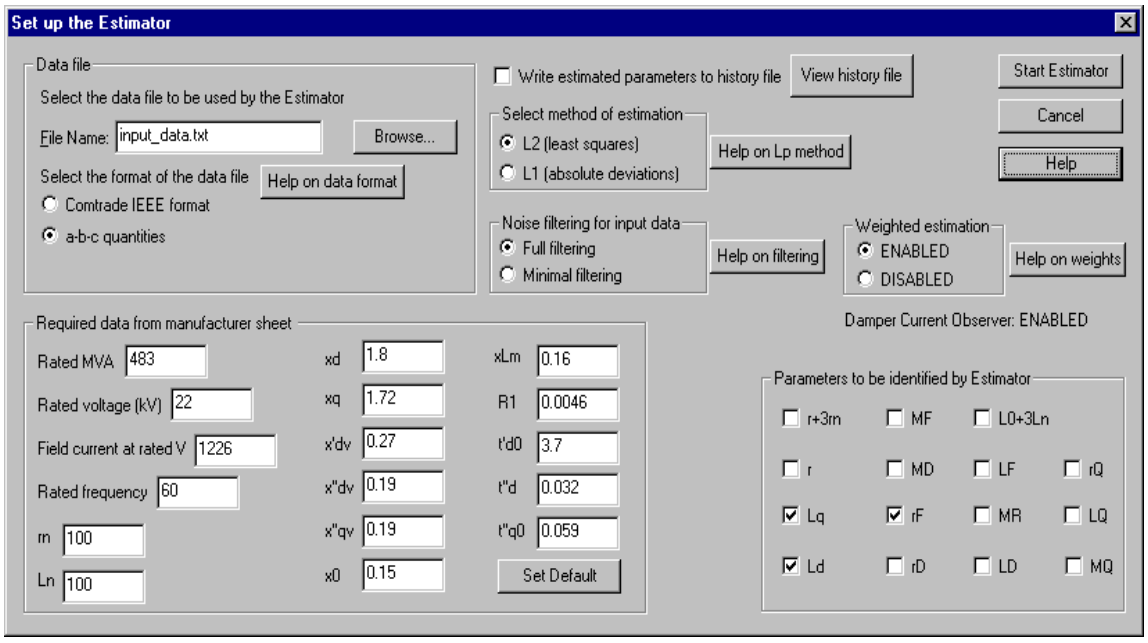

Fig. 4.1 Input window of the estimator

The parameter estimation method described in this report requires a base set of values of selected machine parameters. The user inputs the required parameters as contained in the manufacturer data sheet of the synchronous machine or default values available in the program can be used. Subsequent to basic data entry, the user selects various options pertaining to the estimation process. It is possible to perform either a least squares estimation (*L2* minimization) or a minimization of absolute deviations using the *L1* norm.

Further, the user may select the level of filtering that is desired. Of the two options, the full filtering is preferred since it will minimize the noise content in the measured signals. Finally, the user is given the option to apply weights to the measurements. This is particularly useful if it is known that certain measurements are less reliable than other measurements. Further documentation on all the options is provided through context-sensitive help or through the buttons that are located on the input window.

The final step of the estimation process is to select the parameters that are to be estimated. For the test GUI implemented, the user has the opportunity to select up to five parameters for estimation. This selection can be done by simply clicking on the check box corresponding to the parameter to be estimated as shown in Fig. 4.1.

The resulting output window after estimation can be seen in Fig. 4.2. On the left side of the output window, the user can see the parameters selected previously and their estimated value in per unit. The rms error on the lower right side of the estimator is a measure of confidence on the estimated parameters and is given by,

$$rms\ error = \sqrt{residual / \#of\ measurements}$$

$$(residual)^2 = \{[H][\hat{x}] - [z]\}^T \{[H][\hat{x}] - [z]\},$$

where $\hat{x}$ is the vector of the estimated parameters. Finally, a confidence level is indicated and has three states: high, average or low. In this fashion, the user can verify whether the measurements used are reliable or not.

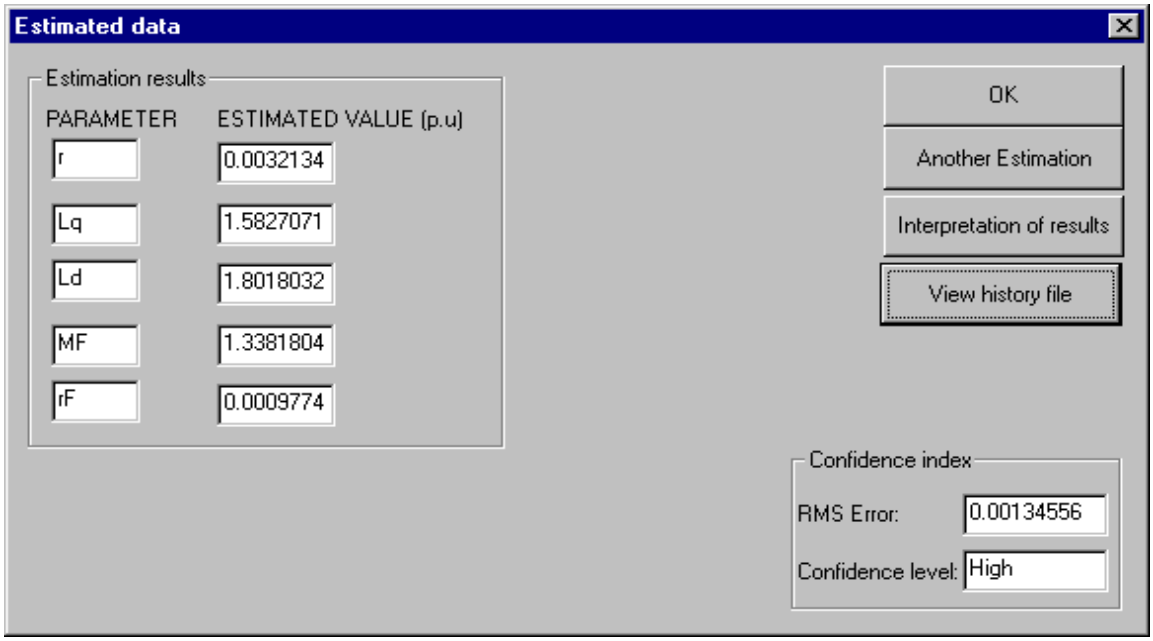

Fig. 4.2 Output window of the estimator

4.3 Listing of the Code and Flow Charts

A listing of the Matlab code, and flow charts for the GUI program appear in appendices of reference [69].

5 Conclusions and Comments

5.1 General Comments

A method to identify synchronous machine parameters from on-line measurements is shown. The method is based on least squares estimation and a simple formula for the derivative operator. To illustrate the potential of the estimation algorithm, the method was implemented for use with a Visual C++ engine and graphic user interface so that the practicing power engineer may link machine measurements taken in an on-line environment with the *Estimator*. An observer for identification of the unmeasurable damper winding currents is also presented. A saturation model was implemented for the generator inductances. Parameter estimation results using on-site measured DFR data show that the machine parameters are estimated accurately for most parameters of interest. Multiple parameters were also estimated accurately: the accuracy of estimation does not degrade when multiple parameters are estimated.

5.2 Comments from Industry

The research work performed in this project attempts to solve a well defined industry problem namely the identification of synchronous generator parameters at various operating levels and the tracking of parameters over time to potentially prevent system outages. A number of utilities and private companies have expressed an interest in this research work and the graphic user interface that is being developed. A number of industry members were involved directly or indirectly in this work and at times offered suggestions, comments, and constructive criticism about the development of the estimator.

All the issues raised by the industry are of practical manner. Some of the major issues include the unavailability of damper winding current measurements and the implementation of a saturation model for synchronous generator inductances. Some other issues that have been discussed are the differences in the configuration of the exciter in synchronous generators, the extension of this research work to other generators, and the improvement of the confidence in the results by using measurements from various generators. Table 5.1 summarizes some of the comments and concerns received by industry members during private discussions or during various presentations of this research work at international conferences.

5.3 Research Conclusions

In this report, a method to identify synchronous generator parameters from on-line measurements is presented. Knowledge of parameter values at different operating levels enables the correct representation of synchronous generators in stability studies and other routine power engineering studies. Proper representation of synchronous generators leads to increased accuracy in the results obtained from these studies as well as better operation and maintenance of the power system network. Additionally, the ability to foresee turn to turn short circuits in the generator field winding potentially enables the engi-

neers to avoid forced outages, thus saving the company huge amounts of money in down-time, rewinding of the generator, and lost dividends from the operation of the generator.

The method proposed in this report is based on least squares estimation of a system of equations based on measurements obtained while the generator is connected to the power system and serves its load. The on-line collection of measurements makes the method superior to off-line methods since it is possible to estimate generator parameters at various operating levels. The developed model of the system was shown to contain seven differential equations that represent the stator and the rotor of the generator as well as three damper windings.

Table 5.1 Comments from the power engineering industry

Area	Industry comment	Plan of action
Exciter	Is the estimator applicable to brushless exciter applications?	The estimator requires voltage and current measurements from the field winding. It is necessary for the exciter to have brushes in order to be able to obtain these measurements. However, it may be possible to develop an observer for the field voltage and current. This subject is under investigation.
Damper windings	The damper windings cannot be measured. How does the estimator obtain these measurements?	Chapter 3 describes an observer for damper winding currents. Results from simulated data verify its operation.
Magnetic saturation	Can magnetic saturation be implemented in the estimator?	A model for magnetic saturation is currently used as shown in Chapter 3. A model to estimate the *q* axis characteristic from the *d* axis characteristic has been developed by a number of researchers and is also presented in Chapter 3.
Superconducting synchronous condensers	Can the estimator be applied to a superconducting synchronous condenser?	The idea proposed in this research work can be applied to any generator that can be described by a model similar to the one of a round rotor synchronous generator.
Further experience	Is it possible to obtain further experience with the estimator using data from other generators?	A number of synchronous generator data have been obtained from APS. These data pertain to six different generators (both steam and gas turbines).

One of the most important obstacles in the parameter estimation algorithm is the unavailability of damper winding currents. Currently there is no proven technology for the di-

rect measurement of damper winding currents using physical instruments. Moreover, damper windings are often fictitious and they are an effect of eddy currents in the rotor path. Therefore it is necessary to estimate damper winding currents. An observer for the estimation of damper currents that is based on the model of the system and *a priori* knowledge about the system was proposed in this work and implemented in the parameter estimation algorithm. Comparison to both steady state and transient simulated measurements showed that the damper currents were estimated accurately.

Magnetic saturation affects some of the generator inductances significantly. In order to enable estimation of parameters at various operating levels, it is imperative to model saturation effectively so that the estimated parameters reflect the true state of the system. A saturation model was implemented in this dissertation based on knowledge of the saturation curve of the direct axis. A saturation factor that was calculated from the saturation model was used to modify the values of inductances that were used in the estimation process. Parameter estimation results show that magnetic saturation is represented effectively. A possible improvement of the saturation representation is to calculate separate saturation factors for the direct and quadrature axes. Because of the unavailability of q axis saturation data, it is necessary to approximate the q axis saturation characteristic. A method to estimate the q axis open circuit characteristic from the available d axis open circuit characteristic is shown in Chapter 3.

Noise suppression is of major concern in this research work. Actual generator data always contain noise that needs to be reduced in order to improve the accuracy of the estimated parameters. Several types of digital filters have been considered in order to filter out high frequency noise in the stator and rotor measurements. The Butterworth filter is selected to be implemented because of its desirable characteristics in the passband, and especially because of the small amount of ripple in its response. A multiple parallel filtering method was proposed to implement noise filtering in an effective manner because of the spread of the frequency spectrum of the signals. Multiple parallel filtering in effect applies the same filter a number of times to slowly attenuate all frequency components that are located in the transition band of a signal. For "noise" that is actually harmonics, in either the field or armature, a small possible improvement might be obtained by modeling the effects of these harmonics rather than simply discarding the harmonic portion of the spectrum.

The synchronous generator models and the proposed method were verified using synthetic data obtained from the solution of the differential equations of the model and from the simulation of the generator in EMTP. The latter method allowed the estimation of generator parameters with a maximum error of 0.39%, while the stator resistance and the field resistance were estimated exactly.

The proposed method was subsequently tested using on-line measurements from synchronous generators. In case study R-NC-01-10 described in full in [69], the field resistance was estimated with a deviation of 0.8% for all three proposed models for generator FC5HP. The direct axis inductance L_d was estimated with a deviation of 2.4% for both

models 2.1 and 2.2, while the quadrature axis inductance L_q was estimated with a deviation of 1.0% for model 2.1 and 0.2% for model 2.2 respectively. In the case of model 2.2x, the direct axis mutual inductance L_{AD} was estimated with a deviation of 5.9%, while the quadrature axis mutual inductance L_{AQ} was estimated with a deviation of 2.0%. It is possible that the deviation of the estimated parameters from the manufacturer supplied parameters is due to inaccurate modeling of saturation, change of generator parameters over time, and the fact that the rotor of the generator under study has been rewound at least three times during its operating history. Therefore it is possible that the manufacturer supplied parameters do not reflect the present state of the generator.

In the companion doctoral dissertation, reference [69], it was demonstrated that multiple parameter estimation is feasible. A number of case studies performed using both synthetic and actual measurements illustrated that the accuracy of the estimation does not degrade as the number of parameters increases. This enables the estimation of more than one parameter at a time and it is a particularly useful result since there is often uncertainty in more than one generator parameter.

In order to ascertain the validity and the accuracy of the proposed algorithm for other synchronous generators, and to examine whether it is possible to estimate parameters at different operating points, a number of case studies were performed. Data sets from gas turbines GT1 and GT2, as well as from steam turbines ST1 and ST2 indicated a consistency in the estimated parameters over a range of operating points. A decreasing trend in the value of the mutual inductances was observed as the generators were driven deeper into the saturation region. This is consistent with magnetic saturation theory, since the apparent value of the inductance is expected to decrease as the magnetic field intensity increases beyond the saturation threshold of the magnetic material. Further, the estimated unsaturated inductances at all operating points had small deviations from the mean for all generators under study. This shows a consistency in the representation of saturation at all operating levels. It should also be noted that for the steam turbine units the stator resistance was unavailable. Nevertheless, consistent estimates were obtained.

Table 5.2 presents possible sources of deviation from manufacturer supplied parameters. These deviations may be due to inaccuracies in the estimated parameters and the modeling of the generator, or due to inaccuracies in the manufacturer supplied parameters.

The method presented in this report is developed to be used with a Visual C++ engine and graphic user interface (GUI), so that the practicing power engineer may link synchronous generator measurements taken in an on-line environment with the *Estimator*. The GUI application is user friendly and self guiding so as to enable prompt estimation of the desired parameters. The required data that are needed to perform the estimation process can be read off the manufacturer data sheet for the generator under study, and can be supplied to the input screen of the *Estimator*. The data file and the desired parameters that need to be estimated can also be selected on the input screen. The estimated parameters are then displayed on the output screen.

5.4 Future Steps

The results obtained from the proposed method and their subsequent analysis in this report demonstrate that the parameter identification algorithm proposed is potentially an accurate method for the estimation of generator parameters. Therefore, future steps need to be directed towards the enhancement of the accuracy of the results and the utilization of the acquired knowledge for the improvement of certain features of the algorithm.

One of the most important issues that deserve attention is the modeling of magnetic saturation. A saturation model was proposed and implemented in this research work. Because of the unavailability of q axis saturation data, the saturation in the two axes of the generator was assumed to be the same. However, this is not generally true. A method for the estimation of the q axis characteristic from the d axis characteristic was shown. This method needs to be applied into the parameter estimation algorithm and ascertain its validity.

The operational parameters of six synchronous generators were estimated through multiple data sets for each generator. Nevertheless, it is necessary to test the proposed algorithm with a variety of generators from different utilities and different manufacturers to verify the applicability of the estimation method. A greater range of operating points needs to be examined to draw solid conclusions and possibly improve the parameter estimation procedure.

Furthermore, in order to fully explore the capabilities of this methodology, it is required to apply the proposed method in the transient case. Estimation of generator parameters using transient data will potentially prove to be a powerful method for the better understanding of the behavior of a generator in such situations and possibly the improvement of models that are currently being used in a number of power engineering studies.

An interest from various industry members was expressed in the possibility to use the proposed method for the identification of model parameters for other types of generators such as salient pole generators and superconducting synchronous condensers. One of the future steps of this research work is to explore this possibility.

Table 5.2 Principal sources of differences between estimated and manufacturer parameters

Type of deviation	Source of deviation	Description of deviation
Inaccuracy in estimated parameters	Filtering	It may be possible that in some cases noise is not filtered completely, or that some frequency components of interest are filtered out.
Inaccuracy in estimated parameters	Harmonics	Harmonics in the measured signals were treated as noise. It may be possible that some of the harmonic components are not noise and that these components have an effect on the actual machine performance.
Inaccuracy in estimated parameters	Linear model	The model representing the synchronous generator is a linear model. However, physical systems are generally nonlinear. Representing a nonlinear model as linear introduces a degree of inaccuracy.
Inaccuracy in estimated parameters	Representation of magnetic saturation	Saturation is a highly nonlinear, complex phenomenon. To represent saturation a number of assumptions are made. Some of these assumptions have an impact on the accuracy of the estimates.
Inaccuracy in estimated parameters	Modeling	A synchronous generator is a complex system with many parameters. In order to develop a practical model of the system, assumptions need to be made as to whether certain components of the system deserve modeling. It is possible that some of the neglected components have an effect on the machine performance at certain operating levels.
Inaccuracy in estimated parameters	Measurements	Noise, incomplete metering, spikes, and A/D conversion error cause inaccuracies in the measurements. A filtering mechanism cannot extract perfect measurements from noisy measurements and therefore the estimated parameters will contain a certain amount of error.
Inaccuracy in manufacturer parameters	Manufacturer supplied parameters not accurate	Generators are manufactured based on design data. In some cases these design data are shown on the manufacturer stability data sheet. Therefore the actual parameters of each manufactured generator may differ from the design (desired) parameters.
Inaccuracy in manufacturer parameters	Manufacturer supplied parameters not accurate	It is possible that some of the parameters reported on the manufacturer stability data sheet are not measured directly but are calculated parameters. ANSI Standard C50.13-1977 indicates which tests should be performed on a generator, and which can be substituted by results obtained from tests on a duplicate generator. For example, transient and subtransient reactances are typically calculated, not measured.
Inaccuracy in manufacturer parameters	Machine repairs	Often machines undergo repairs (e.g. rewinding the field of the rotor). These repairs cause changes in the machine parameters. Sometimes the changes are significant.
Inaccuracy in manufacturer parameters	Differences in operating point and operating conditions	The machine parameters reported in the manufacturer data sheets are measured at specific operating conditions and a certain level of excitation and temperature. The operating conditions of the machine in the estimation interval are probably different. Further, aging causes changes in the physical properties of the machine parts; these changes are reflected in the machine parameters.

The GUI application that was developed in this research work has been designed to enable a user friendly estimation. Multiple data formats can be read and the estimation procedure is automated. Several supplementary features for further improving the appearance and operation of the application are under consideration for implementation. Such features include the display of a level of confidence and a range for the estimated parameters, and the storing of the estimated parameters over time to enable tracking of possible generator malfunction. The GUI application will be offered to a number of electric utilities for further testing and constructive criticism on its features and capabilities. After appropriate testing and enhancement of its features, it is desired to commercialize the prototype application by developing it into a software package.

Appendix A Construction of a Damper Current Observer

A.1 Introduction

This appendix contains some additional details on the construction of a damper current observer. An observer is a control system with initially unspecified parameters for which those parameters are adjusted in order to allow the observer to have a specified dynamic response. Since the damper windings of a synchronous generator are often not windings at all (i.e., they may be damper bars and rotor cage elements), these circuits are very difficult to accurately model, and basically impossible to instrument. The appendix gives some concepts on this subject, and an engineering solution is presented.

The concepts given here are reprinted from the authors' papers [67, 69]

A.2 Development of an Observer for Damper Winding Currents

Usually, available data for synchronous generators are the stator phase currents and voltages at the terminals of the machine, and the field voltage and current. In order to formulate the parameter estimation problem, it is necessary to have measurements for the damper currents i_D, i_G, and i_Q. Since it is not possible to measure the damper currents directly using physical instruments, even in the case that the damper windings are not fictitious, it is necessary to estimate the damper currents by means of an *observer* prior to the implementation of the state estimator for the generator parameters.

The general concept of an observer is as follows: certain states of a physical system may be difficult to measure or calculate. These unobserved states may nonetheless be needed to calculate an estimate of the machine parameters. An 'observer' is a dynamic system that is constructed so that the unobserved states may be estimated. The observer is adaptive: parameters of the observer are adjusted methodically so that the output of the machine simulation agrees with the actual measured machine output. Fig. A.1 shows the concept of an observer. For the construction of the observer, the following expressions from Chapter 2 are used,

$$-v_D = 0 = -r_D i_D - \frac{1}{\omega_B} L_{AD} i'_d - \frac{1}{\omega_B} L_{AD} i'_F - \frac{1}{\omega_B} (L_{AD} + \ell_D) i'_D$$

$$-v_G = 0 = -r_G i_G - \frac{1}{\omega_B} L_{AQ} i'_q - \frac{1}{\omega_B} (L_{AQ} + \ell_G) i'_G - \frac{1}{\omega_B} L_{AQ} i'_Q$$

$$-v_Q = 0 = -r_Q i_Q - \frac{1}{\omega_B} L_{AQ} i'_q - \frac{1}{\omega_B} L_{AQ} i'_G - \frac{1}{\omega_B} (L_{AQ} + \ell_Q) i'_Q$$

where for the purposes of the development of the observer the current derivatives are replaced by the forward difference formula,

$$i'(t) \approx \frac{i(t+\Delta t) - i(t)}{\Delta t} .$$

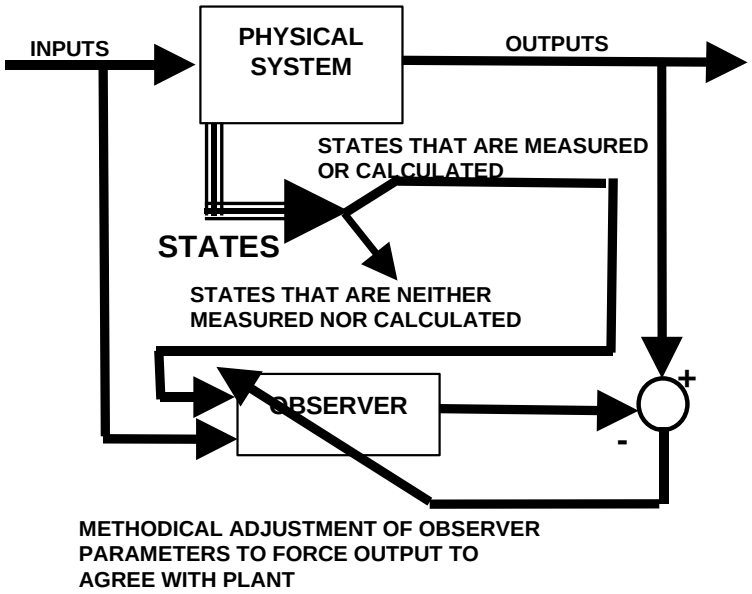

Fig. A.1 Concept of an observer for a dynamic system

Solving for the several damper currents, an expression can be obtained in terms of known measurements and the value of i_D at the previous step.

$$i_D(n+1) = (1 - \frac{r_D \omega_B \Delta t}{L_{AD} + \ell_D}) i_D(n) - \frac{L_{AD} \Delta t}{L_{AD} + \ell_D} (i'_d(n) + i'_F(n))$$

$$i_G(n+1) = \left[1 - \frac{(L_{AQ} + \ell_Q) r_G \omega_B \Delta t}{k_{AQ}} \right] i_G(n) + \left[\frac{L_{AQ} r_Q \omega_B \Delta t}{k_{AQ}} \right] i_Q(n) + \frac{L_{AQ} \Delta t}{(L_{AQ} + \ell_G)} \left[\frac{L_{AQ} \ell_G}{k_{AQ}} - 1 \right] i'_q(n)$$

$$i_Q(n+1) = \left[1 - \frac{(L_{AQ} + \ell_G) r_Q \omega_B \Delta t}{k_{AQ}}\right] i_Q(n) + \left[\frac{L_{AQ} r_G \omega_B \Delta t}{k_{AQ}}\right] i_G(n) - \left[\frac{L_{AQ} \ell_G \Delta t}{k_{AQ}}\right] i'_q(n),$$

where

$$k_{AQ} = (L_{AQ} + \ell_Q)(L_{AQ} + \ell_G) - L_{AQ}^2 .$$

These equations enable the calculation of the damper currents. All parameters can be accurately calculated using manufacturer's data, while the time varying quantities are available measurements. The only ambiguity in the observer equations is the value of $i_D(0)$, $i_G(0)$, and $i_Q(0)$. These are needed to initiate the observation process. Nevertheless, the initial conditions can be assumed to be zero without loss of accuracy as will be shown in the two case studies in the next section.

A.3 Case Studies Using a Damper Winding Currents Observer

The foregoing concept of parameter estimation was tested in two ways: in simulated models; and utilizing actual generator measurements and manufacturer's data. The simulation approach is considered first.

A synchronous generator was simulated using the Electromagnetic Transients Program (EMTP) both in the steady state and in transient mode. EMTP is suitable for testing the estimation algorithm because data from the simulation are free of noise, and one has access to all machine parameters and signals. Furthermore, EMTP provides the simulated damper currents in the direct and quadrature axes. Therefore, a means of testing the observer is provided. The simulation tests support the application of the observer in the real data case.

The machine under consideration is a cross-compound generator located in the southwest U.S.A. The generator contains a high pressure unit rated at 483 MVA and a low pressure unit rated at 426 MVA. This example is chosen because subsequently, a real-life example of the same machine, with measurements taken by a digital fault recorder (DFR) will be used. At this point it suffices to state that the measurements required are the three phase stator voltages and currents, and the DC field voltage and current. The measurements are assumed to be error free for the simulation tests. The results of the tests are shown in Chapter 3 of this report.

A.4 Configuration of The State Estimator

State estimation is a process during which a number of unknown system state variables or parameters are assigned a value based on measurements from that system. Typically, the number of measurements (or number of equations) is much greater than the parameters to be estimated. In this case the system is overdetermined and the solution is found in a least

squares sense. That is, the sum of the squares of the differences between the estimated and the measured parameters is minimized.

Since the last three equations in Section A.2 have been used for the development of the observer, the remaining four equations are rearranged into the form

$$Hx = z$$

to obtain the estimated parameters by

$$\hat{x} = H^{+} z \ ,$$

where H^{+} is the pseudoinverse of H. Matrix H (the *process matrix*) is of dimension $m \times n$ and contains the coefficients of the unknowns, which are either obtained by direct measurements of current and voltages, or via the observer in the case of the damper currents, or via calculation in the case of the derivatives. The formula for the derivatives is the forward difference formula. The vector z has dimension m and it contains known parameters, or measurements or a combination of the two. Fig. A.2 illustrates in block diagram form the idea of the observer, the data manipulation and the parameter estimation algorithm.

For example, if parameters L_{AD}, L_{AQ} and r_F are to be estimated, the damper current expressions can be rearranged in the form $Hx = z$ to obtain,

$$\begin{bmatrix} 0 & 0 & 0 \\ \dfrac{(i'_d + i'_F + i'_D)}{\omega_B} & \omega(i_q + i_G + i_Q) & 0 \\ -\omega(i_d + i_F + i_D) & \dfrac{(i'_q + i'_G + i'_Q)}{\omega_B} & 0 \\ \dfrac{(i'_d + i'_F + i'_D)}{\omega_B} & 0 & i_F \end{bmatrix} \begin{bmatrix} L_{AD} \\ L_{AQ} \\ r_F \end{bmatrix} = -\begin{bmatrix} r + 3r_n & 0 & 0 & 0\,0\,0\,0 \\ 0 & r & \omega\ell_q & 0\,0\,0\,0 \\ 0 & -\omega\ell_d & r & 0\,0\,0\,0 \\ 0 & 0 & 0 & 0\,0\,0\,0 \end{bmatrix} \begin{bmatrix} i_0 \\ i_d \\ i_q \\ i_F \\ i_D \\ i_G \\ i_Q \end{bmatrix}$$

$$-\frac{1}{\omega_B} \cdot \begin{bmatrix} L_0 + 3L_n & 0 & 0 & 0 & 0\,0\,0 \\ 0 & \ell_d & 0 & 0 & 0\,0\,0 \\ 0 & 0 & \ell_q & 0 & 0\,0\,0 \\ 0 & 0 & 0 & \ell_F & 0\,0\,0 \end{bmatrix} \begin{bmatrix} \dot{i}_0 \\ \dot{i}_d \\ \dot{i}_q \\ \dot{i}_F \\ \dot{i}_D \\ \dot{i}_G \\ \dot{i}_Q \end{bmatrix} - \begin{bmatrix} v_0 \\ v_d \\ v_q \\ -v_F \\ -v_D \\ -v_G \\ -v_Q \end{bmatrix}$$

In this way, the four unknown parameters and their coefficients are isolated on the left hand side, and all elements of the right hand side are known. Moreover, the right hand side reduces to a vector and therefore the system takes the final form $Hx = z$.

The linear system $Hx = z$ represents multiple time steps. Each measurement results in an equation of the form $Hx = z$. At each subsequent time step, the new data are augmented to the existing H matrix and z vector to create an overdetermined system.

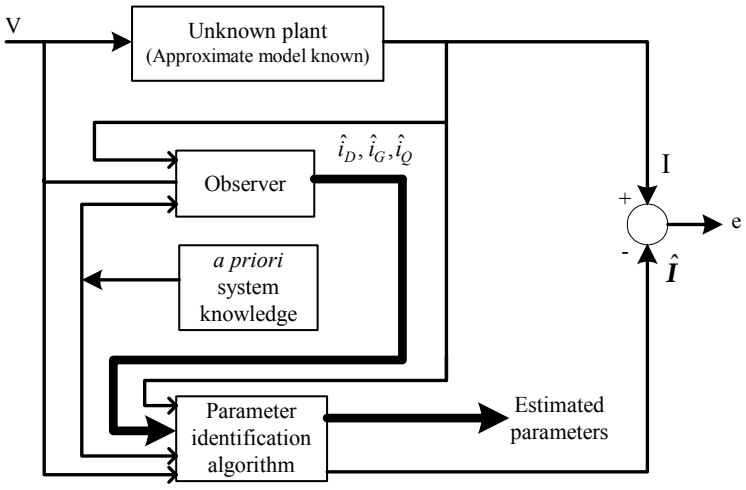

Fig. A.2 Block diagram for observer implementation and parameter identification algorithm

6 Appendix B Bad Data Detection, Rejection and Filtering

B.1 Introduction

Real data have errors resulting mainly from meter and communication errors, incomplete metering, or inaccuracy of metering equipment. Therefore, prior to any estimation it is necessary to perform bad data detection and rejection, and filtering of the noise.

Details of the actual digital filters studied, and their implications on data acquisition and instrumentation appear in Appendix D.

In the field circuit, the main frequency components of interest are at or near DC. On the other hand, in the stator measurements it is possible to perform filtering in the AC measurements (50-60 Hz range), or in the 0*dq* transformed signals (at or near DC). In the synchronous machine parameter estimation application, it was found that the stator measurements are most effectively filtered after the 0*dq* transformation. Fig. B.1 shows the filtering and bad data detection/rejection configuration.

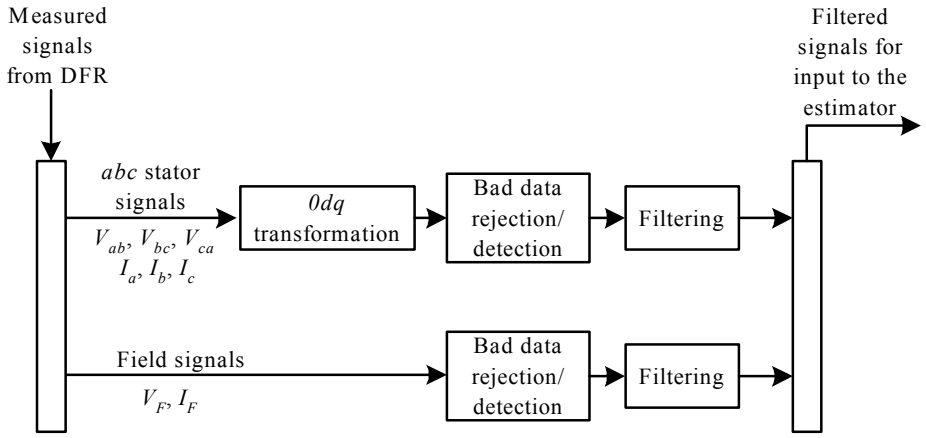

Fig. B.1 Filtering and bad data detection/rejection configuration

B.2 Transformation / Filtering Sequence

After the transformation of the *abc* voltages and currents into 0*dq* signals through Park's transformation, a filter is applied to remove outliers from the measurements. Such outliers appear in the form of spikes, in the time domain plot of each signal. They are caused by metering errors and can be safely removed without risking inaccuracies in the estimation process. If a spike in any one signal is detected, then the whole measurement at that time is removed from the data set.

A second filter was implemented for the removal of random noise. Frequency domain plots of the measured signals indicate the existence of noise in a wide range of frequencies from the main frequency component up to the Nyquist frequency. This noise is detrimental to the estimation process, especially in the calculation of derivatives. A small random noise content in consecutive measurements is amplified when divided by the time step between the measurements (Δt is in the order of 0.1 ms). A Butterworth filter is used to implement the filtering. Butterworth filters are characterized by a magnitude response that is maximally flat in the passband and is characterized by monotonicity in the passband and stopband regions.

B.3 Implementation of a Butterworth Filter

To compensate for the shallower rolloff characteristic of a Butterworth filter, the data are filtered successively by passing them through the same filter until the frequency components that are due to noise are minimized. Filter characteristics are chosen depending on the location and on the size of the noisy frequency components, but in general, the filters for all the signals have a cutoff frequency of approximately 10 Hz and a stopband frequency of 100 Hz with a stopband attenuation of about 60-80 dB. Fig. B.2 depicts the direct axis voltage component in the time domain as calculated from measurements obtained at the generator terminals, while Fig. B.3 shows the filtered signal after applying a spike filter and multiple Butterworth filters.

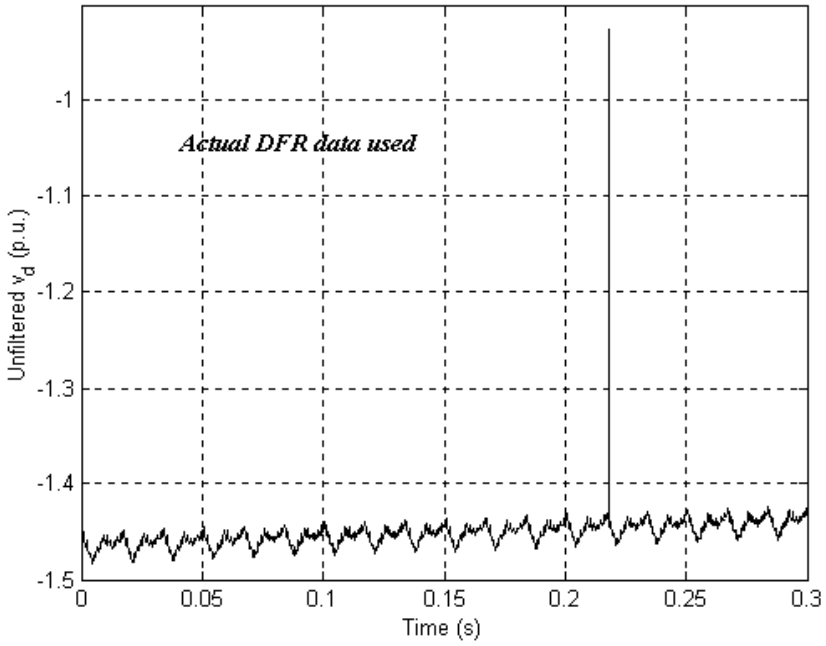

Fig. B.2 Unfiltered direct axis voltage in the time domain

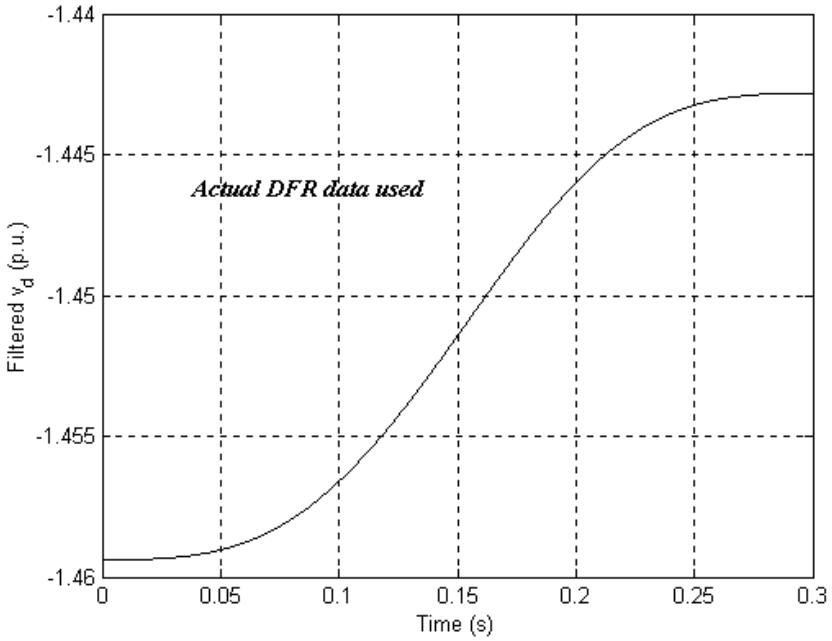

Fig. B.3 Filtered direct axis voltage in the time domain

Appendix C Magnetic Saturation

C.1 Magnetic Saturation in Synchronous Machines

In order to represent saturation in stability studies several assumptions are made. The reason for this is that a rigorous treatment of synchronous machine performance including saturation is a futile exercise. Hence, one typically looks for a practical method for dealing with saturation effects based on semi-heuristic reasoning, carefully chosen approximations, simplicity of model structure, data availability, and accuracy of results.

In the approach used in the modeling in this work, several simplifying assumptions are made in determining saturation. The effects of saturation are represented as,

$$L_{AD} = K_{sd} L_{ADu}$$

$$L_{AQ} = K_{sq} L_{AQu}$$

where L_{ADu} and L_{AQu} are unsaturated values of L_{AD} and L_{AQ}. The saturation factors K_{sd} and K_{sq} identify the degrees of saturation in the direct and quadrature axis, respectively. The *d*-axis saturation is determined from the open circuit characteristic. Typically the saturation curve is divided into three segments, which are defined by threshold values of the flux linkage λ. Suitable approximations for the behavior of λ are made based on the operating segment and thus, appropriated expressions for K_{sd} are derived. It is commonly assumed that for salient pole machines, since the path for the *q*-axis flux is largely in air, L_{AQ} does not vary significantly with saturation of the iron portion of the path. Hence, typically the saturation factor K_{sq} is assumed to be equal to 1.0 for all loading conditions.

In the case of round rotor machines, magnetic saturation should be accounted for in both axes. In general the saturation factor K_{sq} can be determined from the no-load saturation characteristic of the *q*-axis. However, *q*-axis saturation data are typically not available. As a result one normally makes the assumption that K_{sq} is equal to K_{sd}. This essentially assumes that the reluctance of the magnetic path is homogeneous around the periphery of the rotor.

C.2 Improved Modeling

An approach to improved saturation modeling using *q*-axis saturation characteristics derived from finite-element analysis is shown in [19], [20]. Kundur [20] shows a method to calculate the saturation function. References [20, 62,] and [70] address these issues.

In the parameter estimation method shown in the present work, L_{AD} and L_{AQ} (as well as other parameters) are estimated for a given set of operating data. Estimation of parameters using data from an actual synchronous generator operating at different load levels, indicates that inductances L_{AD} and L_{AQ} are the inductances that are most affected by saturation and these quantities vary considerably.

Appendix D Data Acquisition Details

D.1 Introduction

This appendix provides a detailed overview and results from data processing techniques applied to filtering current and voltage signals of a synchronous generator. The information given in this appendix is essentially a reprint of reference [68].

The synchronous generator data are inputs to an estimator, which is used for synchronous machine parameter identification. The scope of this research includes filtering these data to obtain satisfactory results (minimum residual error) for the estimator. The choice of the filter to be designed depends on many factors including the filter performance, ease of design, and simplicity of implementation. A goal of this work is to provide the parameter estimator with multiple filter types for the user to select from.

The primary challenge addressed in this paper is the filtering of the phase quantities. It is a problem in the sense that the phase information imbedded in these quantities should not be distorted by the filtering. The results presented herein provide a technique to meet these requirements.

D.2 Synchronous Machine Mathematical Model

The mathematical model developed for synchronous machine parameter estimation is depicted in Fig. D.1 [1]. The model consists of three stator windings, one for each phase; one field winding, representing the field excitation; two damper windings, one each for the direct (D) and the quadrature (Q) axes, and the neutral.

The instantaneous terminal voltage *v,* for the windings can be represented by a general equation,

$$v = -r\,i - \dot{\lambda}$$

where *r* is the winding resistance, *i* is the current and $\dot{\lambda}$ is the first derivative of flux linkage. This equation arises from the fact that the terminal voltages are a function of rotor position .

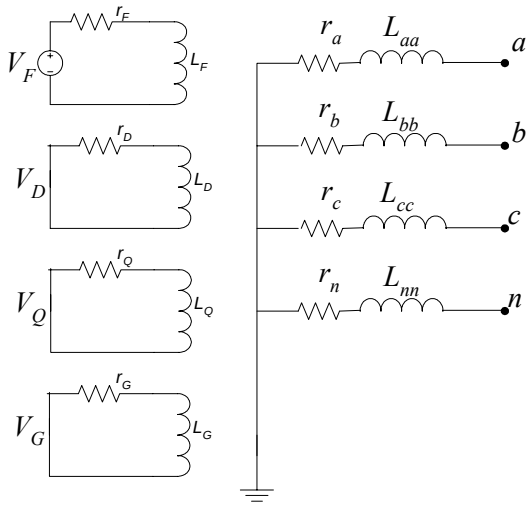

Fig. D.1 Synchronous machine model

The three-phase time-variant phase quantities are difficult to analyze owing to the fact that both the magnitude and the phase of the quantities must be preserved. It is necessary to convert these quantities to time-invariant equivalents. This can be accomplished using a series of transformations, which convert the three-phase stationary phase quantities (i_a, i_b, i_c and v_a, v_b, v_c) into three rotating quantities (i_d, i_q, i_0 and v_d, v_q, v_0). For a balanced generator, the *0* component can be neglected.

The development of the model for the *0dq* axes frame has been described in the main body of this report. The final simplified model is given by the matrix equation,

$$\begin{bmatrix} v_0 \\ v_d \\ v_q \\ -v_F \\ 0 \\ 0 \end{bmatrix} = \begin{bmatrix} r+3r_n & 0 & 0 & 0 & 0 & 0 \\ 0 & r & \omega L_q & 0 & 0 & \omega k M_Q \\ 0 & -\omega L_d & r & -\omega k M_F & -\omega k M_D & 0 \\ 0 & 0 & 0 & r_F & 0 & 0 \\ 0 & 0 & 0 & 0 & r_D & 0 \\ 0 & 0 & 0 & 0 & 0 & r_Q \end{bmatrix} \begin{bmatrix} i_0 \\ i_d \\ i_q \\ i_F \\ i_D \\ i_Q \end{bmatrix}$$

$$- \begin{bmatrix} L_0+3L_n & 0 & 0 & 0 & 0 & 0 \\ 0 & L_d & 0 & kM_F & kM_D & 0 \\ 0 & 0 & L_q & 0 & 0 & kM_Q \\ 0 & kM_F & 0 & L_F & M_R & 0 \\ 0 & kM_D & 0 & M_R & L_D & 0 \\ 0 & 0 & kM_Q & 0 & 0 & L_Q \end{bmatrix} \begin{bmatrix} \dot{i}_0 \\ \dot{i}_d \\ \dot{i}_q \\ \dot{i}_F \\ \dot{i}_D \\ \dot{i}_Q \end{bmatrix}$$

The inputs to this equation are the field quantities and the transformed phase quantities. In the current vector, the damper currents i_D and i_Q are shown. These two quantities, which cannot be measured, have to be predicted using an observer [3].

D.3 Park's Transformation

As mentioned earlier the phase quantities have to be transformed to a rotating frame of axes to obtain transformed signals independent of phase (angle) information. Park's transformation is used for the above purpose. The Park's transformation equation is as follows

$$P = \sqrt{\frac{2}{3}} \begin{bmatrix} \frac{1}{\sqrt{2}} & \frac{1}{\sqrt{2}} & \frac{1}{\sqrt{2}} \\ \cos(\theta) & \cos\left(\theta - \frac{2\pi}{3}\right) & \cos\left(\theta + \frac{2\pi}{3}\right) \\ \sin(\theta) & \sin\left(\theta - \frac{2\pi}{3}\right) & \sin\left(\theta + \frac{2\pi}{3}\right) \end{bmatrix},$$

where θ, in radians, is given by the equation

$$\theta = \varpi_R t + \delta + \frac{\pi}{2},$$

where ϖ_R is the rated angular frequency in rad/s and δ is the synchronous torque angle. The conversion is shown in the following equation,

$$i_{dqo} = P\, i_{abc},$$

where i_{abc} is the phase vector that has to be converted to the *dq0* frame of axis. The transformed phase quantities are shown denoted by i_{dqo}.

Park's transformation converts the 60 Hz ac signals into pure dc. However the behavior of the Parks transformation for higher order harmonics of the fundamental is yet to be investigated. Simple observation of plots show that the higher order harmonics are mapped into oscillations around the dc signal (obtained for the fundamental). The filtering of these quantities involve the removal the oscillation and to obtain the dc component of the signal.

D.4 Moving Average Filters

The moving average filter, as the name suggests, averages a set of samples from an input signal to produce each point of the output. This filter is useful when the filtering requirements involve extracting the dc component.

Moving average filtering is performed in the time domain and is easy to encode. The form of the *n*-point moving average filter used here is

$$y[k] = \frac{1}{n} \sum_{k}^{k+n-1} x[k]$$

where n is the window length (number of points in the moving average). The proper selection of the number of points enables selective filtering. This idea is applied for our application.

D.5 Digital Filtering

The digital filtering techniques used in this project are limited to the Infinite Impulse Response (IIR) type and the moving average filter (MAF). The classical IIR filters tested for this application include the Bessel, Butterworth, elliptic, and Chebyshev I and II filters. This section provides a brief overview of the form and behavior of these filters.

Figure D.2 shows the basic filter response for design purposes. The filter response is divided into three sections: the passband, the transition band, and the stop band region. The filter performance is determined by its behavior in the above-mentioned regions. An ideal filter has the smallest passband and stop band ripple, and steepest transition band (fastest roll-off). Apart from this the filter should have large stop band attenuation.

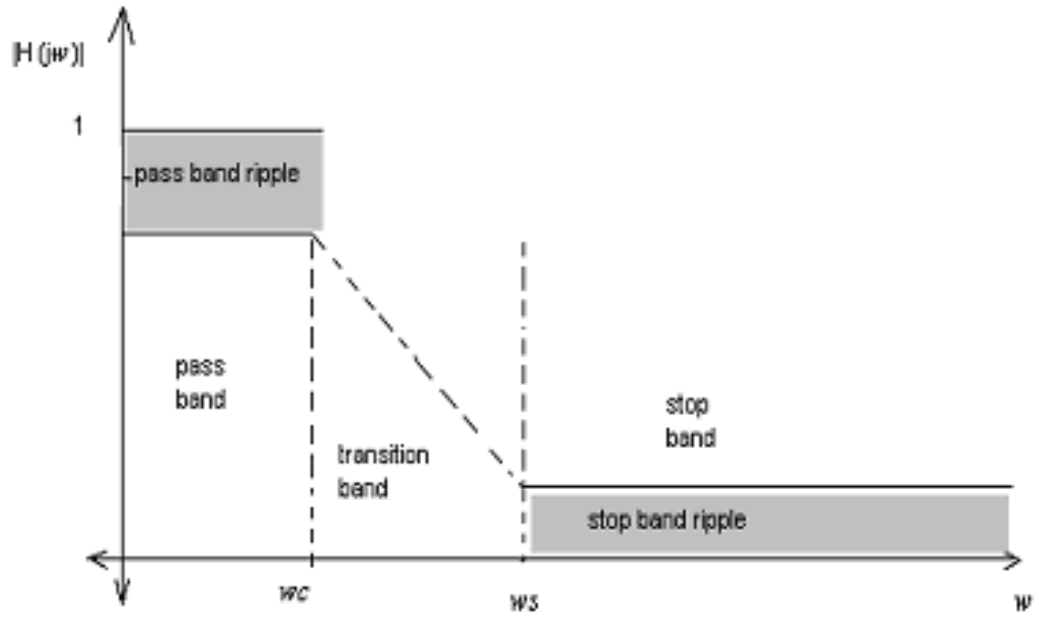

Fig. D.2 Template of magnitude response of designed IIR filters.

D.6 Butterworth Filter

The Butterworth filter has a response that is maximally flat in the passband region; hence this filter is also called a maximally flat filter. The frequency response (amplitude response) of a Butterworth low pass filter for increasing orders is shown in Fig. D.3. As the order increases the transition band steepness increases. This class of filters sacrifices the roll-off steepness for achieving maximally flat response (smoothness).

The Butterworth filter transfer function for order n is given by the equation

$$\left|H(j\varpi)\right|^2 = \frac{1}{\sqrt{1+\varpi^{2n}}}.$$

where ω is the frequency normalized to the cutoff frequency; at the cutoff frequency the gain of the filter is –3 db.

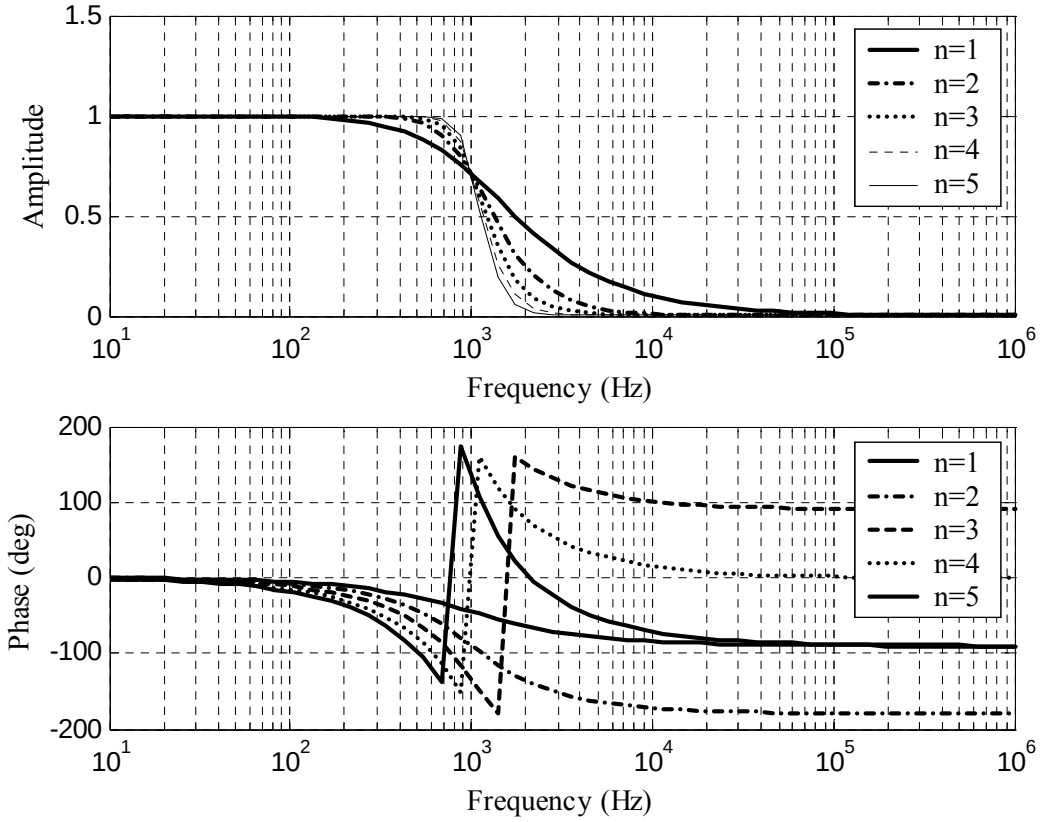

Fig. D.3 Frequency response of the Butterworth filter for increasing orders

D.7 Chebyshev I Filters

The Chebyshev I filter is equiripple in the passband with a stop band magnitude response that is maximally flat. It minimizes the difference between the ideal and the actual frequency response. The frequency response for increasing orders is shown in Fig. D.4.

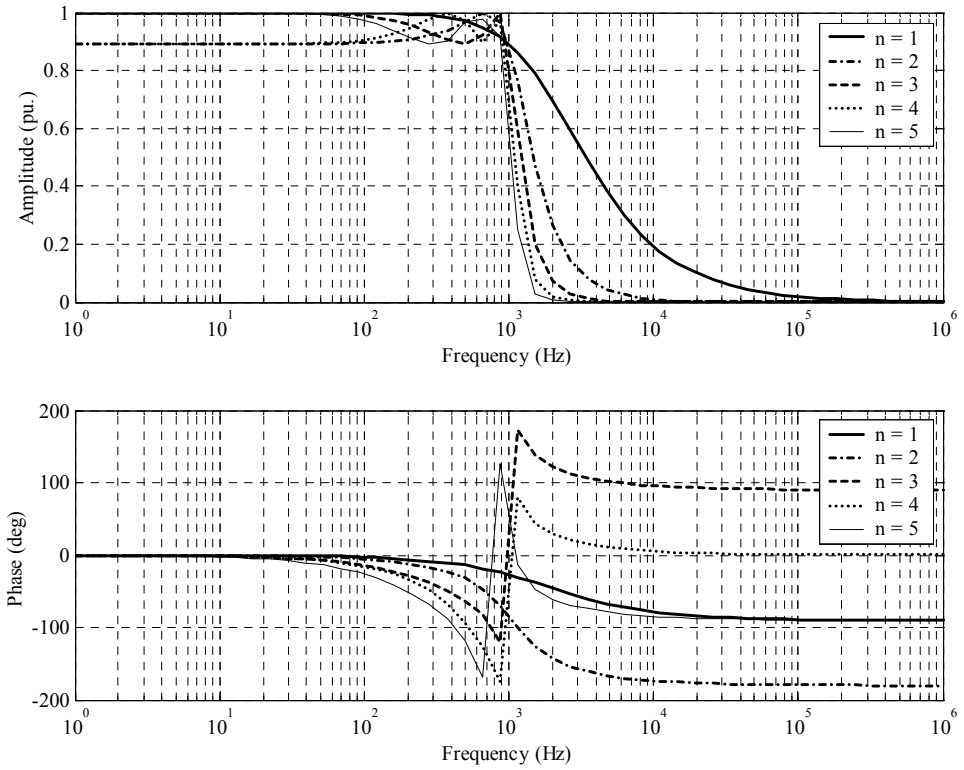

Fig. D.4 Frequency response of the Chebyshev I filter for increasing orders.

The Chebyshev I filter transfer function is given by

$$\left|H(j\varpi)\right|^2 = \frac{1}{\sqrt{1+\varepsilon^2 C^2{}_n(\varpi)}}$$

where ε is a constant and $C_n^2(\varpi)$, called the Chebyshev polynomial, is

$$C_n^2(\varpi) = \cos[n \arccos(\omega)]$$

This shows that the magnitude function of this filter attains 1 at the zeroes of the $C_n(\varpi)$ for the passband region; beyond that $C_n(\varpi)$ has no zeroes and the amplitude function is severely attenuated. In the passband the amplitude function attains the minimum value of

$1/\sqrt{1+\varepsilon^2}$ at the points $|C_n(\varpi)|$ attains the maximum value of 1. These are the ripples in the passband. The Chebyshev filter is also called an equiripple filter because the passband ripples are of equal magnitude.

D.8 Elliptic Filters

Elliptic filters offer steeper roll-off characteristics than Butterworth or Chebyshev filters, but are equiripple in both the passband and stop band. These filters give the best possible performance for a given order among the different types of filters. But the elliptic filter algorithm is computationally intensive compared to the other filters.
The elliptic filter transfer function is

$$|H(j\varpi)|^2 = \frac{1}{\sqrt{1+\varepsilon^2 R_n^2(\varpi)}}$$

where n may be chosen to be even or odd, and $R_n(\varpi)$ is given by

$$R_n(\varpi) = \begin{cases} \prod_{i=1}^{n/2} \dfrac{(\varpi_{2i-1}^2 - \varpi^2)}{(1-\varpi_{2i-1}^2\varpi^2)} & for\ n = 2,4,6,\ldots \\ \varpi \prod_{i=1}^{n/2} \dfrac{(\varpi_{2i}^2 - \varpi^2)}{(1-\varpi_{2i}^2\varpi^2)} & for\ n = 3,5,7,\ldots \end{cases}$$

The frequency response of this filter is shown in Fig. D.5.

D.9 IIR Filter Performance and Comparison

Bessel and Chebyshev II filters were also tested. The Bessel filter has a rounded amplitude response, with a very slow and monotonous roll-off. The Chebyshev II filters are inverse Chebyshev I filters. These filters do not roll off as fast as the Chebyshev I type filter. Based on early comparisons and testing, the Bessel and Chebyshev II filters were eliminated from consideration.

The performance of the three IIR type filters in the passband, stop band and the transition band is compared in Table D.1 [67]. The elliptic filter has an obvious advantage of faster roll off; however, it is much more complex to encode.

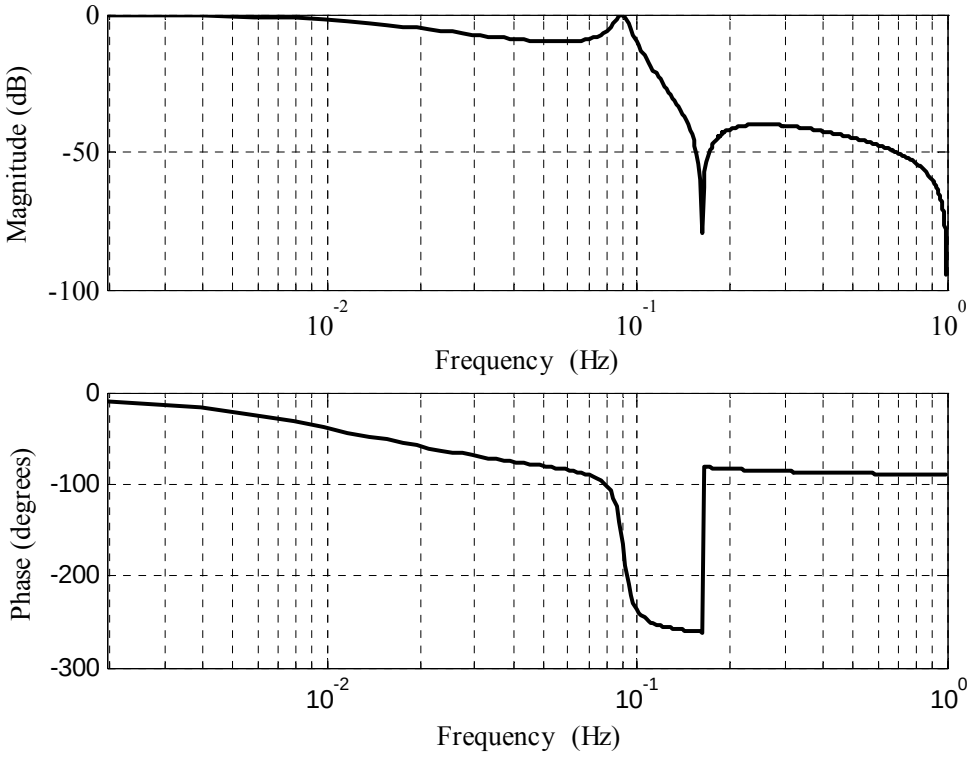

Fig. D.5 Frequency response of an elliptical filter

Table D.1 Comparison of the performance characteristics of three IIR filter types considered for the project

	Butterworth	*Chebyshev I*	*Elliptic*
Passband	Smooth, maximally flat	Rippled	Equiripple
Stop Band	Smooth	Smooth	Equiripple
Transition Band	Monotonic, and less attenuation	Steeper roll off	Steeper roll off
Comments	Acceptable performance is obtained at an order higher than other types	The order required is less than Butterworth, however more than that of elliptic	It designs the filter with the least order

D.10 Data Acquisition and Processing: A Test System

A block diagram for the test system is presented in Fig. D.6. The field voltage and current excite the generator field winding. This current is the output of a six-pulse uncontrolled rectifier, which is given a three-phase 60 Hz input.

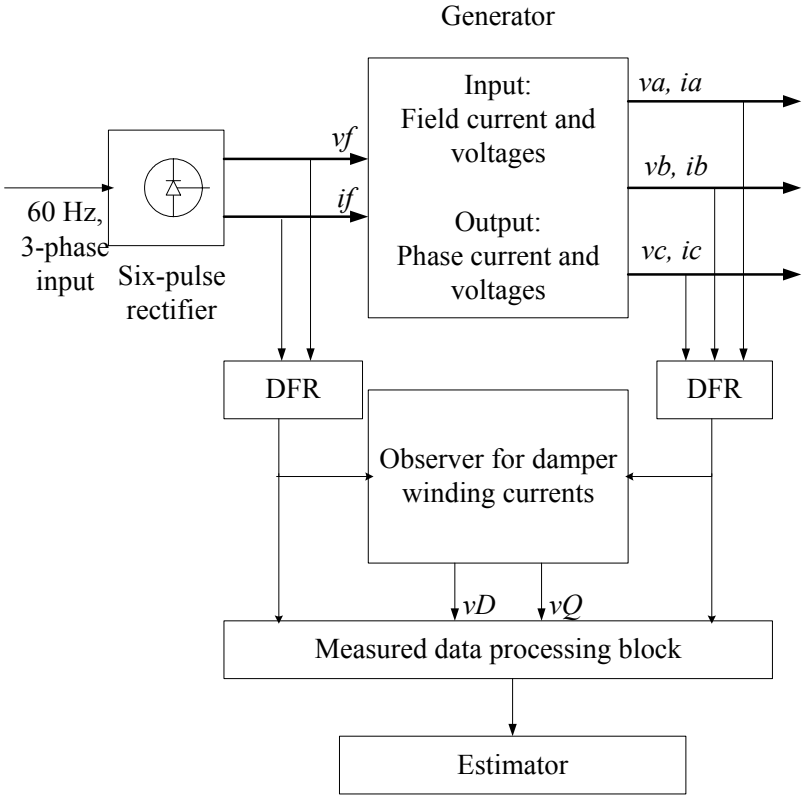

Fig. D.6 Block diagram of the overall system

The generator output is a set of three-phase currents and voltages. Both the input and the output quantities are measured using a digital fault recorder (DFR). Apart from the phase quantities, knowledge of the damper currents is also essential for the parameter estimation. As mentioned in the previous section, these quantities have to be estimated using an observer, as they cannot be measured using conventional instruments.

Examination of recorded data shows that these measurements have to be processed before they can be used for parameter estimation. This measured data processing block is discussed in the next section. The processed data are provided to the estimator.

The measurements available for parameter estimation are the stator phase currents, the terminal voltages, and the field voltages and currents. Operational data are obtained from a 483 MVA generator**.** These data are from online measurements of the quantities using a DFR.

The data processing block described in the previous section is shown in Fig. D.7. The measurements from the DFR are processed in this manner.

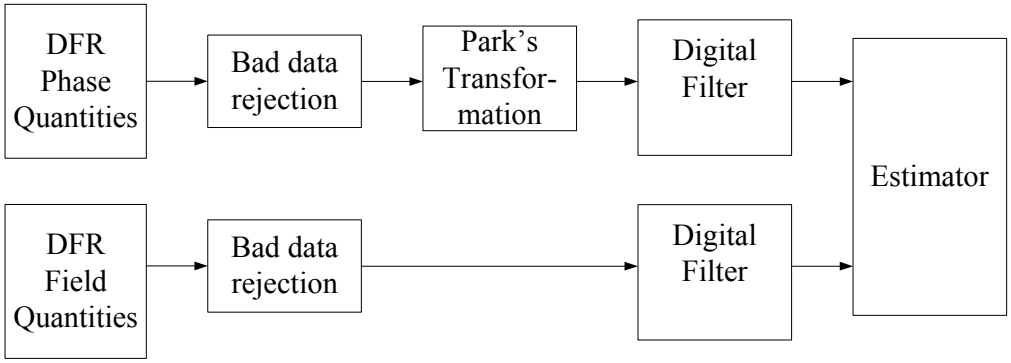

Fig. D.7 Block diagram for processing measured data

D.11 Bad Data Rejection

Due to measurement errors, high amplitude spikes may contaminate the recorded signal. These spikes in the signal may cause filter misoperation. These spikes are termed as bad data, and have to be eliminated form the signal. To accomplish this, a maximum deviation is set for the given signal and the adjacent samples are compared. If the difference exceeds the deviation, the latter datum is erased from the data. The maximum deviation is set by observation and experience for the particular application.

D.12 Data Filtering Analysis

The measurements are taken at a sampling frequency (f_S) of 10 kHz. The data are analyzed in two distinct sets. The first set is the field quantities that are DC in nature; the other set is the three-phase ac voltages and currents at 60 Hz. The data records are 0.32 seconds in length.

Field Voltage and Current Data
The field quantities obtained from the DFR are plotted in Fig. D.8. These plots give insight into the nature of the noise that might be present in the measurements. The plots in Fig. 8 show the presence of high frequency noise along with the expected DC component. In addition, it can be seen that the field current signal has a slowly varying component with a period of roughly 0.1 sec (10 Hz). Figure D.9 shows the compressed signal shown in Fig. D.8. The slowly moving component is more evident from Fig. D.9.

The frequency response of the measured quantities is provided in Fig. D.10. It should be noted that there is a considerable influence of the frequencies at 300 Hz and 420 Hz, which

correspond to the fifth and seventh harmonics of the fundamental frequency. This behavior is expected from a signal obtained from a six-pulse rectifier. A ~10 Hz component is seen in both the current and voltage spectra.

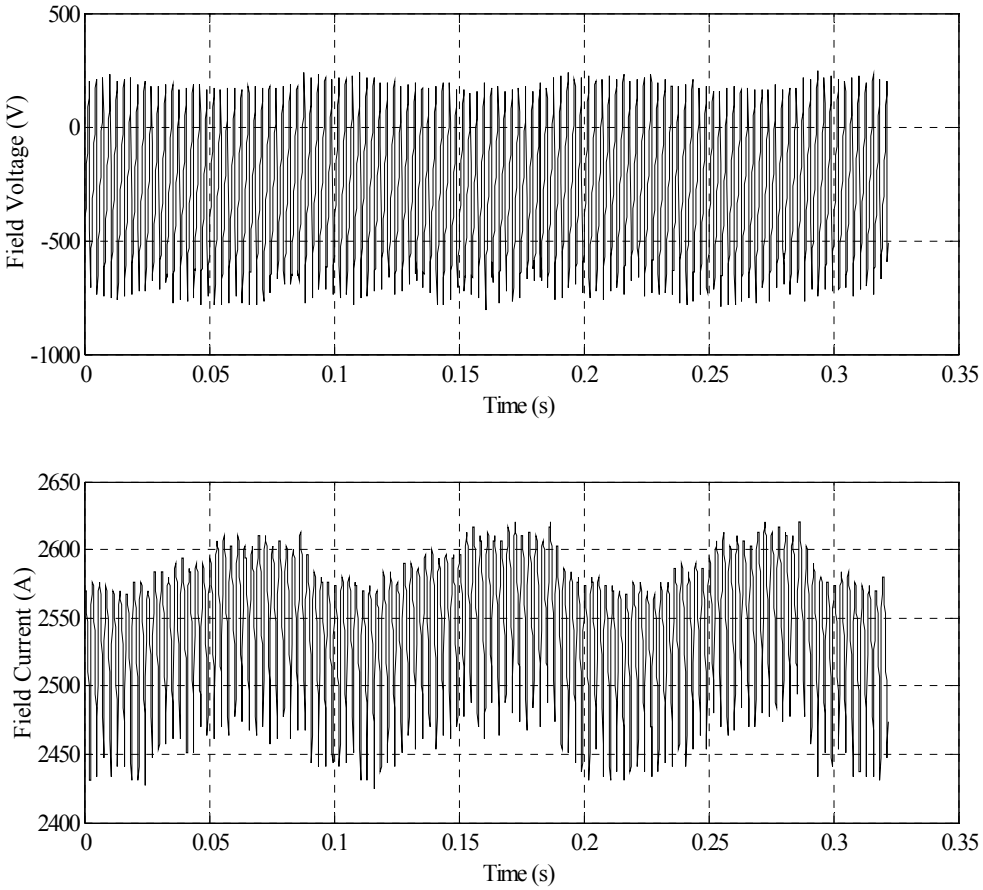

Fig. D.8 Field current and voltage signals indicating the presence of noise

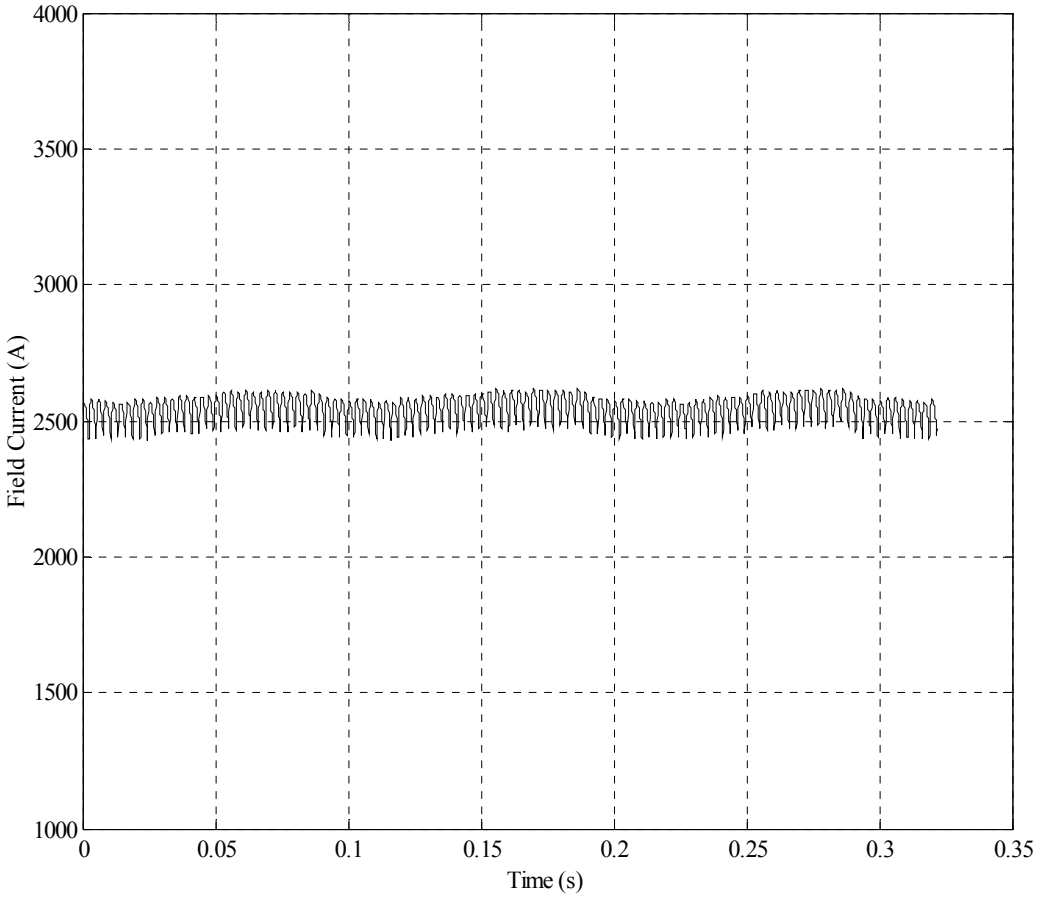

Fig. D.9 Field current signal replotted on expanded ordinate axis to show low frequency behavior.

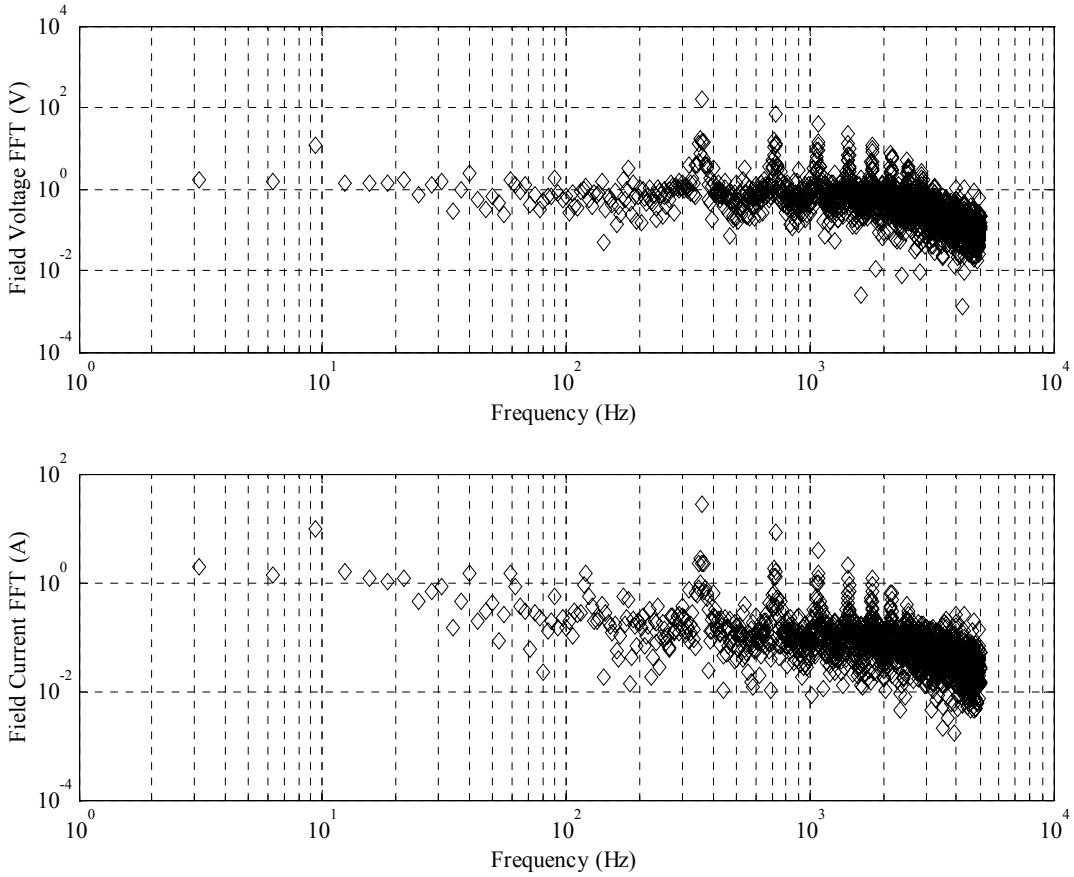

Fig. D.10 Frequency response in field current and voltage plots indicating the presence of noise and bad data. (The dc value is not shown in the plot.)

Filtering of Field Quantities

For the field quantities it is desired that the low frequency component mentioned earlier be preserved, while the higher frequency components are removed. Also the current vector is seen to have a first order derivative. The derivative of current is obtained in the estimator using a small time step ($1/f_S$)**.** To avoid errors in the derivative calculations the filtered signals should be ripple free.

To accomplish this, a definite filtering strategy is chosen. First, the data are passed through a moving average filter whose results are shown in Fig. D.11. Close examination of the data shows that the remaining low frequency component has a period of about 0.101 sec. From testing, we select a 500-point moving average filter (MAF) to remove the high frequency components. The MAF is easily encoded, and it leaves only a small high frequency ripple in the field voltage signal as shown in Fig. D.11. Using the MAF has reduced the data set from 3219 samples to 3219-500=2719 points.

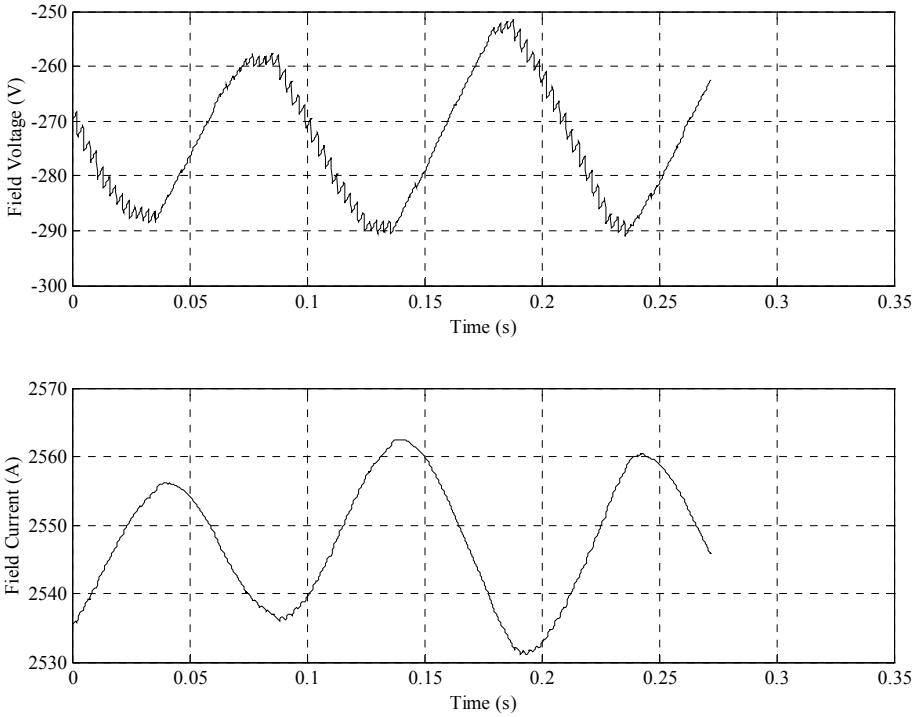

Fig. D.11 Time domain plots for the moving average filtered field quantities

Applying any of the classical filters can remove the remaining high frequency ripple. To investigate the performance of the three different filter types, the cutoff frequency for each filter was varied from 1 to 20 Hz. The criterion for comparing the filter performance is the directly calculated field resistance, obtained from the ratio of the filtered field voltage and current,

$$r_F = \frac{v_F}{i_F}$$

The manufacturer provided field resistance value is 9.72×10^{-4} p.u. Fig. D.12 shows the field resistance values computed from the filtered data. It was found that the elliptical filter provided the largest stop band attenuation while maintaining filter stability.

The elliptic filter is chosen here for post MAF processing of the field quantities. This filter was optimally designed to an order, n of 4. The filtered data of Fig. D.13 show that a smooth, ripple-free low frequency signal is obtained. Figure D.14 shows the frequency response of the filtered field quantities given in Fig. D.13.

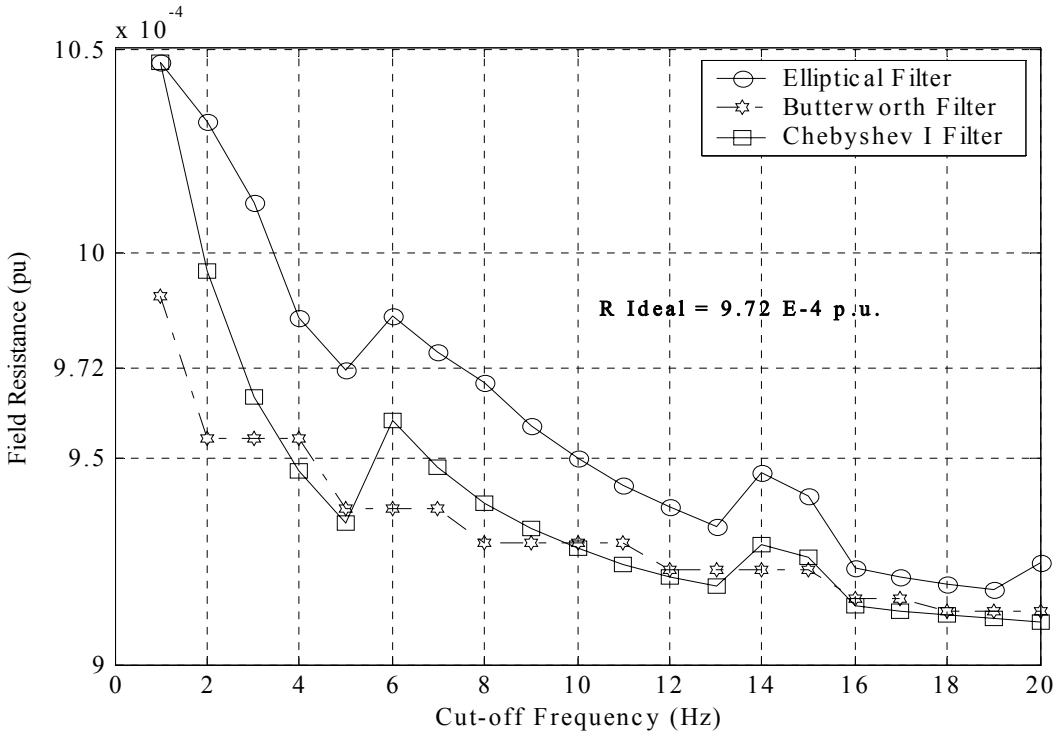

Fig. D.12 Filter performance comparison for different cutoff frequencies

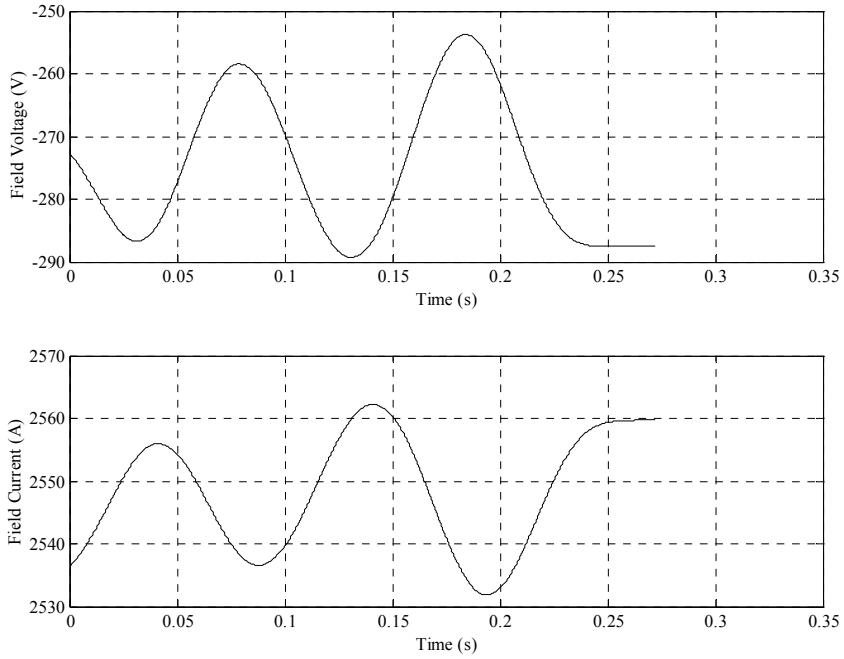

Fig. D.13 Field quantities after 500-point moving average followed by fourth-order elliptic filtering at 20 Hz cut-off and 200 Hz stop band frequencies

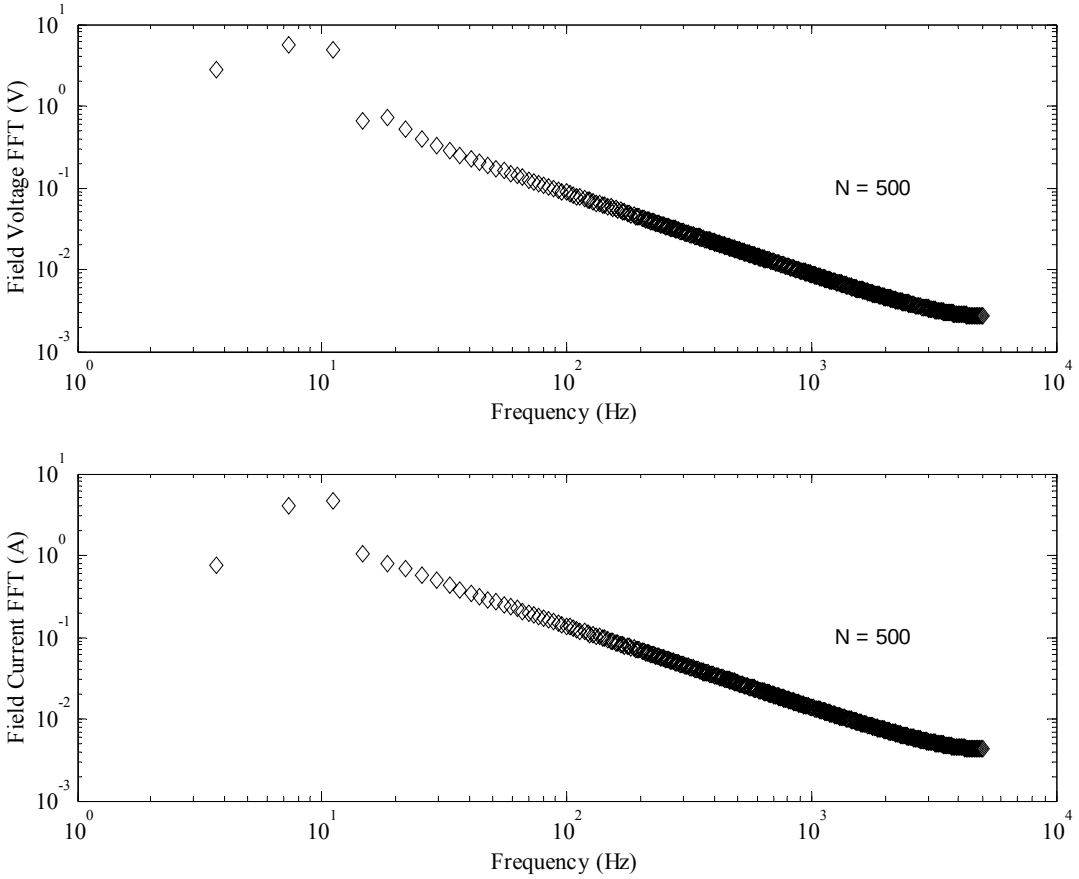

Fig. D.14 Frequency response of field current and voltage after filtering with a moving average filter and elliptic filter

An alternate strategy to obtain the same results as those from the MAF and elliptic filter combination is to use the IIR type filters with stringent cutoff conditions. The results obtained using an elliptical filter with cut-off at 12 Hz are shown in Fig. D.15. The IIR filters designed to obtain results such as these are relatively high order (around $n \sim$ 8-10). This plot shows the loss of the initial samples due to "the slow start" of the filter. Thus, the first approach of using a 500-point moving average filter followed with a classical IIR filter is found to be more effective.

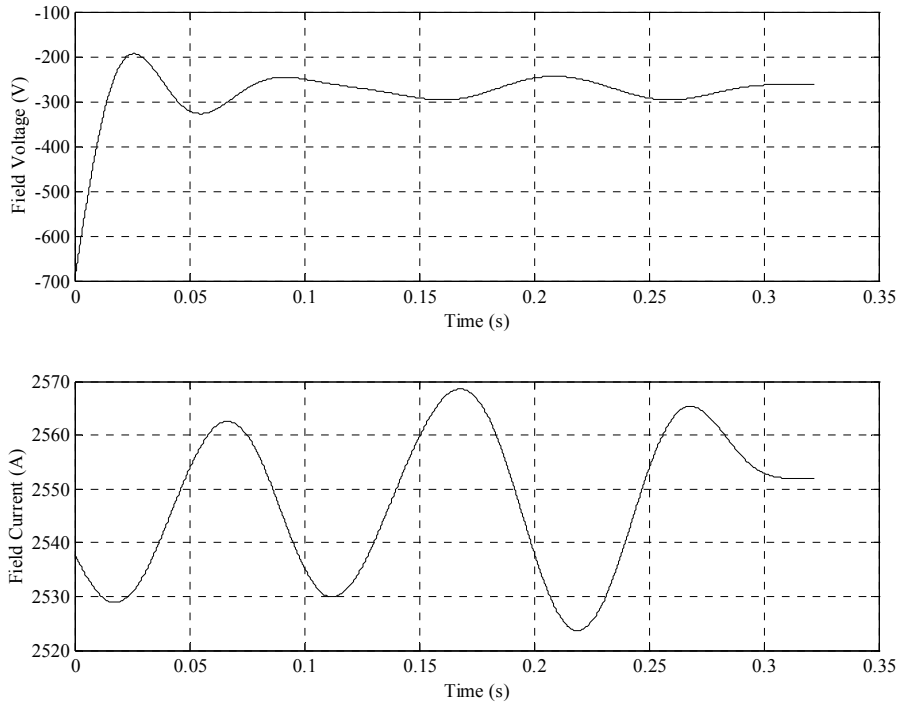

Fig. D.15 Filtered field quantities using eighth-order elliptic filter at 12 Hz cut-off and 100 Hz stop band frequencies

Phase Voltage and Current Data

Plotting the field quantities provided considerable insight regarding the noise present in those signals. The same approach is used to analyze the noise present in the phase quantities. Fig. D.16 shows the phase *A* voltage and current, which are representative of all three phases. The corresponding frequency response plots are shown in Fig. D.17. These plots fail to yield any valuable information, which would help in the investigation of the noise influence on the signal.

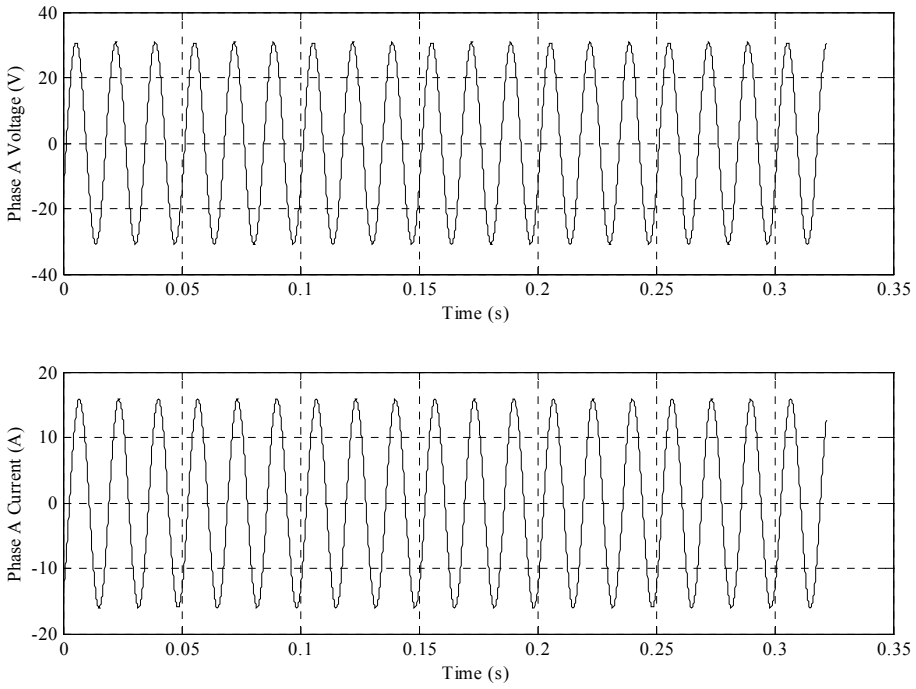

Fig. D.16 Time domain plots for phase A current and voltage

Fig. D.17 Frequency response of phase A current and voltage

Recall that before the phase quantities can be filtered, they are passed through Park's transformation. An examination of Park's transformation shows that the 60 Hz fundamental components in a signal are converted into a non-oscillating signal with frequency 0 Hz. Further, higher order harmonics are transformed into low frequency variations in the output signal.

To investigate the phase quantities for the presence of noise Park's transformation is first applied to the data. The time domain plots of transformed phase voltage and current (v_d and i_d) are shown in Fig. D.18. Figure D.19 shows the frequency response of the transformed quantities.

Figures D.18 and D.19 show that the transformed quantities are not DC; this indicates the presence of noise in the original data. Close examination of the Fig. D.18 shows that the transformed phase quantities have a dc component, which is biased by a ramp signal. Also like the field quantities, the phase quantities have a definite low frequency component of around 10-12 Hz. Unlike the field voltage the transformed phase voltage is seen to have a spike. For successful implementation of the moving average filter, the spike is first eliminated using the bad data rejection algorithm.

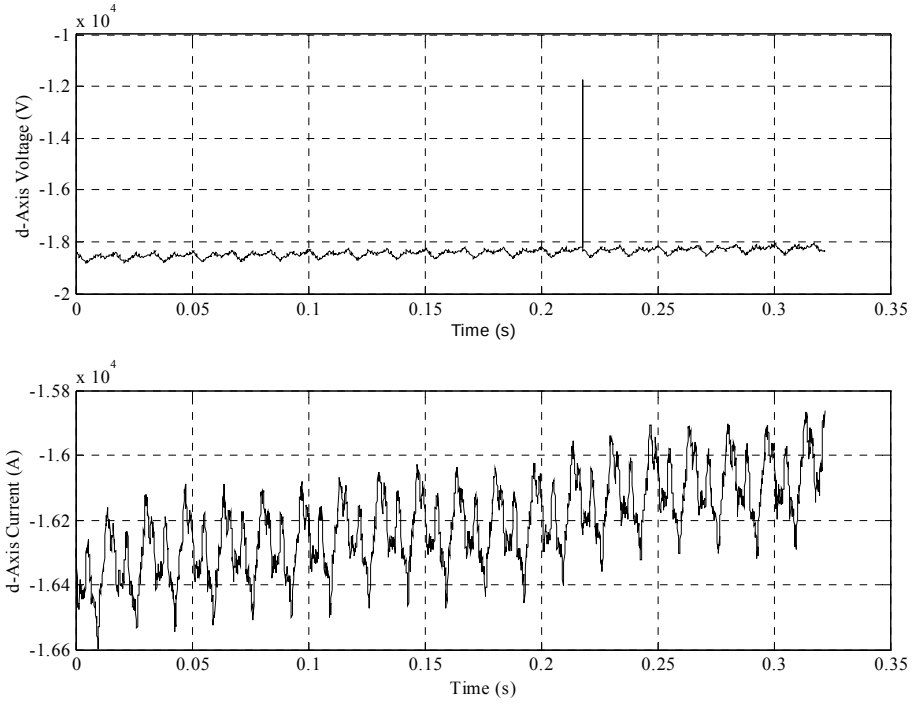

Fig. D.18 Time domain plots for the d-axis voltage and current

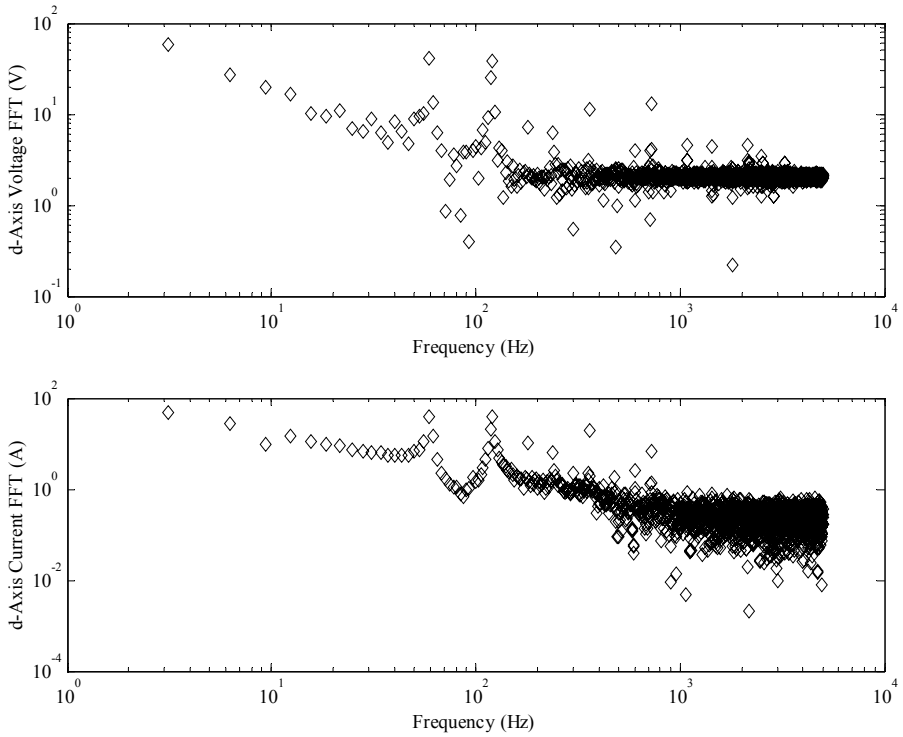

Fig. D.19 Frequency response in field current and voltage plots indicating the presence of noise and bad data

Filtering of Phase Quantities

As seen in the previous section, the slowly moving component around the dc signal has to be preserved while filtering out the periodic high frequency noise. Also, the fact that the current quantity derivatives are required for the estimator, as mentioned earlier, the filtered signals should be smooth.

As seen in the field measurements, the low frequency signals have a period of around 0.101 seconds, thus by setting the window length of the moving average to around 500 points, the high frequency distortions can be removed. The moving average filtered signals are shown in Fig. D.20. There is a small ripple even after the application of the MAF. This small ripple content remaining in the signals is eliminated using an elliptic filter set to around a 12 Hz cut-off, similar to the case of the field filtering. The results are shown in Fig. D.21. Likewise, *0* and *q* axes quantities, being similar to the *d*-axis, receive a parallel filtering regiment to achieve the desired results.

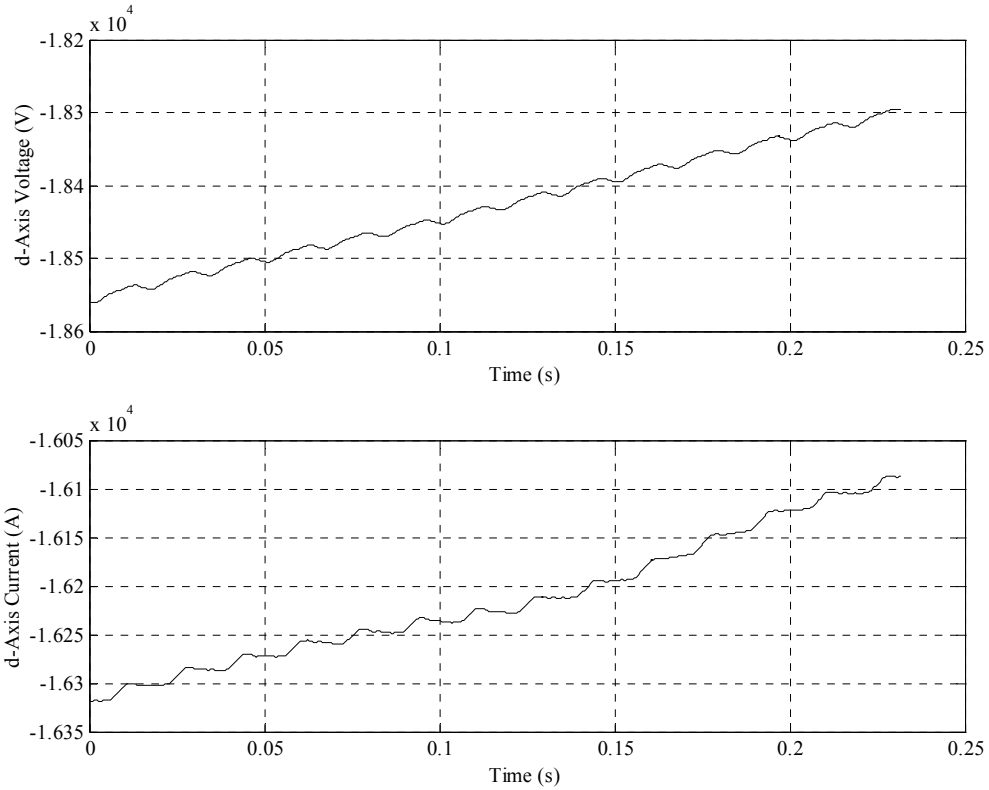

Fig. D.20 Time domain plots for the d-axis quantities (transformed phase quantity) after 500 point moving average filter

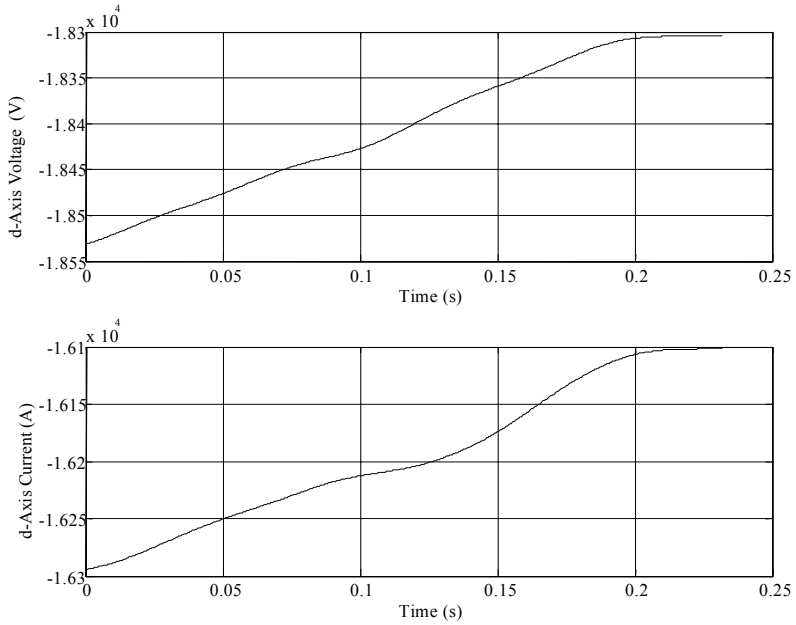

Fig. D.21 Transformed phase quantities after 500-point moving average followed by fourth-order elliptic filtering at 20 Hz cut-off and 200 Hz stop band frequencies

D.13 Estimated and Expected Results

To provide a quantitative means of indicating the performance of the filter, both filtered and raw data are passed through the estimator. The estimator has the capability of determining multiple parameters. Some results from analyzing these data are given in Table D.2. Those results show that the estimation error after filtering the components is reduced. The improvement in the L_{AQ} estimation, suggests that the estimator accuracy can be improved by designing effective filters.

Table D.2 Results before and after filtering the data sets

All values in per unit		Before Filtering		After Filtering	
Parameter	Actual	Estimate	Error	Estimate	Error
L_{AD}	1.64	1.2611	23.1%	1.2647	22.8%
L_{AQ}	1.56	1.516	6.1%	1.5375	1.14%
r_F	8.454e-4	8.1472e-4	3.6%	8.34e-4	0.89%
R	0.0046	0.1487	3132%	-0.012	377%

D.14 Summary

The project involves the implementation of the designed system in a graphical user interface (GUI). The reported results were obtained using MATLAB; but the data processing algorithm has to be converted into C++ code to implement the GUI. The GUI is expected to provide the user the option of choosing the type of filtering.

Table D.2 shows that designing more accurate filters can reduce the error in the estimated quantities. The phase filtering has to be improved to obtain better results.

Appendix E Zero Phase Filtering and Park's Transformation

E.1 Introduction

This appendix describes data processing of synchronous generator current and voltage measurements, which are used to estimate the machine parameters via Park's transformation. The data preprocessing employs infinite impulse response (IIR) digital filters. The challenge is to filter the measurement data while preserving the phase information within the ac voltage and current. This problem is addressed by converting the phase quantities into a time-invariant frame of reference using Park's transformation. The influence of Park's transformation on higher harmonics is analytically studied here to track the conversion of the harmonics into the transformed domain. Park's transformation is analyzed for positive, negative and zero sequence inputs of different frequencies under balanced and unbalanced conditions. Strategies using filters before and/or after Park's transformation are applied to simulation as well as operational generator data from an electric utility. Results demonstrate that the machine parameter estimation error is reduced from the application of the digital filtering.

The work shown in this appendix is essentially that of reference [68].

E.2 Measured Data Processing Block

Current and voltage data were sampled from four synchronous generators. Data were obtained from machines located at the Four Corners Generating Station and the Redhawk Generating Station of Arizona Public Service Company. The measurement system for data collection is depicted in Fig. E.1, and a brief description follows. The generator, the object of the parameter estimation, draws DC field excitation (v_f and i_f) from a three-phase six-pulse rectifier. Both the field and phase quantities (voltage and current) are measured using a Digital Fault Recorder (DFR). These quantities are to be processed in the estimator. However, the data obtained from the DFR need to be preprocessed in order to obtain accurate estimates. This is achieved in the measured data processing block, which includes Park's transformation.

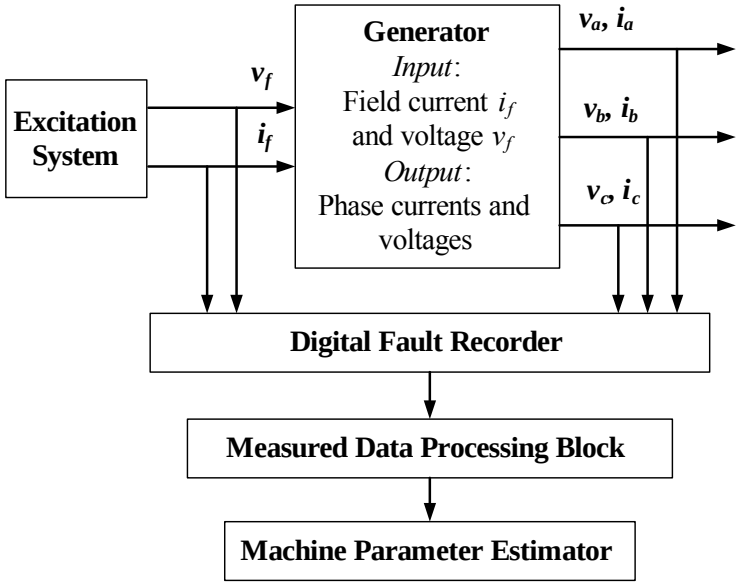

Fig. E.1 Block diagram of the generator, the data measurement using a digital fault recorder (DFR), and the data processing system

This paper details the design of this measured data processing block. Classical Infinite Impulse Response (IIR) filters and moving average filters, implemented as digital filters isolate the signal information from the noisy measurements. Park's transformation is used as a data analysis and processing tool for the phase signals.

The filtering problem can be divided into two parts, namely, field filtering and phase filtering. The filtering process as a whole can be perceived from the schematic in Fig. E.2. The requirement for field filtering is more easily defined. The generator field excitation is DC in nature; hence, the required signal information is carried by the 0 Hz frequency component. The DC component can be isolated from the noise using a simple low-pass elliptic filter in conjunction with a moving average filter.

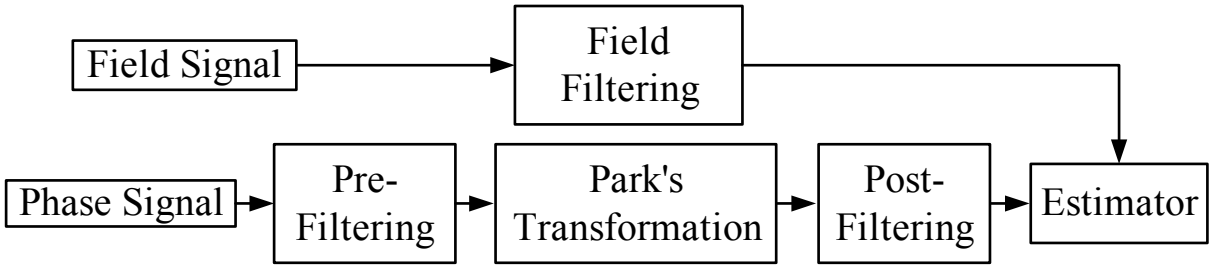

Fig. E.2 Schematic showing strategy for phase and field filtering

The phase signal filtering is the more interesting case, where we define the filtering requirements as:

1. The phase signal has magnitude and phase components, which both should be preserved while processing the data. However, the IIR filters distort the phase information of the signal, and hence, cannot be applied directly.
2. For a phase signal, the information-carrying component is the synchronous (60 Hz) frequency. To isolate this signal, a sharp band pass filter has to be implemented, thus increasing the complexity of the design.

The above-mentioned problems can be solved effectively by considering the strategy shown in Fig. E.2. The block diagram shows that for phase signal filtering, the signal could potentially be filtered either before or after Park's transformation. Pre-filtering involves application of IIR filters before Park's transformation such that fewer harmonic frequencies enter the transformed domain. If pre-filtering is employed, then a methodology, such as zero-phase filtering described in Section E.3, must be instituted.

In Park's transformation, the phase quantities are transformed to a rotating frame of axis. The required 60 Hz component is thus transformed to a 0 Hz frequency. In the case of post-filtering, the phase filtering effort simplifies to one similar to that of field filtering, that is, a low-pass filter applied after Park's transformation.

However, there is an issue with the post-filtering scheme. The original phase signal is not a pure 60 Hz sinusoid, it has higher frequency components, which can be termed as noise, and the three phases may not be perfectly balanced. When a signal of this nature is passed through Park's transformation, the frequency composition in the transformed domain is unknown. It is important to know the nature of the harmonic frequencies before applying filtering in the transformed domain. Hence, Section E.4 studies these harmonics in the transformed *d-q* domain. Furthermore, Section E.4 also shows that imbalance can result in the loss of parts of the original 60 Hz signal when transformed to higher order harmonics, which would (unfortunately) be removed by post filtering.

E.3 Zero-phase Filtering Technique

The classical IIR filters used in this project are the standard filter functions from the literature. However, these filters have been implemented here in a special manner so that the algorithm results in the most effective filtering. Specifically, IIR filters are nonlinear in nature; they tend to distort the phase information of a signal. This is an important issue while performing the phase signal filtering. To avoid this distortion, the IIR filters can be applied as zero-phase filters; this is essential for pre-Park's transform filtering.

Zero-phase filtering involves forward and then backward filtering of the same signal. The filtering process is shown in Fig. E.3. The filtering is done in such a way that the phase changes due to forward and backward filtering cancel out each other, while the magnitude of the filter is squared. This is analytically demonstrated below.

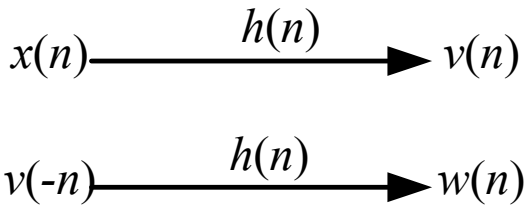

Fig. E.3 Zero-phase filtering system

In Fig. E.3 the input signal $x(n)$ is processed by a filter with impulse response given by $h(n)$. The (forward) filtered signal is designated by $v(n)$

$$v(n) = h(n) * x(n)$$

Using Z-domain representation

$$V(z) = H(z) \cdot X(z)$$

This is the forward filtering. Now, the forward filtered signal is reversed and re-filtered by the same filter (with impulse response $h(n)$) yielding a signal $w(n)$.

$$w(n) = h(n) * v(-n)$$

Equivalently in the Z-domain

$$W(z) = H(z) \cdot V(z^{-1})$$

To obtain the final filtered signal, the re-filtered signal is inverted to yield $y(n)$

$$y(n) = w(-n)$$

Equivalently in Z-domain

$$Y(z) = W(z^{-1}) \tag{E.1}$$

Using the Flip Theorem, the expression given in Equation (E.1) can be represented as follows

$$\text{if} \quad w(n) \xrightarrow{Z} W(z),$$

$$\text{then} \quad w(-n) \xrightarrow{Z} W(z^{-1}), \quad \text{and}$$

$$Y(z) = W(z^{-1}) = H(z^{-1}) \cdot V(z) = H(z^{-1}) \cdot H(z) \cdot X(z)$$

On the unit circle z can be replaced by $e^{j\omega T}$

$$Y(e^{j\omega T}) = H(e^{-j\omega T}) \cdot H(e^{j\omega T}) \cdot X(e^{j\omega T})$$

Thus, it can be seen that the phase angles in the two H terms being equal and opposite to each other cancel out. Therefore, the original input signal is effectively filtered twice without any change in the phase.

E.4 Analysis of Park's Transformation

Park's transformation maps the three-phase quantities to a rotating frame of axes to obtain transformed signals which are (ideally) non-oscillating in nature. The Park's transformation equation can be represented in a form of a matrix. This transformation converts the three-phase stationary phase quantities (i_a, i_b, i_c and v_a, v_b, v_c) into three (actually two) rotating quantities (i_d, i_q, i_0 and v_d, v_q, v_0) where d, q and 0 are transformed axes on a rotating frame of reference. The idea is to convert the self-inductances into a non-oscillating frame of reference. The Park's transformation matrix is

$$P = \sqrt{\frac{2}{3}} \begin{bmatrix} \frac{1}{\sqrt{2}} & \frac{1}{\sqrt{2}} & \frac{1}{\sqrt{2}} \\ \cos(\theta) & \cos\left(\theta - \frac{2\pi}{3}\right) & \cos\left(\theta + \frac{2\pi}{3}\right) \\ \sin(\theta) & \sin\left(\theta - \frac{2\pi}{3}\right) & \sin\left(\theta + \frac{2\pi}{3}\right) \end{bmatrix}$$

where θ is given as

$$\theta = \omega t + \delta + \pi/2$$

where ω is the (synchronous) angular frequency and δ is the synchronous torque angle. The multiplication factor $\sqrt{2/3}$ is included to normalize the matrix computations. The transformation can be shown as

$$\begin{bmatrix} i_0 \\ i_d \\ i_q \end{bmatrix} = P \begin{bmatrix} i_a \\ i_b \\ i_c \end{bmatrix} \quad \text{and} \quad \begin{bmatrix} v_0 \\ v_d \\ v_q \end{bmatrix} = P \begin{bmatrix} v_a \\ v_b \\ v_c \end{bmatrix}$$

where i_{abc} and v_{abc} are the phase vectors that have to be converted to the $0dq$ axis frame. The transformed phase quantities are denoted by i_{0dq} and v_{0dq}.
At this point, Park's transformation is studied for the three sequence components: positive, negative and zero sequence. Park's equation is a linear sum of cosine products. This fact can be expressed mathematically as

$$i_0 = \sqrt{\frac{1}{3}}\left[\, i_a + i_b + i_c \,\right]$$

$$i_d = \sqrt{\frac{2}{3}}\left[i_a \cos(\theta) + i_b \cos\left(\theta - \frac{2\pi}{3}\right) + i_c \cos\left(\theta + \frac{2\pi}{3}\right)\right] \tag{E.2}$$

$$i_q = \sqrt{\frac{2}{3}}\left[i_a \sin(\theta) + i_b \sin\left(\theta - \frac{2\pi}{3}\right) + i_c \sin\left(\theta + \frac{2\pi}{3}\right)\right]$$

Essentially identical expressions also result for v_0, v_d and v_q, but for brevity are not explicitly shown.

As mentioned, the objective of this section is to analyze the behavior of Park's transformation under harmonic conditions. To generalize the calculations, n^{th} order phase quantities are considered as seen in the expression,

$$\begin{aligned} i_a &= I_a \cos[n(\omega t)]; \quad i_b = I_b \cos\left[n\left(\omega t - \frac{2\pi}{3}\right)\right]; \\ i_c &= I_c \cos\left[n\left(\omega t + \frac{2\pi}{3}\right)\right] \end{aligned} \tag{E.3}$$

Using Equation (E.3), Equation (E.2) can be represented as

$$i_d = \sqrt{\frac{2}{3}}\left\{ I_a \cos(n\omega t)\cos(\theta) + I_b \cos\left[n\left(\omega t - \frac{2\pi}{3}\right)\right]\cos\left(\theta - \frac{2\pi}{3}\right) + I_c \cos\left[n\left(\omega t + \frac{2\pi}{3}\right)\right]\cos\left(\theta + \frac{2\pi}{3}\right)\right\}$$

Using the trigonometric identity, $2\cos\alpha\cos\beta = \cos(\alpha+\beta) + \cos(\alpha-\beta)$

$$i_d = \frac{1}{2}\sqrt{\frac{2}{3}}\left\{ I_a[\cos(n\omega t + \theta) + \cos(n\omega t - \theta)] + I_b\left[\cos\left(n\omega t + \theta - \frac{2(n+1)\pi}{3}\right) + \cos\left(n\omega t - \theta - \frac{2(n-1)\pi}{3}\right)\right] + \right.$$
$$\left. I_c\left[\cos\left(n\omega t + \theta + \frac{2(n+1)\pi}{3}\right) + \cos\left(n\omega t - \theta + \frac{2(n-1)\pi}{3}\right)\right]\right\}$$

Substituting $\theta = \omega t + \delta + \pi/2$

$$i_d = \sqrt{\frac{1}{6}}\left\{ I_a\left[\cos\left((n+1)\omega t+\delta+\frac{\pi}{2}\right)+\cos\left((n-1)\omega t-\delta-\frac{\pi}{2}\right)\right]+I_b\left[\cos\left((n+1)\omega t+\delta+\frac{\pi}{2}-\frac{2(n+1)\pi}{3}\right)+\right.\right.$$
$$\left.\left.\cos\left((n-1)\omega t-\delta-\frac{\pi}{2}-\frac{2(n-1)\pi}{3}\right)\right]+I_c\left[\cos\left((n+1)\omega t+\delta+\frac{\pi}{2}+\frac{2(n+1)\pi}{3}\right)+\cos\left((n-1)\omega t-\delta-\frac{\pi}{2}+\frac{2(n-1)\pi}{3}\right)\right]\right\}$$

A similar approach for i_q (using the identity $2\sin\alpha\cos\beta=\sin(\alpha+\beta)+\sin(\alpha-\beta)$), and i_0 quantities leads to

$$i_q = \sqrt{\frac{1}{6}}\left\{ I_a\left[\sin\left((n+1)\omega t+\delta+\frac{\pi}{2}\right)+\sin\left((n-1)\omega t-\delta-\frac{\pi}{2}\right)\right]+I_b\left[\sin\left((n+1)\omega t+\delta+\frac{\pi}{2}-\frac{2(n+1)\pi}{3}\right)+\right.\right.$$
$$\left.\left.\sin\left((n-1)\omega t-\delta-\frac{\pi}{2}-\frac{2(n-1)\pi}{3}\right)\right]+I_c\left[\sin\left((n+1)\omega t+\delta+\frac{\pi}{2}+\frac{2(n+1)\pi}{3}\right)+\sin\left((n-1)\omega t-\delta-\frac{\pi}{2}+\frac{2(n-1)\pi}{3}\right)\right]\right\}$$

$$i_0 = \sqrt{\frac{1}{3}}\left\{ I_a\cos[n(\omega t)]+I_b\cos\left[n\left(\omega t-\frac{2\pi}{3}\right)\right]+I_c\cos\left[n\left(\omega t+\frac{2\pi}{3}\right)\right]\right\} \qquad \text{(E.4)}$$

It should be noted that for n = 1, 4, 7…, the expression in Equation (E.4) represents positive sequence quantities, while for n = 2, 5, 8…, the formula represents negative sequence quantities. Consequently, a derivation is performed below for each of the three sequences.

E.5 Processing of Harmonics of Distinctive Sequence

Positive Sequence Harmonics

For a positive sequence harmonic signal, the phase sequence is i_a-i_b-i_c. For a perfectly balanced case

$$I_a = I_b = I_c = I \quad \text{and} \quad I_a + I_b + I_c = 3I$$

For balanced signals with positive sequence harmonic, the cosine terms in Equation (E.4) with frequencies of the order (n+1) are spaced 120° and are eliminated due to their balanced nature, while the components with frequencies of order (n–1) are preserved and appear in the transformed domain as

$$i_0 = 0$$

$$i_d = \sqrt{3/2}\ I\cos[(n-1)\omega t-\delta-\pi/2]$$

$$i_q = \sqrt{3/2}\ I\sin[(n-1)\omega t-\delta-\pi/2]$$

From the above formulae it can be seen that the fundamental frequency, 60 Hz (n = 1) is converted into a DC signal. Similarly, each high frequency component is reduced by 60 Hz as shown in Table E.1.

Table E.1 Park's transformation output frequency for positive sequence inputs

Original Phase Quantities		Transformed Quantities			
		Balanced Condition		Unbalanced Conditions	
n	Frequency (Hz)	n–1	Frequency (Hz)	n+1	Frequency (Hz)
1	60	0	0	2	120
4	240	3	180	5	300
7	420	6	360	8	480
10	600	9	540	11	660

Equation (E.4) can also be analyzed for the unbalanced case. An imbalance will cause the $(n+1)^{th}$ terms to remain in the expression, although these $(n+1)^{th}$ frequency components will be of small magnitude. Table E.1 also gives the frequency distribution for the unbalanced case.

Negative Sequence Harmonics

For a negative sequence harmonic signal, the phase sequence is i_a-i_c-i_b. For the balanced negative sequence harmonic signals, the cosine terms in Equation (E.4) with frequencies of the order (n–1) are spaced 120° and are eliminated due to their balanced nature, while the components with frequencies of order (n+1) are preserved and appear in the transformed domain as

$$i_0 = 0$$

$$i_d = \sqrt{3/2}\, I \cos\left[(n+1)\omega t + \delta + \pi/2\right]$$

$$i_q = \sqrt{3/2}\, I \sin\left[(n+1)\omega t + \delta + \pi/2\right]$$

From the above formulae, the negative sequence components are increased by +60 Hz in the transformed domain. Accordingly, the high frequency components are transformed as shown in Table E.2.

Table E.2 Park's transformation output frequency for negative sequence inputs

Original Phase Quantities		Transformed Quantities			
		Unbalanced Conditions		Balanced Condition	
n	Frequency (Hz)	n–1	Frequency (Hz)	n+1	Frequency (Hz)
2	120	1	60	3	180
5	300	4	240	6	360
8	480	7	420	9	540
11	660	10	600	12	720

For negative sequence unbalanced signals, reasoning similar to that for the positive sequence can be applied. It can be concluded here that an imbalance causes the $(n\text{-}1)^{th}$ term to remain in the equation, although the $(n–1)^{th}$ frequency components will be of a small magnitude. Table E.2 also gives the frequencies for an unbalanced case.

Zero Sequence Harmonics
For a zero sequence harmonic signal, all phases are in the same direction. For a balanced zero sequence harmonic, all the cosine terms in Equation (E.4) are spaced 120° apart and are eliminated due to their balanced nature, hence for this case, zero sequence components do not appear in the transformed domain.

For the unbalanced case, the resulting zero sequence components will be a vector addition of three cosine terms. Thus, the frequency of the zero axis component is same as before transformation.

E.6 Simulation Results

To quantify the amount of allowable imbalance, simulated data were generated where the imbalance was systematically increased by 1% of the signal amplitude. The simulated signals were 60-Hz phase voltages of magnitudes: v_a, v_b and v_c where $v_b = a \cdot v_a$ and $v_c = b \cdot v_a$. The imbalance factors a and b were chosen such that a varies from 1.00 to 1.05, and b ranges from 1.00 to 0.95.

Table E.3 shows the component frequencies and their magnitudes in the transformed domain. The following observations are made from the tabulated values:

- For an ideal case, with zero imbalance, the factors a and b are unity. In this case, the phase signals are transformed into d, q and 0 axis components of exclusively zero frequency; and the magnitude of the 0- axis component is negligible.
- Further imbalance is introduced in the phases of the fundamental, as shown in Table 3. The 60 Hz fundamental of the phase signals is divided into two parts, a DC and a

120 Hz component. This 120 Hz component carries a small part of the signal information.

- Increase in the imbalance factors increases the contribution to the 120 Hz component in the transformed domain; this is because the magnitude of the 120 Hz component is proportional to the signal imbalance. Similarly, the zero sequence components are split into a 0 Hz and a 60 Hz component.

From the above observations, it can be inferred that cases of imbalance might introduce higher frequency components (120 Hz), which cannot be termed as noise; instead, these are components carrying signal information and should be preserved. However, unless there is a huge disturbance (imbalance), Park's transformation performs the desired operation without any discrepancies.

E.7 Implications to Post Transform Filtering Strategy

It can be seen from the above discussion that the frequencies are shifted in the transformed domain. A challenging case occurs for post filtering of the negative sequence harmonic frequency. From Table E.2 it can be seen that the negative sequence harmonic frequency is shifted by +60 Hz. Thus, to eliminate a fifth-order harmonic (300 Hz), the filter cutoff should be set below 360 Hz. Under balanced circumstances, a filter with cutoff at 330 Hz will suffice the requirement, however under unbalanced circumstances the 300 Hz harmonic is split into 240 Hz and 360 Hz as seen in Table E.2. Hence, for effective elimination of the fifth harmonic, the filter cutoffs would have to be reduced to less than 240 Hz.

Furthermore, under unbalanced conditions the signal information carried by the 60 Hz component is split into the DC and the 120 Hz components (as seen in Table E.1) which would have been only DC under balanced conditions. Moreover, Table E.3 shows that the loss in signal information is proportional to the amount of imbalance. Thus, the post transform filter cutoffs must be chosen carefully so that no signal information is lost.
Taking all the cases into consideration it can be concluded that a strategy involving both pre and post-filtering will be beneficial. Thus the signal should undergo pre-filtering before Park's transformation followed by post-filtering as shown in Fig. E.2. This filtering strategy is proposed by the paper and is studied in the next section.

Table E.3 Magnitude of transformed quantities for different unbalanced cases

Imbalance factors	*d* axis		*q* axis		*0* axis	
	Frequency (Hz)	Magnitude	Frequency (Hz)	Magnitude	Frequency (Hz)	Magnitude
$a = 1.00$	0	612.37	0	1060.7	0	~0
$b = 1.00$						
$a = 1.01$	0	1133.75	0	462.29	0	0.077
$b = 0.99$	120	4.85	120	9.47	60	4.22
$a = 1.02$	0	1133.21	0	464.19	0	0.15
$b = 0.98$	120	7.62	120	8.43	60	8.43
$a = 1.03$	0	1133.75	0	468.99	0	0.23
$b = 0.97$	120	10.02	120	10.13	60	12.64
$a = 1.05$	0	1131.10	0	468.83	0	0.39
$b = 0.95$	120	18.482	120	10.07	60	21.07

E.8 Phase Signal Filtering and Results

The three IIR filters investigated in this research were Butterworth, Chebyshev type I, and elliptical. Different tests were performed to determine the best filtering strategy for this application. After performing preliminary tests with these filter types to analyze their performance in the frequency domain, the elliptical filter was chosen.

Data obtained from operational generators were tested with the proposed filtering strategies. After testing with these strategies, the filtering strategy involving both pre and post filtering was seen to be giving the best results. The effect of filtering can be visualized graphically through plots, and quantitatively through the estimation results. This section uses the *d*-axis voltage data to exemplify the filter application. Figure E.4 shows the time domain plot of the *d*-axis voltage data as obtained from Park's transformation without any pre-filtering.

The synthetic data analysis indicates the importance of pre-filtering the phase data. Pre-filtering would prevent higher harmonic noise from entering Park's matrix which causes a pre-emptive elimination of the harmonics in the transformed domain. The zero-phase filtering strategy was therefore implemented to carry out phase signal filtering such that the phase information of the signal is not distorted. However, zero-phase filtering is not perfect; after filtering, a small distortion is evident in the phase response near the cutoff frequency, hence to prevent such phase distortions, cutoff frequencies are set to eliminate harmonics of order 5 and higher.

As an example of pre-filtering, the sampled data after zero-phase filtering are presented in Fig. E.5. This signal is input to Park's matrix. After the pre-filtered signal is transformed, post-filtering is implemented using an elliptical filter of order 4. The results of filtering the transformed phase data can be seen from Fig. E.6.

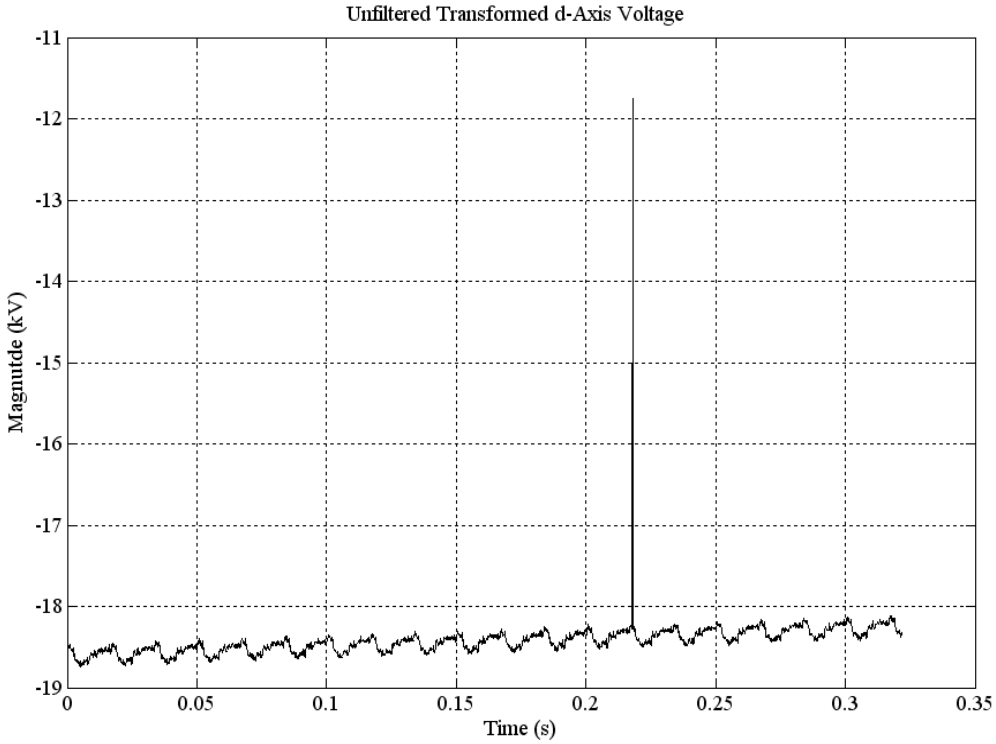

Fig. E.4 Magnitude of d-axis voltage from Park's transformation without filtering

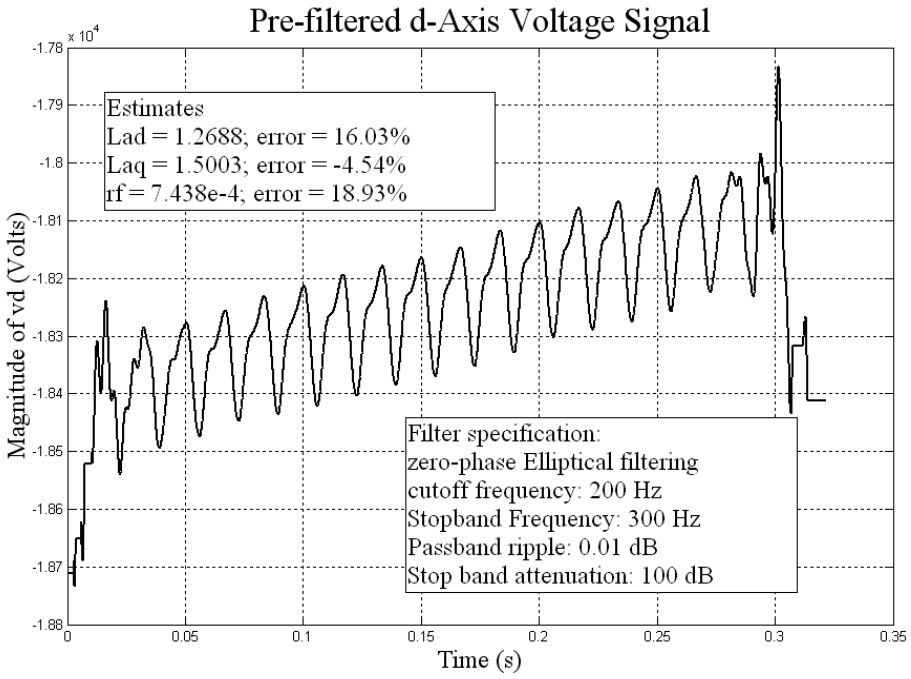

Fig. E.5 Pre-filtered phase data showing filter specifications and magnitudes of the estimates

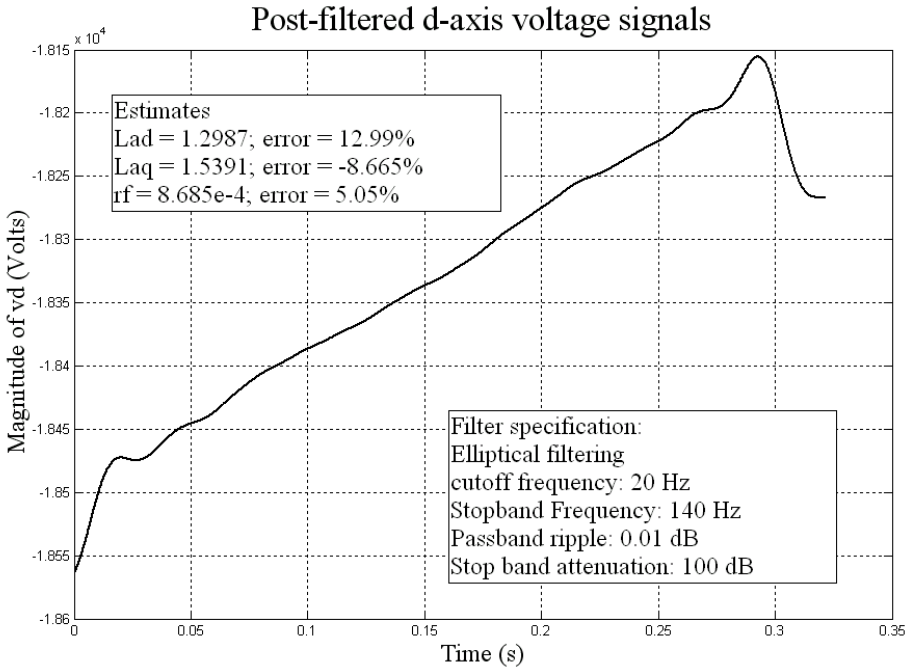

Fig. E.6 Post-filtered phase data showing filter specifications and magnitudes of the estimates

The combined effect of pre and post filtering can be seen from Table E.4, which shows the parameter estimates before and after the application of the filtering algorithm. The data samples were obtained from the first Four Corners machine (FC1). The estimates are compared to the ideal parameter values as provided by the manufacturer. Table E.4 demonstrates that the designed filtering algorithm improves the L_{AD} estimate quality at a minimal increase in the error of L_{AQ}. Additionally, the difference between the manufacturer-provided field resistance (r_f) and the estimate with signal filtering is less than half the difference without filtering. Eight other data sets were tested with the same filtering procedure, and the results were similar to those of Table E.4.

Table E.4 Results with pre- and post-filtering of data set FC1

Parameter	Manufacturer Value	Without Filtering		With Filtering	
		Estimate	Difference	Estimate	Difference
L_{AD} (p.u.)	1.5051	1.2504	17%	1.2987	13%
L_{AQ} (p.u.)	1.4332	1.5391	–7.4%	1.5387	–8.7%
r_f (mΩ)	0.0845	0.0809	11.8%	0.0868	5.5%

L_{AD} is the direct axis magnetizing mutual inductance,
L_{AQ} is the quadrature axis magnetizing mutual inductance, and
r_f is the field winding equivalent resistance.

E.9 Conclusions

This research successfully defines the application of digital signal processing techniques to power systems measurements. Park's transformation is used as a signal processing tool, rather than an analysis tool to perform effective phase signal filtering. Detailed analysis of the behavior of Park's transformation under the influence of higher harmonic inputs and unbalanced input was studied and documented as part of this research. Moreover, an accurate and effective digital filtering technique was designed and tested to provide filtering for the current and voltage signals obtained from a synchronous machine.

The phase signals that were tested with this algorithm were relatively noise-free, and therefore, resulted in only a marginal improvement in the quality of estimates. Applicability of the filtering algorithm should be tested for more data sets including some cases where there is a large amount of harmonic noise.

Appendix F The Brushless Exciter Case

F.1 An Approach to Brushless Exciter Models and Identification

Paper [47] by Heydt aims to identify synchronous generator parameters from on-line data measured at the terminals of the machine using the generator field current I_f and field voltage. An observer for estimation of synchronous generator damper currents is designed and implemented by equations (14)~(15) in [47]. However, for a brushless excitation system shown as Figure F.1, these two values cannot be directly measured. Accordingly, a key issue for a brushless exciter is how to estimate these unknown values and how to relate these values to other measurable quantities such as through the current from the exciter filed winding. Our approach can detect generator's potential internal faults to avoid the potential catastrophe caused by failure of brushless exciters, which are typically installed on large generation units. In addition, we can use these two estimated values as pseudomeasurement values to plug in the observer equation [47] to estimate generator damper currents.

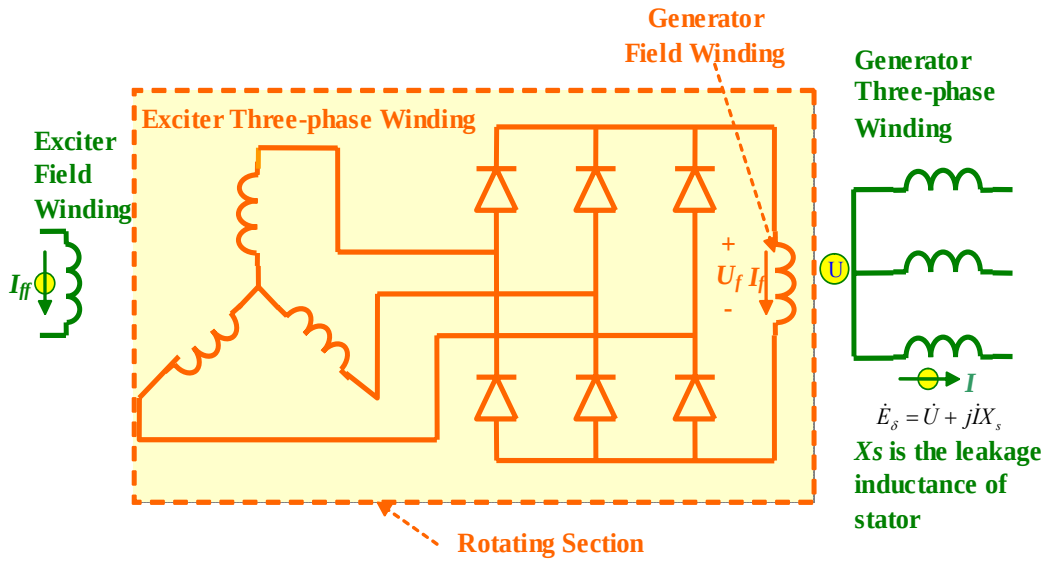

Fig. F.1 A brushless excitation system

Some difficulties are:

- It is difficult to directly measure and monitor the data on the rotor side.
- The characteristic fault signal may be overlapped by a big noise, and thus the SNR (Signal-to-Noise) is rather low. Moreover, with different types of faults, the fault signals may locate at different frequency bands, thus it is difficult to detect the signal by common filtering technique.

- The characteristic of brushless exciter fault is very complex. Fault at different locations may cause some similar featured values at stator side. So we cannot identify and locate different types of internal faults by using one or two feature values.

Accordingly, it is necessary to develop a scheme to detect the internal faults of brushless exciters. Accordingly, design a method to estimate generator's field current and voltage values. Based on estimated values, develop a scheme to detect the possible internal fault of the brushless exciter system by relating the field current and voltage to the measurable quantity from the exciter field winding. Details about this work will be addressed as follows:

A method to estimate field current and voltage of a generator

An indirect measure method is usually used in literature [22 - 24], here a brief review of it will be given before further discussion: place a search coil (inductor) in the stator slots of the exciter alternator (locate the coil in the *q* axis), then we can measure the sixth harmonic component of the voltage induced in the coil. During normal operation, the magnitudes of the sixth harmonics are in proportion to the armature current of exciter alternator, which means that it is also in proportion to generator's field current If, so we can measure If indirectly by the measure of magnitude of the sixth harmonics component of the voltage induced in the coil.

The above idea is based on the following assumptions: the field windings of generator is a big induction load of the exciter alternator, thus the current wave in the armature windings can be taken as a square wave, which can be decomposed as a series of odd harmonics. With the Y-connection of the armature windings of exciter alternator, there is no passageway for 3rd harmonics. So there only have 1st, 5th, 7th, 11th, 13th, 19th… harmonics exist in secondary armature reaction magnetic field. The 1st harmonic is stationary related to the search coil, so it will not induce voltage in the coil. The 5th, 11th, 17th … harmonics are in opposite rotation direction compared with exciter alternator, so they will induce 6th harmonics in the search coil. The 7th, 13th, 19th … harmonics are in the same rotation direction with exciter alternator, and they will also induce 6th harmonics in the search coil. With normal operating conditions, the magnitude of 6th harmonics are in proportion to the armature current of brushless ac exciter, thus also in proportion to generator's field current If. Thus we can measure If indirectly by the measure of magnitude of the sixth harmonics component of the voltage induced in the coil. Drawback of this method: this method requires installing a search coil in rotating part, thus it will make the excitation system less reliable and impose a maintenance burden. Moreover, the faults of bridge rectifier or faults between the windings of exciter will make the harmonic change and this method will no longer be accurate.

An identification method to estimate the field current

I_f is mainly influenced by armature reaction and the saturation of the magnetizing. The armature reaction is in proportion to stator current I, while the saturation effect of the magnetizing can be denoted by E_δ, here

$$\dot{E}_\delta = \dot{U} + j\dot{I}X_s$$

Xs denotes the leakage inductance of stator, $\dot{U}$ and $\dot{I}$ denote the stator voltage and current. From the characteristic curve of magnetizing saturation, we know that saturation effect is nearly in a linear relation to E_δ.

Approximate *If* as,

$$I_f = K_1 + K_2 I + K_3 E_\delta \tag{F.1}$$

With (F.1), if we can get enough samplings of *I* and *U* and I_f, we can determine K_1, K_2, K_3 by identification method. As we know, *I* and *U* can be directly measured from the stator side, so the question is how to get samplings of I_f. When generator is under maintenance, we can temporarily add a sensor to measure current and convert the current signal to a light signal, then we can do field test with different operation conditions. A receiver in stator side will capture the light signal, thus we can get the samplings of I_f. After enough samples, we can uninstall those sensor and converter from armature and use identified K_1, K_2, K_3 to estimate I_f.

Estimation of the field voltage

With the estimated I_f by using the identified model (F.1), calculate the field voltage U_f by

$$U_f = R_f I_f ,$$

here R_f denotes the resistance of the exciter windings. However, R_f will vary with average temperature T_f of exciter windings as

$$R_f = \frac{235 + T_f}{235 + T_0} R_{f0} \tag{F.2}$$

Here T_o and R_{fo} denote the average temperature and resistance of exciter windings under rated operation condition. It is difficult to measure T_f of the rotating exciter windings directly. To measure T_f, a possible way is to install a temperature sensor on the armature and transfer the temperature signal into light signal, then with the light signal receiver in the stator side we can measure T_f indirectly. However, this method need to install sensor and signal converter in armature and is difficult to maintain reliability. Moreover, the maintenance of sensor and converter is also very difficult. So here we give a simple and feasible method to

estimate T_f. We know that the temperature rise of exciter windings ΔT_f is in proportional to I_f^2

$$K = \frac{\Delta T_f}{I_f^2} = const \tag{F.3}$$

K is nearly a constant, and can be given as a parameter by the manufacturer. Therefore we can calculate the average temperature of exciter windings as

$$T_f = T_{f0} + \Delta T_f = T_{f0} + KI_f^2 \tag{F.4}$$

With (F.1), (F.2) and (F.4), calculate the field voltage as

$$U_f = R_f I_f = \frac{235 + T_{f0} + KI_f^2}{235 + T_0} R_{f0} I_f \tag{F.5}$$

F.2 Selection of Exciter Model

A brushless exciter is an alternator-rectifier exciter, as shown in Fig. F.2, and this type of exciter employs rotating rectifiers with a direct connection to the synchronous machine field thus eliminating the need for field brushes.

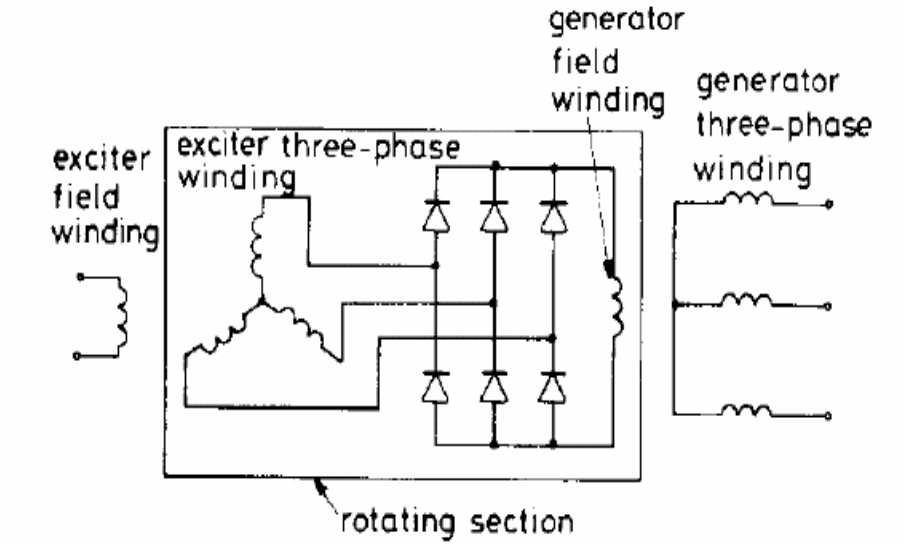

Fig. F.2 Brushless exciter-generator

The excitation system under consideration is a Westinghouse brushless excitation system (also known as the IEEE AC1A type excitation system). This is a field controlled alternator rectifier exciter. The main exciter's output is determined by the Trinistat three phase power

amplifier, whose firing angle is determined by the Trinistat firing circuit. The signal mixer generates an error signal which is fed into this firing circuit, which, in turn, determines the firing angle used. Under normal operating conditions, the output of the voltage error detector, which compares the actual terminal voltage to a specified reference voltage, establishes the signal mixer output. The main exciter field current is fed back through the damping module to produce a closed loop configuration. This helps stabilize the system and maintain a constant voltage output. The load compensator provides compensation for the transformer impedance or line drop at the output of the generator. All of these devices, together, are considered to be the pilot exciter, which supplies the field current to the main exciter.

A model suitable for simulating the performance of this exciter, using available system stability software such as ETMSP, is the IEEE standard AC1A exciter. A model of this exciter is shown in Fig. F.3. This model is linear with the exception of the rectifier operation function ($F_{EX} = f(I_N)$) and the saturation function of the main exciter ($S_E(V_E)$).

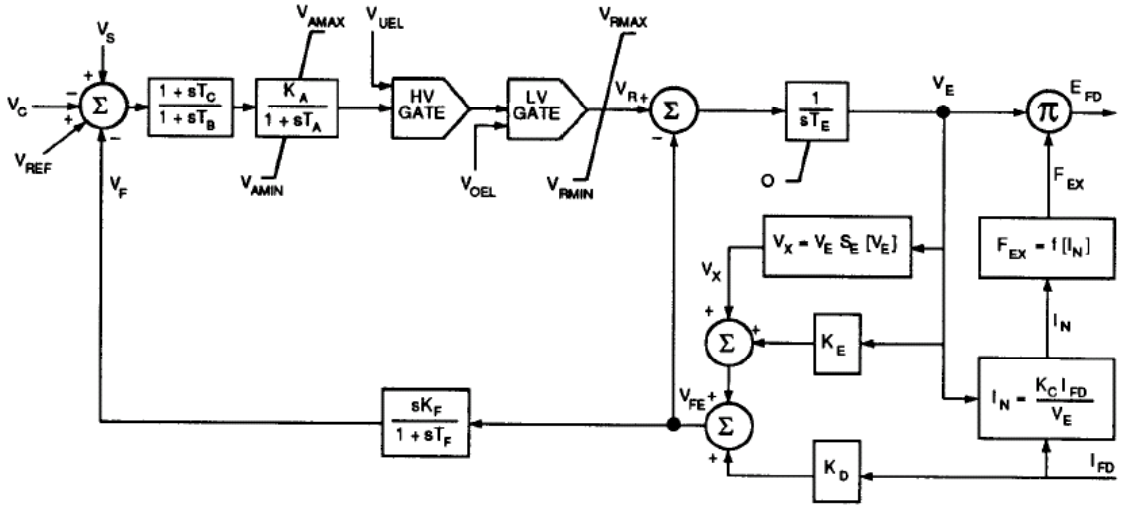

Fig. F.3 Type AC1A-alternator-rectifier excitation system

In Fig. F.2, there are 12 parameters to estimate, including T_A, T_B, T_C, T_F, T_E, K_A, K_C, K_D, K_E, K_F, a and b. The a and b parameters of the saturation function $S_E(V_E)$. The time constants, T_B and T_C, are used to model equivalent time constants inherent in the voltage regulator. The time constant T_A, and gain K_A are associated with the voltage. T_e is the time constant of the exciter block. The value of K_e reflects the setting of the shunt field rheostat. The term $F_{EX}=f(I_N)$ is the rectifier operation function. The time constant T_F, and gain K_F are associated with the damping block.

The software package ETMSP is a widely recognized tool for the simulation of the power system. It was extensively analyzed by many utility companies and is found to accurately simulate the response of actual excitation system during the open circuit operation of the generator. As a consequence, if the parameters of exciter model in ETMSP can be estimated,

then so can the actual exciter parameters. In this study, the parameter estimation process is based on estimating the parameters of exciter model in ETMSP. The ETMSP acts as the actual system to provide input-output data for parameter estimation.

F.3 Input-Output Data Collection

The first step in parameter estimation is to collect the input and output data that are physically measurable in the actual system. The measurable signals are listed in Table F.1, where E_{FD} is the exciter output voltage; I_{FD} is the exciter output current; V_R is the regulator output; V_{FE} is the signal proportional to exciter output current; V_F is the excitation system stabilizer output; V_E is the exciter voltage back of commutating reactance.

Table F.1 Measurable signals - synchronous machine instrumentation

E_{FD}
I_{FD}
V_R
V_{FE}
V_F
V_E

F.4 Parameter Estimation with Linear Functions

The brushless exciter model is built by Simulink. Its Simulink model is depicted in Fig. F.4. To effectively utilize all measurable signals and simplify the estimation process, based on the obtainable input/output signals, the whole exciter model is broken up into several parts. Each part can be described by a transfer function relating an output signal to an input signal.

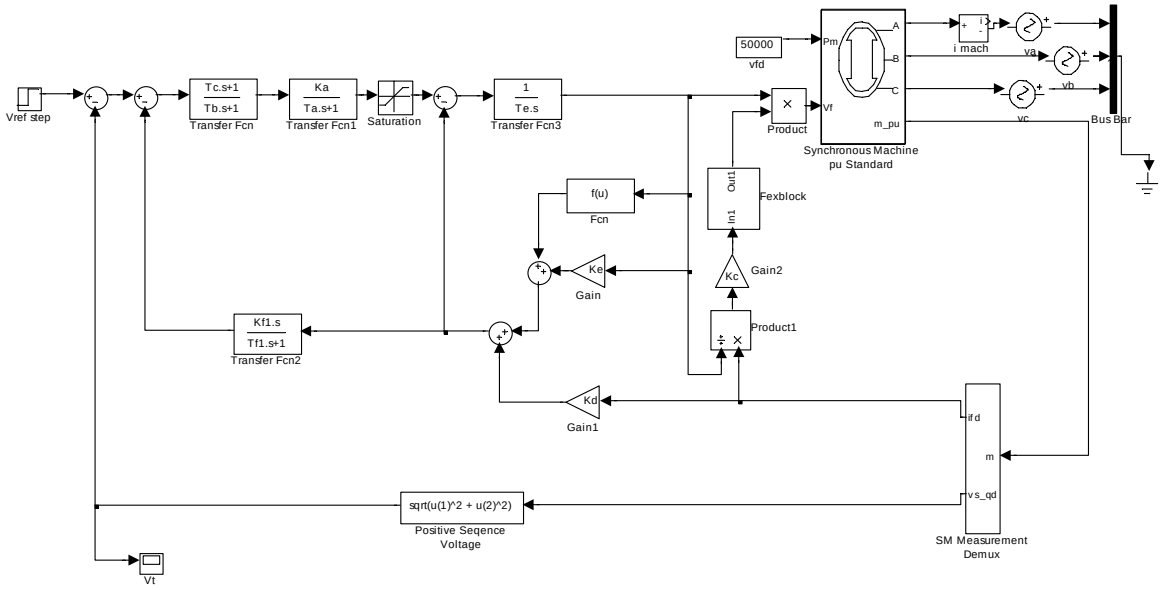

Fig. F.4 Simulink model of brushless exciter

To determine the parameters of each part (except the rectifier operation function and the saturation function of the main exciter), the least square method is employed. The task is to minimize the objective function as follows

$$J(\theta) = \frac{1}{N}\sum_{k=1}^{N}[y(k) - \hat{y}(k,\theta)]^2$$

where $y(k)$ is the measured output;

$\hat{y}(k,\theta)$ is the prediction output;

θ is the estimated parameter vector.

The state space model is used as prediction model.

$$\hat{y}(k,\theta) = A(\theta)\hat{x}(k,\theta) + B(\theta)u(k)$$

$$\frac{d\hat{x}(k,\theta)}{dt} = C(\theta)\hat{x}(k,\theta) + D(\theta)u(k)$$

$$t = kT$$

where T is the sampling period.

The minimization of J can be solved by Newton-type iterative algorithms. Beginning with initial guess, the parameter vector is updated as follows:

$$\theta^{i+1} = \theta^i + \alpha \cdot d^i$$

where α is a constant; d^i is a descent direction.

$$d^i = H(\theta^i)^{-1} \cdot g(\theta^i) \tag{F.6}$$

where $H(\theta^i)$ is the hessian matrix; $g(\theta^i)$ is the gradient vector.

F.5 Parameter Estimation with Nonlinear Functions

A common expression of the saturation function is the exponential function as,

$$S_E(E_{FD}) = a \cdot e^{b \cdot E_{FD}} \tag{F.7}$$

where a and b are constants.

For the exciter load saturation curve, only values (S_1, S_2) for two points (E_1, E_2) are provided. Based on the two points given, the following can be obtained,

$$b = \frac{\ln(\frac{E_1 \cdot S_1}{E_2 \cdot S_2})}{E_1 - E_2} \tag{F.8}$$

$$a = \frac{E_1 \cdot S_1}{e^{b \cdot E_1}} \tag{F.9}$$

All ac sources that supply rectifier circuits have an internal inductance. This inductance alters the process of commutation and causes a nonlinear decrease in output voltage as a function of rectifier current. The three-phase, full-wave bridge circuits commonly employed have three distinct modes that are determined by the rectifier load current. The rectifier regulation function, shown in Fig. F.5, is a nonlinear function in the normalized exciter load current I_N. The load current I_N is a function of the synchronous machine field current I_{FD}, the exciter voltage V_E, and the rectifier loading factor K_C.

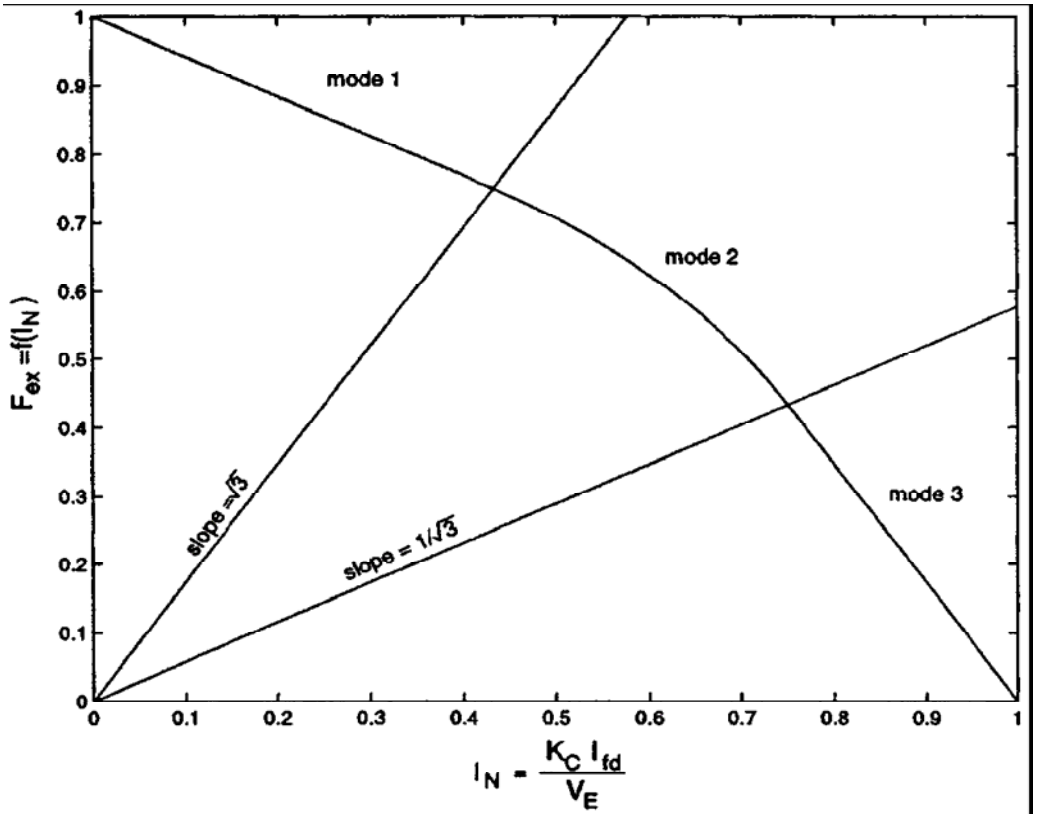

Fig. F.5 Rectifier regulation function

The three modes of operation represented by the following piecewise nonlinear equations

$$F_{EX} = 1 - 0.577 I_N \quad I_N < 0.433 \tag{F.10}$$

$$F_{EX} = \sqrt{0.75 - I_N^2} \quad 0.433 < I_N < 0.75 \tag{F.11}$$

$$F_{EX} = 1.732(1 - I_N) \quad I_N > 0.75 \tag{F.12}$$

$$I_N = \frac{K_C I_{FD}}{V_E} \tag{F.13}$$

I_N is not measurable. But the F_{EX} can be derived by

$$E_{FD} = V_E F_{EX} \tag{F.14}$$

Thus, by the iterative approach, the mode of rectifier can be determined. That yields the corresponding value for K_C.

F.6 Estimation Results

The estimation results are listed in Table F.2. The original parameters are these used by ETMSP to generate input/output data for estimation. The estimated ones are obtained by the least square method.

Table F.2 Estimation results after filtering input data

	Original	Estimated
K_A	275.0000	275.6000
T_A	0.2s	0.1996s
T_B	0.6s	0.6015s
T_C	0.4s	0.3997s
K_F	0.0400	0.0401
T_F	1.5s	1.4972s
T_E	0.6s	0.6026s
K_C	0.1300	0.1300
K_D	1.4000	1.4060
K_E	1.0000	0.9972
a	0.0360	0.0360
b	0.0068	0.0068

Using the estimated parameters, the simulated terminal voltage and field voltage are shown in Fig. F.6 and Fig. F.7 respectively. The curves labeled as "reference" are those obtained by ETSMP. The errors between reference and simulated are plotted in Fig. F.7 and Fig. 8 respectively. The maximum error is less than 6%.

F.7 A Hypothetical Example

In this concluding section, a hypothetical case is shown using data from a Chinese generator. With field test in Pinxu power plant of Anhui province, China, we got samplings of *U, I* and I_f of a generator with different operating conditions, then by the least squares method, K_1, K_2, and K_3 are identified as

$$K_1 \sim K_3 = (-0.354560,\ 0.502152,\ 0.606936)$$

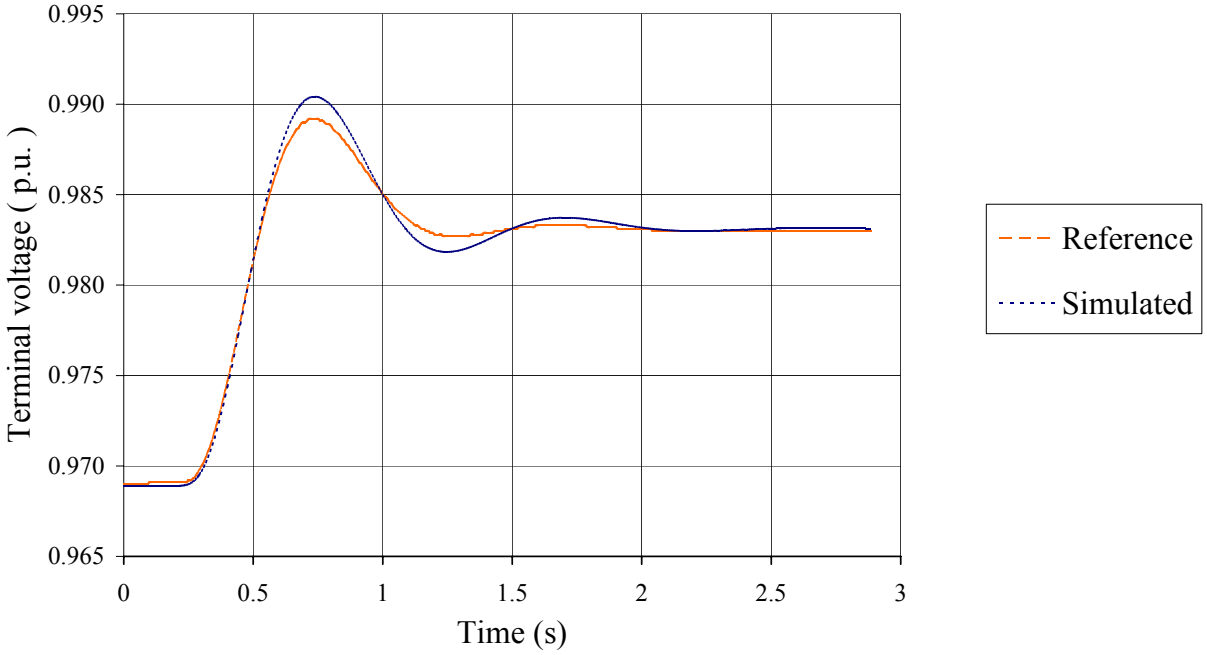

Fig. F.6 Terminal voltage

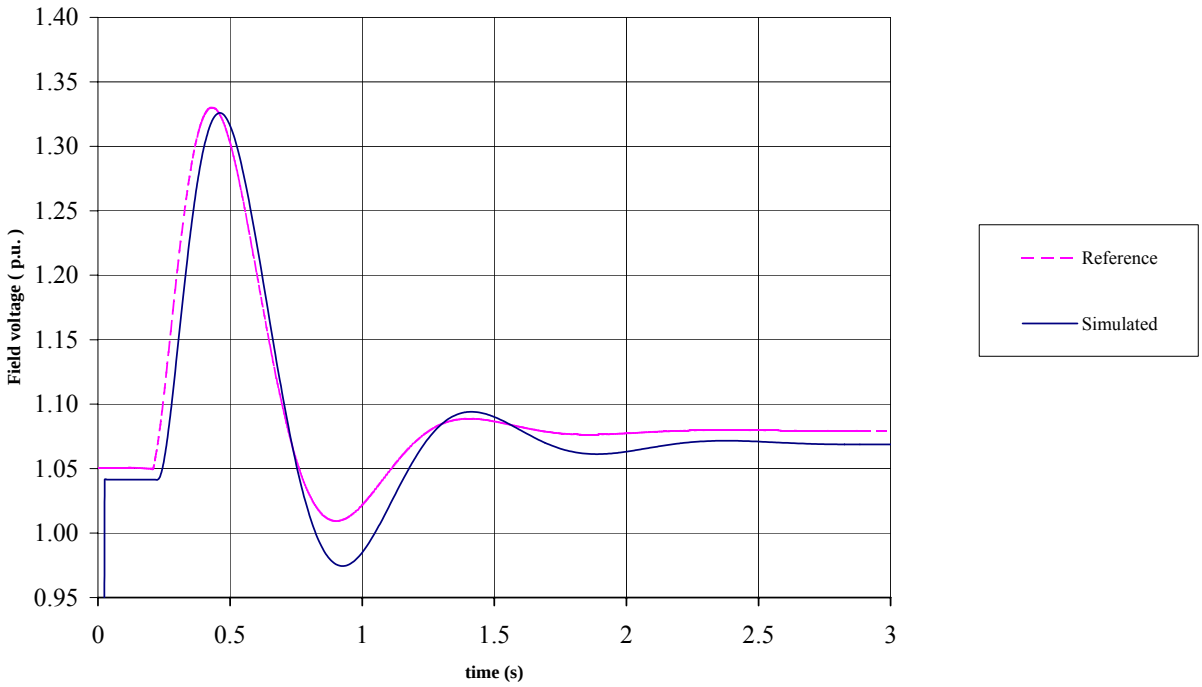

Fig. F.7 Field voltage

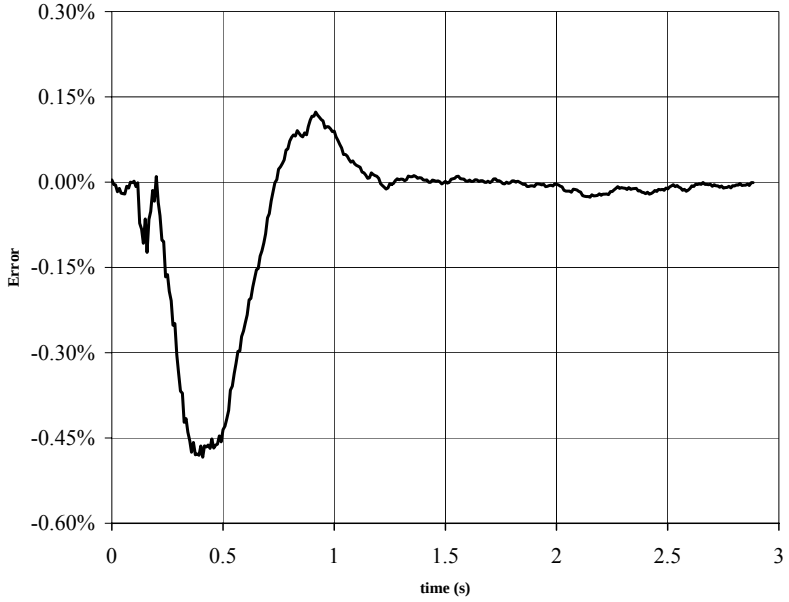

Fig. F.8 Terminal voltage error

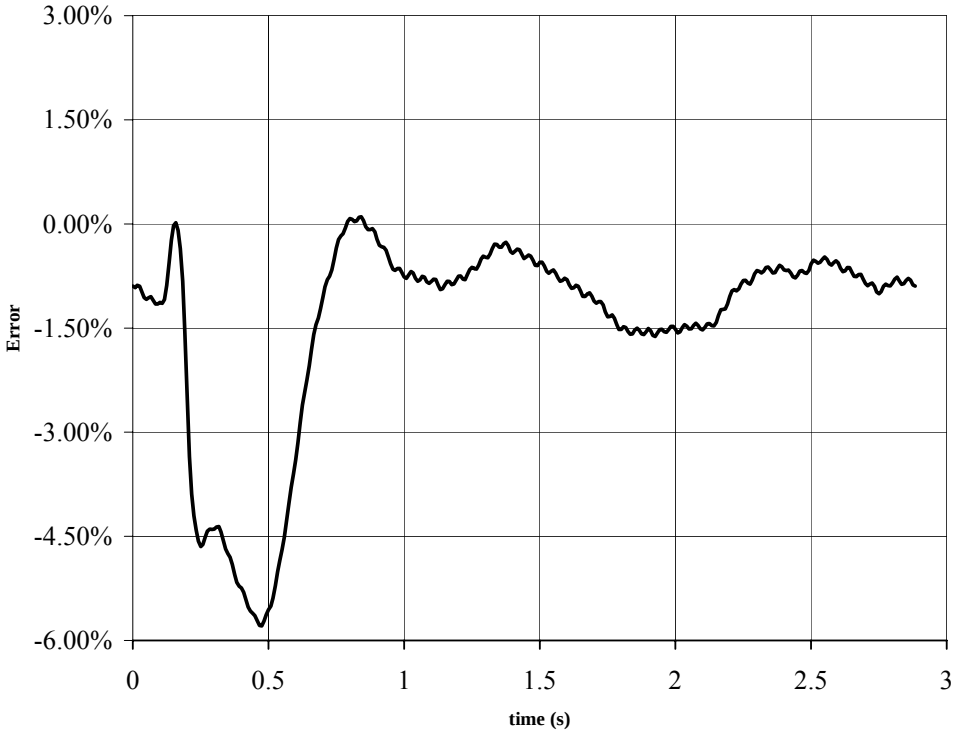

Fig. F.9 Field voltage error

The identification result can be checked with two typical operation mode of that generator, the first operation mode is in normal operation condition, while in the second mode, the generator nearly operates in its limits. In Table F.3, if the measured I_f and the calculated I_f by (F.1) are compared, it is observed that this identification method has enough accuracy. Based on this identified model, we can use the estimated (calculated) value and its relation to the measurable quantity from the exciter field winding to detect potential faults of exciters.

Table F.3 Test example using Chinese machine data

	P(MW)	Q (MVar)	If (Measured from field test)	Estimated If	ΔIf relative error (%)
Operation mode1	597.00	68.00	0.718026	0.734740	2.327
Operation mode2	563.00	107.00	0.664223	0.669973	0.865

F.8 Conclusions Drawn for the Brushless Exciter Case

The results indicated for the brushless exciter case were unable to be tested for actual data. The brushless exciter case was outside the scope of the original project, but the foregoing remarks are a summary of research results. Two actual brushless exciter cases were examined; one was missing several critical measurements, while the other was a machine of unusual design and manufacturer's data could not be obtained. Although the results that are shown in this appendix are promising in terms of constructing an observer for a brushless generator, this conjecture was not proven for actual machine data.

REFERENCES

[1] R. H. Park, "Two-reaction theory of synchronous machines – generalized methods of analysis – Part I," *AIEE Transactions*, vol. 48, pp. 716-727, July 1929.

[2] P. L. Dandeno, P. Kundur, and R. P. Schulz, "Recent trends and progress in synchronous machine modeling in the electric utility industry," *IEEE Proceedings*, vol. 62, pp. 941-950, July 1974.

[3] R. P. Schulz, "Synchronous machine modeling," *IEEE Symposium on Adequacy and Philosophy of Modeling: Dynamic System Performance*, IEEE Publications, 75CH0970-4-PWR, pp. 24-28.

[4] J. L. Dineley and A. J. Morris, "Synchronous generator transient control – Pt I: Theory and evaluation of alternative mathematical models," *IEEE Transactions on Power Apparatus and Systems*, vol. PAS-92, pp. 417-422, Apr. 1973.

[5] R. H. Park, "Two-reaction theory of synchronous machines, Part II," *AIEE Transactions*, vol. 52, pp. 352-355, June 1933.

[6] *Rotating Electrical Machines. Part 10: Conventions for Description of Synchronous Machines*, IEC Standard 34-10-1975, International Electrotechnical Commission, Geneva, 1975.

[7] H. C. Stanley, "An analysis of the induction motor," *AIEE Transactions*, Vol. 57 (Supplement), pp. 751-755, 1938.

[8] G. Kron, *Equivalent Circuits of Electric Machinery*, New York: John Wiley and Sons, Inc., 1951.

[9] W. A. Lewis, "A basic analysis of synchronous machines, Pt. 1," *AIEE Transactions on Power Apparatus and Systems*, vol. PAS-77, pp. 436-455, 1958.

[10] W. B. Jackson and R. L. Winchester, "Direct and quadrature axis equivalent circuits for solid-rotor turbine generators," *IEEE Transactions on Power Apparatus and Systems*, vol. PAS-88, pp. 1121-1136, July 1969.

[11] I. M. Canay, "Causes of discrepancies on calculation of rotor quantities and exact equivalent diagram of the synchronous machine," *IEEE Transactions on Power Apparatus and Systems*, vol. PAS-88, pp. 1114-1120, July 1969.

[12] Y. Yu and H. A. M. Moussa, "Experimental determination of exact equivalent circuit parameters of synchronous machines," *IEEE Transactions on Power Apparatus and Systems*, vol. PAS-90, pp. 2555-2560, Dec. 1971.

[13] *IEEE Guide: Test Procedures for Synchronous Machines*, IEEE Standard 115-1995, Dec. 1995.

[14] *IEEE Standard Procedures for Obtaining Synchronous Machine Parameters by Standstill Frequency Response Testing*, IEEE Standard 115A-1987, May 1987.

[15] G. T. Heydt, *Computer Analysis Methods for Power Systems*, Scottsdale: Stars in a Circle Publications, 1996.

[16] R. J. Hosking, D. C. Joyce and J. C. Turner, *First Steps in Numerical Analysis*, London: Edward Arnold, 1991.

[17] G. Lindfield and J. Penny, *Numerical Methods Using MATLAB*, New Jersey: Prentice Hall, 2000.

[18] M. K. Jain, S. R. K. Iyenkar, and R. K. Jain, *Numerical Methods for Scientific and Engineering Computation*, New York: John Wiley and Sons, 1985.

[19] M. G. Salvadori and M. L. Baron, *Numerical Methods in Engineering*, Englewood Cliffs: Prentice-Hall Inc., 1961.
[20] P. Kundur, *Power System Stability and Control*, New York: McGraw-Hill Inc., 1994.
[21] P. M. Anderson and A. A. Fouad, *Power System Control and Stability*, Ames: The Iowa State University Press, 1977.
[22] R. P. Schulz, R. G. Farmer, C. J. Goering, S. M. Bennett, D. A. Selin, and D. K. Sarma, "Benefit assessment of finite-element based generator saturation model," *IEEE Transactions on Power Systems*, vol. PWRS-2, no. 4, pp. 1027-1033, Nov. 1987.
[23] C. C. Lee and Q. T. Tan, "A weighted-least-squares parameter estimator for synchronous machines," *IEEE Transactions on Power Apparatus and Systems*, vol.1, no. 1, pp. 97-101, Feb. 1977.
[24] P. L. Dandeno, P. Kundur, A. T. Poray, and H. M. Z. El-Din, "Adaptation and validation of turbogenerator model parameters through on-line frequency response measurements," *IEEE Transactions on Power Apparatus and Systems*, vol. PAS-100, no.4, pp. 1656-1664, Apr. 1981.
[25] M. N. T. Nishiwaki, S. Yokokawa, and K. Ohtsuka, "Identification of parameters for power system stability analysis using a Kalman filter," *IEEE Transactions on Power Apparatus and Systems*, vol. PAS-100, no. 7, pp. 3304-3311, July 1981.
[26] Westinghouse Electric Corporation Central Station Engineers, *Electrical Transmission and Distribution Reference Book*, 4th edition, East Pittsburgh: Westinghouse Electric Corporation, 1964.
[27] R. Rosenberg, *Electric Motor Repair*, San Francisco: Rinehart Press, 1970.
[28] H. Saadat, *Power System Analysis*, Boston: McGraw-Hill Inc., 1999.
[29] P. M. Anderson, B. L. Agrawal, and J. E. Van Ness, *Subsynchronous Resonance in Power Systems*, New York: IEEE Press, 1990.
[30] A. E. Fitzgerald, C. Kingsley Jr., and S. D. Umans, *Electric Machinery*, New York: McGraw-Hill Inc., 1983.
[31] P. C. Krause, O. Wasynczuk, and S. D. Sudhoff, *Analysis of Electric Machinery*, New York: IEEE Press, 1995.
[32] A. Keyhani, S. Hao, and G. Dayal, "Maximum likelihood estimation of solid-rotor synchronous machine parameters from SSFR test data," *IEEE Transactions on Energy Conversion*, vol. 4, no. 3, pp. 551-558, Sep. 1989.
[33] A. Keyhani, S. Hao, and G. Dayal, "The effects of noise on frequency-domain parameter estimation of synchronous machine models," *IEEE Transactions on Energy Conversion*, vol. 4, no. 4, pp. 600-607, Dec. 1989.
[34] A. Keyhani, S. Hao, and R. P. Schulz, "Maximum likelihood estimation of generator stability constants using SSFR test data," *IEEE Transactions on Energy Conversion*, vol. 6, no. 1, pp. 140-154, Mar. 1991.
[35] A. Keyhani, H. Tsai, and T. Leksan, "Maximum likelihood estimation of synchronous machine parameters from standstill time response data," *IEEE Transactions on Energy Conversion*, vol. 9, no. 1, pp. 98-114, Mar. 1994.
[36] H. Tsai, A. Keyhani, J. Demcko, and R. G. Farmer, "On-line synchronous machine parameter estimation from small disturbance operating data," *IEEE Transactions on Energy Conversion*, vol. 10, no. 1, pp. 25-36, Mar. 1995.

[37] A. Tumageanian and A. Keyhani, "Identification of synchronous machine linear parameters from standstill step voltage input data," *IEEE Transactions on Energy Conversion*, vol. 10, no. 2, pp. 232-240, June 1995.
[38] H. Tsai, A. Keyhani, J. A. Demcko, and D. A. Selin, "Development of a neural network based saturation model for synchronous generator analysis," *IEEE Transactions on Energy Conversion*, vol. 10, no. 4, pp. 617-624, Dec. 1995.
[39] E. Eitelberg and R. G. Harley, "Estimating synchronous machine electrical parameters from frequency response tests," *IEEE Transactions on Energy Conversion*, vol. EC-2, no. 1, pp. 132-138, Mar. 1987.
[40] E. S. Boje, J. C. Balda, R. G. Harley, and R. C. Beck, "Time-domain identification of synchronous machine parameters from simple standstill tests," *IEEE Transactions on Energy Conversion*, vol. 5, no. 1, pp. 164-175, Mar. 1990.
[41] H. B. Karayaka, A. Keyhani, B. Agrawal, D. Selin, and G. T. Heydt, "Methodology development for estimation of armature circuit and field winding parameters of large utility generators," *IEEE Transactions on Energy Conversion*, vol. 14, no. 4, pp. 901-908, Dec. 1999.
[42] H. B. Karayaka, A. Keyhani, B. Agrawal, D. Selin, and G. T. Heydt, "Identification of armature circuit and field winding parameters of large utility generators," *IEEE Power Engineering Society Winter Meeting*, vol. 1, pp. 29-34, 1999.
[43] H. B. Karayaka, A. Keyhani, B. Agrawal, D. Selin, and G. T. Heydt, "Identification of armature, field, and saturated parameters of a large steam turbine-generator from operating data," *IEEE Transactions on Energy Conversion*, vol. 15, no. 2, June 2000.
[44] J. Rico, G. T. Heydt, A. Keyhani, B. Agrawal, and D. Selin, "Synchronous machine parameter estimation using the Hartley series," *IEEE Transactions on Energy Conversion*, vol. 16, no.1, pp. 49-54, Mar. 2001.
[45] J. Rico, G. T. Heydt, A. Keyhani, B. Agrawal, and D. Selin, "An algebraic approach for identifying operating point dependent parameters of synchronous machines using orthogonal series expansions," *IEEE Transactions on Energy Conversion*, vol. 16, no.1, pp. 92-98, Mar. 2001.
[46] E. Acha and M. Madrigal, *Power Systems Harmonics: Computer Modelling and Analysis*, Chichester: John Wiley & Sons, Ltd., 2001.
[47] E. Kyriakides, G. T. Heydt, and V. Vittal, "On-line estimation of synchronous generator parameters using an observer for damper currents and a graphical user interface," *IEEE Transactions on Energy Conversion*, Aug. 2003, to be published.
[48] A. J. Wood and B. F. Wollenberg, *Power Generation, Operation and Control*, New York: John Wiley and Sons, Inc., 1996.
[49] F. C. Schweppe and J. Wildes, "Power system static state estimation, Pt. I: Exact model," *IEEE Transactions on Power Apparatus and Systems*, vol. 89, pp.120-125, Jan. 1970.
[50] F. C. Schweppe and D. B. Rom, "Power system static state estimation, Pt. II: Approximate model," *IEEE Transactions on Power Apparatus and Systems*, vol. 89, pp.125-130, Jan. 1970.
[51] G. T. Heydt, *Electric Power Quality*, West Lafayette: Stars in a Circle Publications, 1991.

[52] A. V. Oppenheim and R. W. Schafer, *Discrete-Time Signal Processing*, New Jersey: Prentice Hall, 1989.
[53] D. E. Johnson, J. R. Johnson and H. P. Moore, *A Handbook of Active Filters*, New Jersey: Prentice Hall, 1980.
[54] The MathWorks Inc., *MATLAB*, *Signal Processing Toolbox User's Guide*, 2001.
[55] F. Gustafsson, "Determining the initial states in forward-backward filtering," *IEEE Transactions on Signal Processing*, vol. 44, pp. 988-992, Apr. 1996.
[56] J. Kormylo and V. Jain**,** "Two-pass recursive digital filter with zero phase shift," *IEEE Transactions on Acoustics, Speech, and Signal Processing*, vol. 22, Issue 5, pp. 384–387, Oct. 1974.
[57] I. W. Slutsker, "Bad data identification in power system state estimation based on measurement compensation and linear residual calculation," *IEEE Transactions on Power Systems*, vol. 4, no. 1, pp. 53-60, Feb. 1989.
[58] J. L. Durán-Paz, F. Pérez-Hidalgo, and M. J. Durán-Martinez, "Bad data detection of unequal magnitudes in state estimation of power systems," *IEEE Power Engineering Review*, vol. 22, Issue 4, pp. 57-60, Apr. 2002.
[59] W. L. Peterson and A. A. Girgis, "Multiple bad data detection in power system state estimation using linear programming," *Proceedings of the Twentieth Southeastern Symposium on System Theory*, pp. 405 –409, Mar. 1988.
[60] G. T. Heydt, E. Gunther, "Postprocessing of electric power quality data," Journal Electric Machines and Power Systems, No. 8, Volume 24, 1996, p. 847 - 855.
[61] F. P. de Mello and L. N. Hannett, "Validation of synchronous machine models and derivation of model parameters from tests," *IEEE Transactions on Power Apparatus and Systems*, pp. 662-672, Feb. 1981.
[62] S. H. Minnich, R. P. Schulz, D. H. Baker, D. K. Sarma, R. G. Farmer, and J. H. Fish, "Saturation functions for synchronous generators from finite elements," *IEEE Transactions on Energy Conversion*, vol. EC-2, no. 4, pp. 680-692, Dec. 1987.
[63] J. C. Wang, H. D. Chiang, C. T. Huang, and Y. T. Chen, "Identification of synchronous generator saturation models based on on-line digital measurements," *IEE Proceedings on Generation, Transmission and Distribution*, vol. 142, no.3, pp.225-232, May 1995.
[64] F. P. de Mello and L. N. Hannett, "Representation of saturation in synchronous machines," *IEEE Transactions on Power Systems*, vol. PWRS-1, no.4, pp. 8-18, Nov. 1986.
[65] A. Keyhani and H. Tsai, "Synchronous generator saturation modeling from operating data," *IEEE/NTUA Athens Power Tech Conference*, pp. 837-841, Sep. 1993.
[66] M. A. A. Lopez and D. C. Macdonald, "Analysis of synchronous reactances as a function of airgap MMF," *Electric Power Components and Systems Journal*, vol. 30, pp. 345-359, 2002.
[67] E. Kyriakides, G. T. Heydt, "An observer for the estimation of synchronous generator damper currents use in parameter identification," *IEEE Transactions on Energy Conversion*, Vol. 18, March 2002, pp. 175-177.
[68] S. U. Borkar, K. E. Holbert, "Digital Filtering of Synchronous Generator Measurements for Parameter Estimation," *Proceedings of the Seventh IASTED International Conference on Power and Energy Systems*, Clearwater, FL, Nov. 28-Dec. 1, 2004, pp. 454-459.
[69] E. Kyriakides, "Innovative Concepts For On-Line Synchronous Generator Parameter Estimation,: Doctoral Thesis, Arizona State University, Tempe, AZ December 2003.

[70] R. P. Schulz, R. G. Farmer, C. J. Goering, S. M. Bennett, D. A. Selin, and D. K. Sharma, "Benefit Assessment of Finite-Element Based Generation Saturation Model," *IEEE Transactions on Power Systems*, Vol. PWRS-2, No. 4, pp. 1027-1033, Nov. 1987.
[71] S. U. Borkar, "Design of a Digital Filter for Synchronous Generator Parameter Estimation," M. S. E. E. Thesis, Arizona State University, Tempe, AZ, August 2004.
[72] J. P. Martin, C. E. Tindall, "Noninvasive technique for determining parameter values from the sudden short-circuit test data of brushless alternators," IEEE Transactions on Energy Conversion, vol. 15, No. 3, Sept. 2000, pp. 245 – 250.
[73] X. Y. Li, "A microprocessor-based fault monitor for rotating rectifiers of brushless ac exciters using a pattern-recognition approach," IEEE 1994 Instrumentation and Measurement Technology Conference, vol. 1, May 1994, pp. 394 – 397.
[74] S. Kabir, R. Shuttleworth, "Brushless exciter model", IEE Proceedings on Generation, Transmission and Distribution, vol. 141, No. 1, Jan. 1994, pp. 61 – 67.
[75] T. Zouaghi, M. Poloujadoff, "Modeling of polyphase brushless exciter behavior for failing diode operation," IEEE Transactions on Energy Conversion, vol.13, No. 3, Sept. 1998, pp. 214 - 220